Magnetic resonance study of atomic hydrogen stabilized in matrices of hydrogen isotopes below 1 K

Manuscript of the PhD thesis of
Sergei Sheludiakov

Department of Physics and Astronomy
FIN-20014 University of Turku
Finland

February 2017

Acknowledgments

Turku, January 2017

Sergei Sheludiakov

Abstract

In this thesis, we report on an experimental study of H, D and T atoms stabilized in solid molecular matrices of hydrogen isotopes at temperatures down to 70 mK. Being trapped in a molecular H_2 matrix, hydrogen atoms are not completely localized and able to diffuse by quantum tunneling at temperatures below 1 K. Accumulating H atoms in such matrices to high concentrations may lead to a number of fascinating phenomena related to the BEC-like behavior of H atoms or to a transition to the conducting state of a normally insulating hydrogen matrix. We describe different approaches to reaching high concentrations of unpaired atoms in solid films of hydrogen isotopes: an *in situ* electron-impact dissociation of hydrogen molecules in the matrix by running a cryogenic rf discharge in helium vapors and admixing β-radioactive tritium to the gas mixture prior to deposition. The atoms of all three hydrogen isotopes have non-zero electron and nuclear spins and the main experimental techniques used in our study are high-frequency electron spin resonance (ESR) and electron-nuclear double resonance (ENDOR).

Accumulating atoms in D_2:H_2 solid mixtures by running the rf discharge we reached a total concentration of unpaired atoms [H]+[D]$\simeq$4$\times$10^{19} cm^{-3}. Spectacular conversion of D atoms into H due to quantum tunneling isotopic exchange reactions D+H_2 $\rightarrow$HD+H and D+HD$\rightarrow$$D_2$+H was observed in all samples containing deuterium. We were able to measure the rate of the latter reaction in pure HD, $k^{ex}\simeq$3 $\times$ 10^{-27}cm^{3}s^{-1}, which turned out to be nearly independent of temperature down to 0.13 K. We studied the D+HD reaction also in a D_2 matrix with a small, 0.23 %, admixture of HD, and found that it goes with a nearly same rate as in HD. In the D_2 matrix the reactants should diffuse towards each other before the reaction takes place. The diffusion also occurs via quantum exchange of the impurity atom with one of the atoms of the neighboring molecule. Usually the diffusion is a limiting stage for the recombination of unpaired atoms in hydrogen matrices. However, we found that this is not the case for the D_2:0.23 % HD matrix. The very weak dependence of the exchange reaction rate on temperature is a signature of the quantum tunneling character of this process.

We also studied dynamic nuclear polarization (DNP) of H atoms in different matrices of hydrogen isotopes. It turned out that the DNP via the Solid effect, by pumping the forbidden transitions of H atoms, is strongly enhanced by the presence of unpaired deuterium atoms. This behavior is explained in terms of the

Cross effect, which occurs due to the overlap of the forbidden transitions of H with the ESR lines of atomic deuterium. In the strong magnetic field of this work the Solid and Cross effects are well resolved and both may be used for efficient DNP of H atoms. A new and peculiar phenomenon was observed after saturating the center of the ESR spectra which caused a negative polarization of H atoms. We suggest that this DNP effect may be realized due to the formation of H-H or H-D radical pairs coupled by the strong exchange interaction, which have an allowed transition in the center of the ESR spectra in contrast to unpaired H atoms. Formation of the radical pairs was supported indirectly in experiments on saturating satellite transitions which correspond to the flipping of an electron spin of an unpaired atom and a nuclear spin of a neighboring D_2 molecule.

Studying the samples where unpaired atoms were accumulated due to the β-decay of tritium we achieved the record-high concentrations of T and H atoms, $\simeq 1.8 \times 10^{20}\,\mathrm{cm}^{-3}$ and $\simeq 1.1 \times 10^{20}\mathrm{cm}^{-3}$, respectively, by adjusting the thickness and the T_2:H_2 content in the films. We also observed an efficient conversion of T atoms into H due to the isotopic exchange reaction $T+H_2 \to TH+H$. We estimate the rate of this reaction at $70\,\mathrm{mK}$, $k_T^{ex} = 3(2) \times 10^{-26}\mathrm{cm}^3\mathrm{s}^{-1}$. The maximum concentrations of atoms in these samples were limited by the recombination which was stimulated by phonons generated in the matrix due to the β-decay of tritium. Depending on the storage conditions, recombination also appeared in an explosive manner. We suggest that the main mechanism of atomic diffusion in the samples containing tritium is the physical diffusion related to the formation of vacancies in contrast to the diffusion due to tunneling exchange reactions $H+H_2 \to H_2+H$ and $D+D_2 \to D_2+D$ in H_2 and D_2 matrices where unpaired atoms are produced by other techniques.

Preface

This thesis is based on a series of experiments carried out during the years 2012-2016 and six original papers listed below.

[P1]. S. Sheludiakov, J. Ahokas, O. Vainio, J. Järvinen, D. Zvezdov, S. Vasiliev, V. V. Khmelenko, S. Mao and D. M. Lee, Experimental cell for molecular beam deposition and magnetic resonance studies of matrix isolated radicals at temperatures below 1 K, Rev. Sci. Instrum. **85**, 053902 (2014).

[P2]. S. Sheludiakov, J. Ahokas, J. Järvinen, D. Zvezdov, O. Vainio, L. Lehtonen, S. Vasiliev, S. Mao, V. V. Khmelenko, D. M. Lee, Dynamic nuclear polarization of high-density atomic hydrogen in solid mixtures of molecular hydrogen isotopes, Phys. Rev. Lett. **113**, 265303 (2014).

[P3]. S. Sheludiakov, J. Ahokas, J. Järvinen, O. Vainio, L. Lehtonen, D. Zvezdov, V. V. Khmelenko, D. M. Lee, Electron spin resonance study of electrons trapped in solid molecular hydrogen films, J. Low Temp. Phys. **183**, 120 (2016).

[P4]. S. Sheludiakov, J. Ahokas, J. Järvinen, D. Zvezdov, L. Lehtonen, O. Vainio, S. Vasiliev, D. M. Lee, and V. V. Khmelenko, Tunneling chemical exchange reaction $D+HD{\rightarrow}D_2+H$ in solid HD and D_2 at temperatures below 1 K, Phys. Chem. Chem. Phys. **18**, 29600 (2016).

[P5]. S. Sheludiakov, J. Ahokas, J. Järvinen, O. Vainio, L. Lehtonen, S. Vasiliev, D. M. Lee and V. V. Khmelenko, Dynamic nuclear polarization and relaxation of H and D atoms in solid mixtures of hydrogen isotopes, accepted to J. Low Temp. Phys.

[P6]. S. Sheludiakov, J. Ahokas, J. Järvinen, L. Lehtonen, O. Vainio, S. Vasiliev, D. M. Lee and V. V. Khmelenko, ESR study of atomic hydrogen and tritium in solid T_2 and T_2:H_2 matrices below 1 K, accepted to Phys. Chem. Chem. Phys.

My contribution to the papers is following:

P1   I participated in the design, assembly and experimental tests of the sample cell, analyzed the data and wrote a part of the manuscript.

P2   I was responsible for running the experiments, acquiring and analyzing the data.

P3   I was in charge of running the experiments, collecting and analyzing the data and writing a major part of the manuscript.

P4   I made a part of the experiments and data analysis and wrote a part of the manuscript.

P5   I made a part of the experiments and data analysis and wrote a major part of the manuscript.

P6   I made a part of the experiments and data analysis and prepared the manuscript.

Contents

Chapter 1

Background

1.1 Introduction

Hydrogen is the simplest and the most abundant element in the Universe. It is constructed from a proton and a single electron and stands first in the Periodic table. This simplicity results in a special role which hydrogen plays in physics: starting from the first quantum model of an atom by Bohr till the recent race on reaching Bose-Einstein condensation (BEC) triggered by stabilization of the atomic hydrogen gas [1]. Depending on a mutual orientation of their electron spins, two H atoms may either form a molecule with the strongest bond per unit mass when the spins are anti-parallel or exhibit the weakest interaction between two atoms when their electron spins are parallel [2]. Polarizing electron spins requires low temperatures, $\leq 1\,\mathrm{K}$, and a few Tesla high magnetic field where H atoms can be stabilized as a spin-polarized gas. An extensive experimental and theoretical work on the spin-polarized atomic hydrogen gas led to development of the main methods for trapping and cooling neutral atoms and finally culminated in the observation of BEC in vapors of alkali metals [3, 4], and later BEC in the 3D [5] and the Kosterlitz-Thouless transition in the 2D atomic hydrogen gases [6].

Another approach for stabilizing H atoms is based on introducing them into an inert solid matrix where the atom diffusion is suppressed and they cannot recombine back to molecules. This method of matrix isolation has been in use since the 1950s when the NIST initiated a programme on developing propellants based on metastable atomic radicals in solid molecular matrices, such as H and N in H_2 and N_2, respectively. Atomic recombination in hydrogen solids was considered as a promising source of energy. However, the concentrations of H atoms in solid H_2 reached, $< 0.1\,\%$, were substantially smaller than those needed to achieve an improvement over conventional fuels [7].

A later interest to studying H atoms in solid H_2 arose due to outstanding quantum properties of solid hydrogen. Neighboring molecules of hydrogen isotopes in the lattice have an appreciable overlap of their wavefunctions and are able to diffuse either by swapping places, like HD in para-H_2 [8, 9], or by spin-diffusion,

Figure 1.1: Schematic of the exchange reaction H+H_2 →H_2+H taking place in solid H_2.

ortho-H_2 in para-H_2, through a resonant ortho-para conversion [10]. Unpaired H atoms stabilized in solid H_2 are also mobile and migrate by a repetition of exchange tunneling reaction [11, 12]

$$H+H_2 \rightarrow H_2+H. \tag{1.1}$$

The reaction of a hydrogen atom with a hydrogen molecule (1.1) when another H atom is produced (Fig.1.1) is known to be the simplest among chemical reactions and plays a very special role in the field of chemical kinetics [13]. This reaction has a large activation barrier, $\simeq$4600 K, and proceeds at temperatures ~ 1 K exclusively by tunneling [12]. Similar exchange reactions involve a heavier hydrogen isotope, deuterium:

$$D+H_2 \rightarrow HD + H \tag{1.2}$$

$$D+HD \rightarrow D_2 + H. \tag{1.3}$$

These reactions are of fundamental importance in chemistry of the early Universe where they are essential for understanding dynamics of deuterium in the primordial gas [14, 15].

Accumulating H atoms in a H_2 matrix to high concentrations may lead to a number of fascinating quantum phenomena related to the Bose nature of hydrogen atoms. Andreev and Lifshitz [16] and later Chester [17] and Leggett [18] hypothesized that light impurities in a solid become delocalized at low enough temperatures and behave as a gas of quasi-particles, impuritons, which may manifest quantum degeneracy, leading to a so-called supersolid state. In 2004, Kim and Chan [19] reported on a possible detection of supersolidity in ^{4}He which sparked a new interest towards quantum solids. However later experiments and extensive theoretical work did not confirm the onset of supersolidity [20]. Being lighter than ^{4}He atoms, atomic hydrogen stabilized in solid H_2 is one of candidates for observing such a behavior. The BEC transition temperature for H atoms is [21]

$$T_C = \frac{3.31\hbar^2}{m^*k_B} \left(\frac{n}{g}\right)^{2/3}, \tag{1.4}$$

where n is the concentration of H atoms, g is the number of the hyperfine states occupied and $m^* \sim \hbar^2/a^2\Delta$ is their effective mass which is inversely proportional to the bandwidth of the tunneling motion Δ [22], and a is the lattice constant. An estimate of Δ for H in H_2, 10^{-2} K $< \Delta < 1$ K, leads to the transition temperatures $T_C = 1.4$-140 mK at $n = 10^{20}$ cm^{-3} [23] which might be attained experimentally. However, the band motion at the high concentration of atomic impurities becomes destructed due to the lattice distortion they create which makes the impuriton BEC a rather elusive goal.

In addition to that, a strong exchange interaction may occur between the electron clouds of unpaired atoms which would correspond to the formation of a metallic state of a normally insulating H_2 matrix. A similar behavior is well-known in doped semiconductors, such as phosphorus doped silicon, Si:P, where at [P] $\simeq 3 \times 10^{18}$ cm^{-3} the system undergoes a transition to the conducting state. However, such a transition for H atoms is expected to occur at much higher concentrations due to their much smaller size compared to phosphorus donors. Reaching metallic state in solid hydrogen is a "holy grail" of high pressure physics [24] and intensive studies are carried out in this field [25, 26, 27].

In this thesis, we summarize the results of the experimental study of unpaired H, D and T atoms stabilized in the solid matrices of hydrogen isotopes: H_2, HD, D_2, T_2, and their solid mixtures at temperatures below 1 K using the techniques of electron spin resonance (ESR) and electron-nuclear double resonance (ENDOR). The experiments described in the thesis had several goals. The main emphasis was placed on searching possible methods for creating samples of solid molecular hydrogen with the highest concentrations of unpaired atoms where possible effects of quantum degeneracy could be detected. Based on that we elaborated a versatile experimental cell [P1] for studying samples of different solid hydrogen isotopes where atomic radicals could be accumulated to the record-high densities. We employed different techniques for generating unpaired atoms in solid hydrogen films: a cryogenic rf discharge [P2] and a dissociation of molecules due to β-decay of tritium [P6]. The second aim of this work was to broaden the experiments on H in H_2 started in Turku in 2006, where a number of peculiar effects in recombination of H atoms and their nuclear relaxation were detected [23, 28], to other solid hydrogen isotopes: deuterium and tritium. The solid mixtures of hydrogen and deuterium are one of the only systems where isotopic exchange reactions (1.2) and (1.3) could be studied at temperatures below 1 K. Studying solid tritium samples was intriguing due to both achieving high densities of atoms and the explosive recombination of atoms reported previously [29, 30]. Finally, we expected that studying mechanisms of dynamic nuclear polarization (DNP) of atoms in the films may provide additional information about the interactions in our samples.

The thesis is organized as follows. Chapter 1 provides an introduction to the properties of atomic and solid molecular hydrogen isotopes. In addition, the methods of matrix isolation and magnetic resonance are surveyed. The design and performance of the experimental cell are summarized in Chapter 2. The

effects of interactions of hydrogen atoms stabilized in solid matrices on the main spectroscopic parameters, the ESR line width and shape, are discussed in Chapter 3. Chapter 4 is devoted to the experimental study of isotopic exchange reaction (1.3) in pure solid HD and D_2:0.23%HD matrices at temperatures 0.13-1.5 K. The results of studying mechanisms of relaxation and dynamic nuclear polarization in different matrices of hydrogen isotopes are summarized in Chapter 5. An overview of our experiments with solid tritium and tritium-hydrogen mixtures is presented in Chapter 6. Each chapter contains a short introduction in order to familiarize the reader with a subject to be discussed. Six original publications are attached after the Bibliography section.

1.2   Atomic hydrogen, deuterium and tritium

Hydrogen has the simplest atomic structure: one proton, and one $1s$ electron characterized by the Bohr radius $a_0 = 0.53\,\text{Å}$. Both electron and nuclear spins, I and S, are equal to 1/2 and the total angular momentum, $F = I + S = 0, 1$ is an integer. We will consider only the ground $1s$ electron state in this work. In magnetic field it is split into four sub-levels by the hyperfine interaction between electron and nuclear spins. The hyperfine interaction is purely isotropic (contact) and is defined by a non-zero electron density at the nucleus. The anisotropic dipolar interaction is exactly zero for spherically symmetric $1s$ electron orbitals. Within the limit of high magnetic fields ($B \gg A$, A=507 G is the hyperfine constant), there are four good quantum numbers: the nuclear and electron spin numbers I, S and the corresponding magnetic numbers m_I and m_S. The spin-hamiltonian for a free hydrogen atom in magnetic field is

$$\hat{H} = A\mathbf{I} \cdot \mathbf{S} + g_e \mu_B \hat{S}_z B - g_N \mu_N \hat{I}_z B, \qquad (1.5)$$

where g_e and g_N are the electronic and nuclear g-factors, μ_N and μ_B are the nuclear and Bohr magnetons, respectively, and B is magnetic field. The contact interaction $A\mathbf{I} \cdot \mathbf{S}$ introduces non-diagonal components into the hamiltonian and mixes two states out of four: $a = |\text{-}\frac{1}{2}, \frac{1}{2}\rangle$ and $c = |\frac{1}{2}, \text{-}\frac{1}{2}\rangle$. The states $b = |\text{-}\frac{1}{2}, \text{-}\frac{1}{2}\rangle$ and $d = |\frac{1}{2}, \frac{1}{2}\rangle$ are pure quantum states. The energy levels for atoms of all three isotopes can be found by diagonalizing hamiltonian (1.5). The energy levels of H, T and D atoms in high magnetic field are shown in Fig.1.2.

Both T and H nuclei have spins 1/2 and form composite bosons when combined with electrons [31]. The hyperfine constant and the nuclear gyromagnetic ratio $\gamma = g_N \mu_N$ for atomic tritium, $A = 1516\,\text{MHz}$ and $\gamma = 45.4\,\text{MHz/T}$, are slightly larger than those for hydrogen, $A = 1420\,\text{MHz}$, $\gamma = 42.6$ MHz/T (Table 1.1).

The ESR and NMR selection rules and transition probabilities can be found considering the magnetic dipole transition matrix:

$$\langle m_S, m_I | \hat{V} | m_S', m_I' \rangle, \qquad (1.6)$$

a)

$|d\rangle = |\frac{1}{2}, \frac{1}{2}\rangle$

$|c\rangle = |\frac{1}{2}, \text{-}\frac{1}{2}\rangle$

$|b\rangle = |\text{-}\frac{1}{2}, \text{-}\frac{1}{2}\rangle$

$|a\rangle = |\text{-}\frac{1}{2}, \frac{1}{2}\rangle$

b)

$|\zeta\rangle = |\frac{1}{2}, 1\rangle$

$|\epsilon\rangle = |\frac{1}{2}, 0\rangle$

$|\delta\rangle = |\frac{1}{2}, \text{-}1\rangle$

$|\gamma\rangle = |\text{-}\frac{1}{2}, \text{-}1\rangle$

$|\beta\rangle = |\text{-}\frac{1}{2}, 0\rangle$
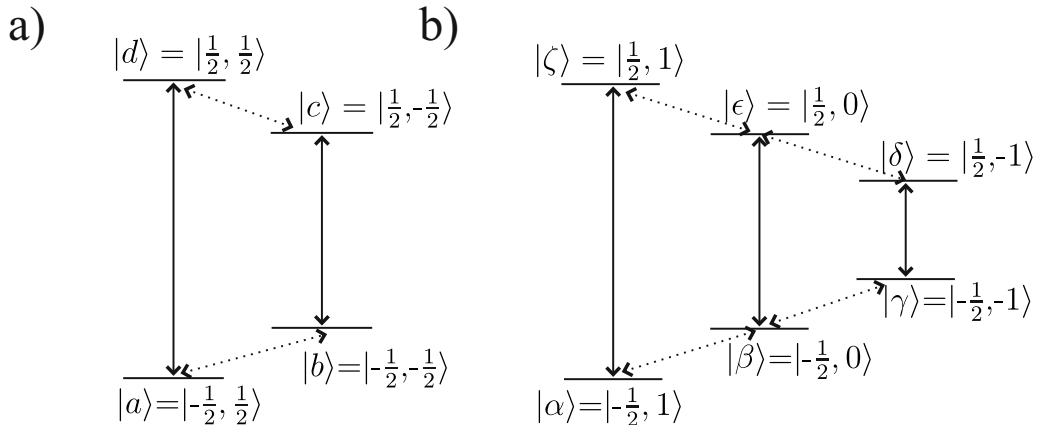
$|\alpha\rangle = |\text{-}\frac{1}{2}, 1\rangle$

Figure 1.2: a) Energy levels of atomic hydrogen and tritium (a) and atomic deuterium (b) in the limit of a high magnetic field. The allowed ESR transitions are shown by solid arrows, the NMR transitions are shown by dotted lines. The spin states are presented as $|m_S, m_I\rangle$.

where the initial and final state should be written in terms of true wavefunctions (see ref. [21]). The excitation operator $\hat{V}$ can be presented in a general form as $\hat{V} = -g_N\mu_N(\hat{I}_x + \hat{I}_y + \hat{I}_z) + g_e\mu_B(\hat{S}_x + \hat{S}_y + \hat{S}_z)$. There are two allowed ESR transitions, $a - d$ and $b - c$, for both H and T atoms, shown by solid lines in Fig.1.2. They can be excited by a transverse oscillating field and correspond to a reversal of the electron spin, $\Delta m_S = \pm 1$, while $\Delta m_I = 0$. In analogy to them, flipping nuclear spins, $\Delta m_I = \pm 1$, $\Delta m_S = 0$, corresponds to the NMR transitions (shown dotted). There are also two forbidden ESR transitions, $a - c$ ($\Delta m_S = \pm 1$, $\Delta m_I = \mp 1$) and $b - d$ ($\Delta m_S = \pm 1$, $\Delta m_I = \pm 1$). The total angular momentum, $I + S$, is conserved for the flip-flop $a - c$ transition. It is forbidden for free atoms by a factor κ^2,

$$\kappa = \frac{A}{(g_e\mu_B + g_N\mu_N)B}, \tag{1.7}$$

here κ is the factor which defines mixing of a and c states. Total angular momentum is not conserved for the flip-flip $b - d$ transition. It is completely forbidden for free atoms. The situation changes in the presence of the dipole-dipole interaction which in contrast to the contact term, $A\mathbf{I} \cdot \mathbf{S}$, mixes all four spin states and the forbidden transitions become partially allowed and can be excited by a transverse oscillating field.

Atomic deuterium has an integer nuclear spin $I = 1$, in contrast to H and T. Its nucleus contains a neutron which has a negative gyromagnetic ratio and the net magnetic moment and the hyperfine constant A are smaller compared to H and T (Table 1.1). The total angular momentum of a D atom is half-integer. Due to the nuclear spin $I = 1$, the ground energy state of a D atom has a six-fold splitting (Fig.1.2). The zero-field splitting is $3/2\,A$ instead of A for H and T. There are in

5

Figure 1.3: Calculated polarization of the electron spins (e), and that of H, D and T nuclear spins in field B=4.6 T.

total three allowed ESR transitions and six forbidden transitions [21, 32].

The equilibrium occupation of the energy levels shown in Fig.1.2 obeys the Boltzmann distribution. The relative population of the energy levels n_m is described by the spin polarization which can be calculated as [33]

$$p = \frac{\sum_m [mn_m]}{I \sum_m n_m}, \tag{1.8}$$

where m is the magnetic quantum number, equal to $-I, -I + 1, \ldots I - 1, I$ and I is the spin number. The electron spins are completely polarized $(P > 99\%)$ for typical conditions of our experiments $(B = 4.6\,\text{T}$ and $T \sim 100\,\text{mK})$, while polarization of the nuclear spins is rather small, $p \simeq 0.1$ (Fig.1.3). An additional parameter, nuclear alignment f_2, should be introduced for describing the energy level occupation for atomic deuterium which has a nuclear spin $I = 1$ [33]:

$$f_2 = \frac{1}{I(2I - 1)} \left(\frac{3 \cdot \sum_m m^2 n_m}{\sum_m n_m} - I(I + 1) \right). \tag{1.9}$$

The super-heavy hydrogen isotope, tritium, is metastable and undergoes β-decay to ^{3}He with a half-life of 12.3 years:

$$\text{T} \rightarrow {}^3\text{He}^+ + e + \bar{\nu}. \tag{1.10}$$

Tritium decay is not accompanied by emission of a γ-quantum and the only possible source of radiation is bremsstrahlung. The decay products along with a ^{3}He$^+$

Figure 1.4: The yields of $\beta-$particles released in tritium decay as a function of their kinetic energy [34].

ion are an electron (e) and an antineutrino ($\bar{\nu}$). Tritium decay is a first-order process:

$$\frac{dN}{dt} = -\lambda N, \qquad (1.11)$$

where $\lambda = 1.782 \times 10^{-9}$ s^{-1} is the probability of a $\beta-$decay per second.

The net kinetic energy of the decay products is $\simeq$18 keV and it is shared by the electron and antineutrino. The recoil energy of the ^{3}He$^+$ ions, $\sim$eV, is much smaller due to a larger mass. The distribution of kinetic energies of electrons released in tritium decay [34] is shown in Fig.1.4. The mean energy of β-particles is $\langle E_K \rangle = 5.7$ keV.

Low decay energy, simple electronic structure and a small nuclear charge make tritium a perfect candidate for measuring the neutrino mass [35]. Tritium as a radioactive material is rather harmless: the β-particles can pass only $\simeq$6 mm in the air while their kinetic energy is not sufficient even for penetrating through the dead outer layer of the human skin.

1.3   Solids of molecular hydrogen isotopes

The solids formed by the hydrogen isotopes represent a special class of the so-called quantum crystals. Due to small masses of particles which form such crystals and their weak interactions, quantum effects have a significant contribution to their properties. The importance of quantum effects was first considered by de Boer

Table 1.1: The main spectroscopic parameters for free H, T, D atoms, and free electrons [36, 37].

	A (MHz)	g_e	I	g_N	$\gamma \equiv g_N \mu_N$ (MHz)
H	1420.405752	2.002284	1/2	5.585695	42.577479
D	218.256235	2.002284	1	0.857438	6.535903
T	1516.701471	2.002284	1/2	5.957925	45.414839
			S		$\gamma \equiv g_e \mu_B$ (MHz)
free electron		2.002319304	1/2		28024.95164

[38] who introduced them as a quantum correction to the law of corresponding states for solids:

$$\Lambda = \frac{h}{\sigma\sqrt{m\epsilon}}, \tag{1.12}$$

where σ and ϵ are the parameters of the Lennard-Jones potential. The de Boer parameter Λ is largest for the lightest solids, ^{3}He (Λ=3.1), ^{4}He (Λ=2.7) [39], and hydrogen isotopes (Table 1.2). As the consequence of the quantum effects, physical properties of molecular hydrogen solids, such as the molar volume, melting temperature or latent heat of vaporization scale according to their de Boer parameters. The Silvera-Goldman potential [2] which accurately describes the interaction between two H_2 molecules has a minimum at the distance σ =3.41Å while the lattice constant of solid H_2 is a =3.79Å. The lattice constant approaches the potential minimum for solid T_2 which has the largest mass among the hydrogens and therefore the smallest amplitude of the zero-point oscillations. The striking decrease of the melting temperature for solid H_2 ($T_m = 13.8$ K) is another consequence of a large amplitude of the zero-point oscillations. Treating H_2 as a classical solid gives an estimate for the melting temperature T_m=25 K [40]. The melting temperature increases with the mass and approaches the classical limit for solid tritium. The data on physical properties of solid hydrogen isotopes are collected in Table 1.2.

The homonuclear hydrogen molecules, H_2, D_2 and T_2, are constructed from indistinguishable atoms and have different spin isomers. The total molecular wavefunction Ψ of a homonuclear molecule is a combination of the electronic wave function $\psi(e)$, rotational $\psi(rot)$, vibrational $\psi(vib)$ and nuclear wave functions $\psi(I)$:

$$\Psi = \psi(e)\psi(rot)\psi(vib)\psi(I), \tag{1.13}$$

it should be either symmetric or anti-symmetric towards permutation of its nuclei. Hydrogen and tritium nuclei are fermions with a spin $I = \frac{1}{2}$ and therefore the total wavefunctions of H_2 and T_2 molecules are anti-symmetric. The electronic wavefunction of H_2, D_2 and T_2 molecules in their ground singlet state, $^1\sum_g^+$, is symmetric, the vibrational wave function depends only on the distance between the atoms and does not change upon their permutation. The nuclear wavefunction

	Λ [39]	hcp lattice a (Å)	fcc lattice a (Å)	V_m (cm^{3}mol^{-1})	T_{tp} (K) [34]
p-H$_2$	1.73	3.79 [2]		23.16 [2]	13.80
n-H$_2$	1.73	3.78	5.31	22.63	13.96
HD	1.41	3.64 [2]	5.18	20.57 [2]	16.60
o-D$_2$	1.22	3.61 [2]		19.95 [2]	18.69
n-D$_2$	1.22	3.60	5.08	19.79	18.73
HT	1.35			20.71* [34]	17.70
DT	1.11			19.29* [34]	19.79
p-T$_2$	1.00	3.47		18.21	20.62

Table 1.2: The main parameters of solid hydrogens [42]: de Boer parameter Λ, the hcp and fcc lattice constants a, molar volumes V_m and the triple point temperatures T_{tp}. The V_m are shown for $T{\to}0$ K. The triple point temperatures for HT and DT are theoretical estimates. *: extrapolation from V_m at melting temperatures.

is anti-symmetric for the even I states and symmetric for the odd ones. The rotational wavefunctions are symmetric for the even $J = 0, 2, 4...$ and anti-symmetric for odd $J = 1, 3, 5...$ [41]. The H$_2$ and T$_2$ molecules in the even J states are characterized by the zero nuclear spins and have $I = 1$ for odd J. The former situation corresponds to the para-state which is the state with the smallest spin degeneracy. The even J states of D$_2$ molecules will also have an even nuclear spin, $I = 0, 2$ (ortho-D$_2$) and an odd, $I = 1$, nuclear spin (para-D$_2$) for the odd J states.

The H$_2$ and T$_2$ gases at 300 K contain $\simeq$75% of ortho-H$_2$ molecules with $I = 1$. Normal D$_2$ at 300 K contains $\simeq$33% of para-molecules with $I = 1$. A transition between the ortho and para states, the so-called ortho-para conversion, is forbidden for isolated molecules but may proceed in solids with a rate of $\leq 1\%$ per hour [2]. The rotational quanta are large, $\Delta E = 170.5$ K for H$_2$ and 86 K for D$_2$, and at low temperatures when only the ground rotational states are occupied, H$_2$ and T$_2$ molecules are in the diamagnetic para-state, while D$_2$ molecules are in the ortho-state where 5/6 of them have a nuclear spin $I = 2$. The heteronuclear molecules constructed from distinguishable atoms, such as HD or HT, are not restricted by the symmetry considerations and do not have spin isomers.

The crystal lattice of solid hydrogen isotopes may vary depending on the ortho-para content and the method the solid was prepared. The solids created by solidifying hydrogen at a saturated vapor pressure always have a hcp lattice. It turned out that the solids condensed from the gas phase much below the triple point tend to have a fcc lattice which is more favorable at temperatures below $\sim$2 K [2]. Both lattice structures have the same packing efficiency, 74%, and every molecule in the lattice site has 12 nearest neighbors. The fcc structure is more symmetric and has only one molecule in the unit cell compared to two molecules per unit cell for the hcp lattice [10].
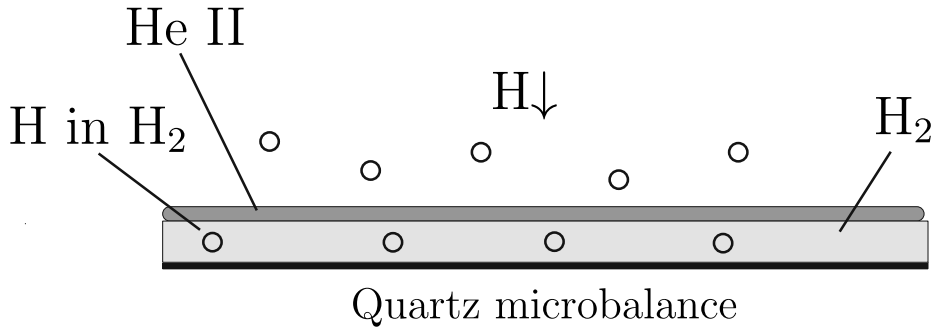
Figure 1.5: Methods for stabilizing H atoms: spin-polarized gas (H↓) and the matrix isolation.

Solid hydrogen does not wet metallic surfaces below its triple point [43] and depositing thin hydrogen films from the saturated vapors results in so-called Stranski-Krastanov growth, when the film appears as a conglomerate of islands connected together by a three-monolayer thick film. The non-equilibrium film deposition of a hydrogen gas onto a cold surface ($\sim$1 K), so-called quench condensing, allows growing smooth thin hydrogen films which turn to bulk polycrystallites after annealing at temperatures $\sim$2.5-3 K for hydrogen and about 4.5 K for deuterium [43, 44].

1.4   Matrix isolation of unpaired atoms of hydrogen isotopes

Unpaired hydrogen atoms are unstable and tend to recombine back to molecules. There are two possible ways to stabilize high concentrations of H atoms: to polarize the electron spins of H atoms in the gas phase (H↓) and suppress their recombination on surfaces [1] or to immobilize H atoms in a solid matrix where their diffusion vanishes [45] (Fig.1.5). The host particles should be inert towards the trapped species and among the most widely used matrices are the solidified noble gases (Ne, Ar, etc.), N_2, and H_2. In our work we consider stabilization of H, D and T atoms in the solid matrices of molecular hydrogen isotopes where unpaired atoms are created *in situ* by dissociating a fraction of host hydrogen molecules using a rf discharge or $\beta-$decay of tritium.

There is a number of methods for introducing H atoms into the matrices of solid molecular hydrogens. It can be carried out either by a co-deposition of the host matrix and unstable radicals [45, 46, 47] or *in situ*, inside an already deposited solid sample by different dissociation techniques such as radiolysis [11], photolysis [48] or by an electron impact [49, 50, 51].

The concentrations of H atoms in solid H_2 created by these methods may vary from 10^{16} to 10^{20} cm^{-3}. The main limitation for stabilizing larger quantities of

unpaired hydrogen atoms is their mobility which leads to a recombination back to molecules when two H atoms encounter each other in neighboring lattice sites. The conservation of energy and momentum does not allow two hydrogen atoms to recombine when they collide in the gas but this restriction is removed in solids where recombination is a two-body process

$$\frac{dn}{dt} = -k^r(T)n^2, \tag{1.14}$$

where n is the concentration of unpaired hydrogen atoms and $k^r(T)$ is the temperature dependent recombination constant. Recombination proceeds in two stages: atomic diffusion and the recombination reaction, H+H$\rightarrow$H$_2^*$. The excess of energy, 4.5 eV, is then transferred to the lattice. The recombination reaction does not have a potential barrier and is considered taking place every time when two hydrogen atoms meet each other in the adjacent sites. The diffusion stage is much slower than recombination and a conventional way to measure the diffusion coefficient for H in H$_2$ is based on finding the recombination rate $k^r(T)$.

The temperature dependence of the recombination rate $k^r(T)$ of hydrogen atoms in solid H$_2$ has two characteristic ranges. The first range corresponds to a thermally activated (classical) diffusion which is related to the formation of vacancies in the lattice. This type of diffusion dominates at temperatures above $\sim$5 K for H in H$_2$ and above $\sim$9 K for D in D$_2$ [50, 52]. The activation energies found experimentally for H in H$_2$ [50], E_a=195 K, match the energy for formation of a vacancy in the para-H$_2$ matrix calculated theoretically [53]. The activation energies for heavier matrices, D$_2$ and T$_2$, are E_a=276 K and E_a=411 K, respectively [54].

A stark difference in the temperature dependence of the recombination rates appears at lower temperatures when the atoms do not have enough energies to surmount the potential barrier and the quantum diffusion based on tunneling starts playing a major role. There are two different views on quantum diffusion of H atoms in H$_2$: physical diffusion related to exchanging positions of H atoms and neighboring H$_2$ molecules similar to that of ^{3}He in ^{4}He and a repetition of the tunneling exchange reactions (chemical diffusion)

$$\text{H+H}_2 \rightarrow \text{H}_2\text{+H} \tag{1.15}$$

$$\text{D+D}_2 \rightarrow \text{D}_2\text{+D.} \tag{1.16}$$

Physical diffusion is related to formation of a free volume for a diffusing particle and its rate should strongly depend on pressure. This was observed for diffusion of ^{3}He in ^{4}He [55]. However, such dependence is not expected for the rates of chemical diffusion. The recombination rates measured experimentally up to 130 bars [12] did not depend on pressure which brought evidence that exchange reaction (1.15) is the main mechanism for diffusion of H in H$_2$ at temperatures $\leq$5 K.

The theory of quantum diffusion in irregular solids was developed by Kagan and co-workers [22, 56, 57]. Diffusion may be presented as a two potential well problem where the transmission coefficient for diffusion has a maximum when the initial and final tunneling states coincide and it vanishes upon the level mismatch. The former case corresponds to a perfect H_2 crystal and the latter case is relevant to an irregular matrix with a significant number of lattice defects and impurities.

Tunneling of a light impurity through a periodic potential of the matrix proceeds within a certain energy band associated with the tunneling probability. The impurity becomes localized in a lattice site if the energy level mismatch is larger than the width of a such energy band. The localization can be removed by phonons which may compensate for the level mismatch. The diffusion coefficient of a particle in an irregular crystal can be characterized by the number of phonons involved. The recombination rate of H atoms in solid H_2 is proportional to T for temperatures $1 < T < 4$ K which is a consequence of a direct process when a single phonon compensates for the mismatch [58]. The situation is different for D in D_2 where the recombination coefficient is proportional to T^9 for $7 < T < 9$ K and becomes almost independent of temperature below 4 K. The T^9 dependence corresponds to the Raman process when two phonons are involved [52]. The diffusion coefficient of H atoms in H_2 is usually extracted from the measurements of the recombination rate of atoms. However the motion of H atoms slows down dramatically when they approach each other due to the level mismatch they impose. Measuring a pure diffusion rate not related to recombination is challenging and still has not been carried out experimentally.

A peculiar dependence of the recombination rate of H in H_2 on temperature was observed below 1 K in the recent works of the group in Turku [23, 28]. It turned out that the recombination rate decrease followed a power dependence much stronger than $\sim T$ as it is prescribed by theory. Finally recombination became immeasurably small at $T = 150$ mK. Similar effects might also be expected for deuterium. The situation is different for tritium atoms where the β-decay results in a creation of non-equilibrium phonons and vacancies. Due to a larger mass and smaller mobility, tritium atoms can be accumulated to higher concentrations compared to H and D. However, this ends up in a collective recombination of atoms in tritiated samples where recombination heat triggers sample overheating and explosive recombination [30].

1.5   Magnetic resonance of atomic hydrogen

Hydrogen atoms have non-zero electron and nuclear spins and can be studied by the methods of magnetic resonance. When the oscillating magnetic field is swept through the Larmor frequency of spin precession, ω_0, the spin system absorbs power of the mm-wave field which is proportional to the square of the oscillating field amplitude H_1 [59, 60]:
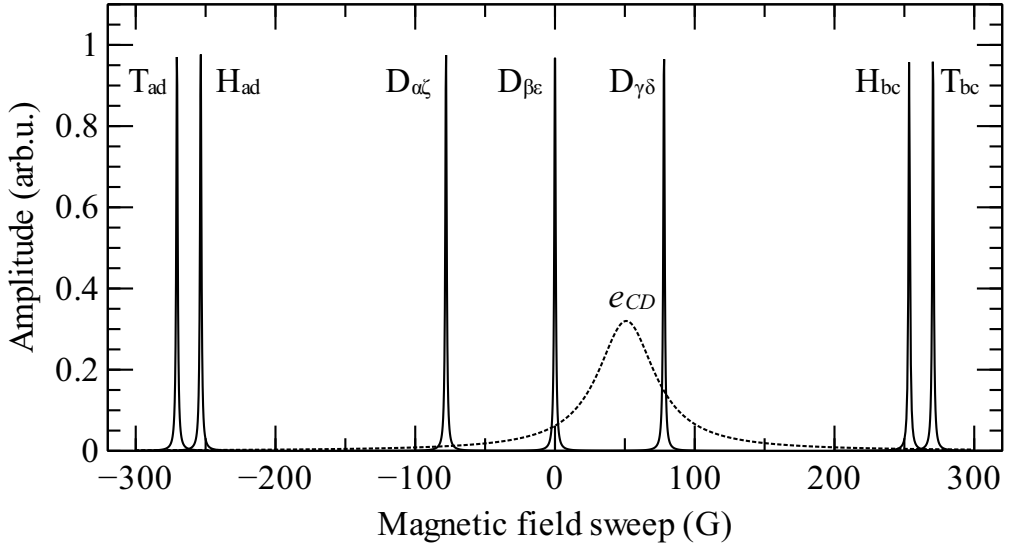
Figure 1.6: A modeled ESR spectrum for unpaired H, T and D atoms. The line from cyclotron resonance of free electrons labeled e_{CD} is shifted from the center of the spectrum by $51\,\mathrm{G}$ in magnetic field $B = 4.6\,\mathrm{T}$. The forbidden transitions are not shown (high-field limit).

$$P = \frac{1}{2}\omega_0 H_1^2 \chi^{''}, \qquad (1.17)$$

where $\chi^{''}$ is the imaginary part of the mm-wave complex susceptibility (absorption), $\chi = \chi' + j\chi''$, which may be related to a number of spins in the sample. Absorption of energy by the spin system may be viewed as an additional source of reducing the cavity quality factor Q,

$$1/Q = 1/Q_u + 1/Q_\chi, \qquad (1.18)$$

where Q_u is the quality factor of the unloaded cavity, i.e. due to resistive and radiation losses, and Q_χ includes the losses due to absorption of the mm-wave power by the sample. If $\chi^{''}$ is uniform through the sample volume, it can be considered as the ratio of the energy stored in the cavity to that absorbed by the sample:

$$Q_\chi = \frac{\int_{cavity} H_1^2 dV}{\chi^{''} \int_{sample} H_1^2 dV}. \qquad (1.19)$$

In addition to absorbing mm-wave power, the interaction of spins with the oscillating field also changes the cavity frequency. This contribution is related to a real component of the complex susceptibility, $\chi^{'}$ (dispersion). The frequency change can be estimated from the change of the velocity of an electromagnetic wave in

the resonator [59]:

$$v = \frac{1}{(\mu\epsilon)^{1/2}} = \lambda f,$$

where ϵ is a dielectric constant and $\mu = \mu_0(1 + \chi)$ is magnetic permeability. The wavelength λ is fixed in the resonator by its physical dimensions. When the susceptibility changes by the amount $\Delta\chi$, and the absorption losses are small, $\Delta\chi'' = 0$, the cavity frequency will shift:

$$\Delta f = \frac{1}{\lambda(\mu_0\epsilon)^{1/2}}[\frac{1}{(\chi')^{1/2}} - \frac{1}{(\chi' + \Delta\chi')^{1/2}}]. \tag{1.20}$$

At the resonance both imaginary and real components of the susceptibility are changed. Absorption and dispersion are related to each other through the Kramers-Kronig relations [59]. The ESR lines may be adjusted to have either an absorption or a dispersion-like shape by changing the effective length of the transmission line before the cavity by a phase shifter.

The sensitivity of methods of magnetic resonance depends on the difference in the population of the energy levels (Fig.1.2) which obeys the Boltzmann distribution. Much smaller energy level splitting for the NMR transitions results in much poorer sensitivity of this method compared to ESR and in many cases does not allow using it directly.

The modeled ESR spectrum for all three atomic hydrogen isotopes is shown in Fig.1.6. The hydrogen spectrum contains two hyperfine lines of the allowed $a - d$ and $b - c$ transitions which are separated by ΔB=507 G, while the deuterium spectrum consists of three ESR lines separated by $\Delta B \simeq 78$ G. The tritium spectrum also contains two lines which are separated by ΔB=541 G. The center of the spectrum, $g = 2.002284$, nearly coincides to the position of the ESR signal of free electrons possessing the g-factor $g_e = 2.002319$ (Table 1.1). The e_{CD} is a cyclotron resonance line of free electrons with g=2. The relative position of this line depends on magnetic field and in our field, $B = 4.6$ T, it is shifted from the center of the ESR spectra by $\Delta B = 51$ G. The widths of the ESR lines of hydrogen isotopes in Fig.1.6, 1.2 G, are equal to those caused by the dipolar interaction of atoms in solid films at their concentration $n \simeq 10^{19}$cm^{-3}. The effects of the matrix on the linewidth are not taken into account.

Chapter 2

Experimental setup

A description of the experimental setup and the sample cell (SC) will be given in this section. The sample cell was used with minor changes in all experiments described in the thesis. The design is partially based on the cells used in previous works of the Turku group [28, 51]. While working on a new design we had two main goals and motivations. First we aimed on developing a method for depositing thin and smooth films of hydrogen isotopes in a controllable manner. For this reason we elaborated a technique of molecular beam deposition where the solid films of hydrogen isotopes are formed by depositing molecules with low kinetic energies which significantly improves the film uniformity. We deposited our films onto a top gold electrode of the quartz-crystal microbalance (QM) which also played a role of the flat mirror of the ESR resonator. This allowed both measuring the mass of the deposited film and recording the ESR signals of unpaired atoms. The QM can also detect onset of possible quantum phenomena related to the non-classical inertia of the sample [18]. At second, the sample cell we designed makes it possible to use the most efficient methods for *in situ* dissociation of molecules in hydrogen films: the techniques of a cryogenic rf discharge and dissociation of molecules by electrons released in β-decay of tritium.

The setup is based on a dilution refrigerator and allows studying very slow chemical processes with the characteristic times of weeks. The design and performance of the experimental cell are presented in paper [P1].

2.1   Sample cell

The experimental setup is based on an Oxford 2000 dilution refrigerator which accommodates the sample cell and a 128 GHz ESR spectrometer. The sample cell (Fig. 2.1) is attached to the mixing chamber of the refrigerator for providing sufficient cooling. The minimum SC temperature achieved in the experiments described in the thesis is $\simeq 70$ mK.

The ESR resonator has a Fabry-Perot open design (FPR). This gives an ad-

Figure 2.1: The sample cell schematic. The helical resonator used for electron-nuclear double resonance (ENDOR) of H atoms is labeled HNMR. The resonators used for measuring ENDOR spectra of D and T are not shown.

vantage of arranging auxiliary rf resonators in a close proximity to the sample and installing capillaries for condensing molecular hydrogen films without distorting mm-wave field in the cavity. The condensing capillaries are directed at the center of the flat mirror of the ESR resonator which also acts as a top electrode of the quartz-crystal microbalance (QM). The lines come from special chambers arranged at the top of the SC and connected to the main cell volume through stainless steel tubing. A small, ∼mmol, amount of hydrogen gas is condensed into the chamber in advance and can be either recondensed onto the surface of the quartz microbalance or used for producing a flux of atomic hydrogen gas when the rf discharge is run there.

The main difficulty in working with thin solid hydrogen films appears from

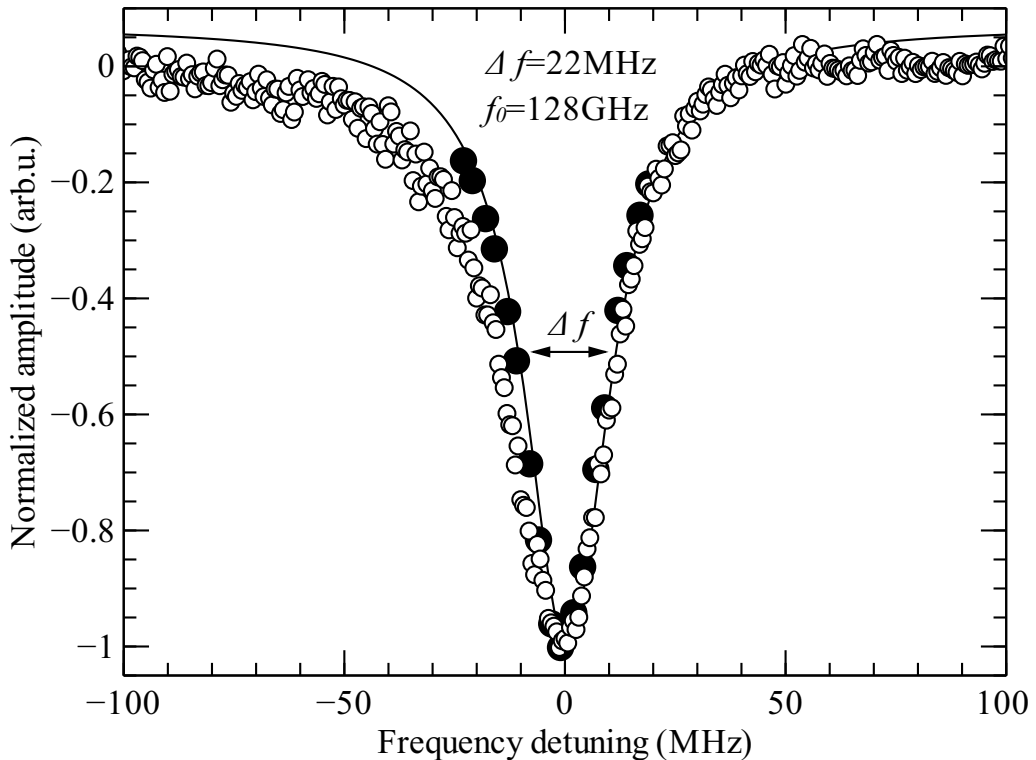Figure 2.2: The ESR resonator curves measured at 300 K (open circles) and 300 mK (filled circles). The cavity width (22 MHz) at 300 mK is determined from the ESR signal of H atoms in solid H_2 upon detuning from the FPR resonance frequency [P1].

non-wetting of metal surfaces below the triple point. The sample cell design allows depositing solid hydrogen films in two different ways: by recondensing solid hydrogens from the sublimation sources or depositing them directly from the room temperature gas handling system. A certain limitation of the first method is an uncertainty in the film composition after recondensing onto the QM. The lighter hydrogens have higher vapor pressures and tend to sublimate first from the source. This results in a larger admixture of lighter isotopes in solid films of heavier hydrogens than expected from the gas composition provided by the manufacturer. We used the first method for creating pure solid films of light isotopes: H_2 and HD while the second technique was employed for depositing pure solid D_2, T_2 and mixture films. The condensing capillaries are heated above melting points of molecular hydrogens (Table 1.2) when the gases were loaded into the sublimation sources or condensed from room temperature directly onto the QM surface.

The main investigation tool in our work is the 128 GHz ESR spectrometer. Its mm-wave block is anchored to the 1 K-pot of the dilution refrigerator and con-

Figure 2.3: The long-term QM-frequency stability at $100\,\mathrm{mK}$ [P1].

Figure 2.4: The gas line of atomic hydrogen a) in an optimized magnetic field gradient and b) after applying a gradient $L_z{=}16\,\mathrm{G/cm}$.

nected to the resonator via a waveguide. The ESR spectrometer is similar to that developed in Turku for experiments with atomic hydrogen gas [61]. It employs a superheterodyne detection scheme and has a sensitivity $\sim 10^{10}$ spins using excitation power $\sim$pW. The maximum mm-wave power available for measurements is of the order of a μW. The flat mirror of the Fabry-Perot resonator also serves as a

18

top electrode of the quartz-crystal microbalance which allows both to study the samples by ESR and determine their mass by the QM. The ESR resonator has a Q-factor of 4700 at room temperature and 5800 at $T =$300 mK (Fig.2.2). Once the setup is closed and the SC is cooled down, there is no possibility to change the FPR frequency. Therefore, in order to measure the cavity resonance curve we used the ESR signal dependence on the cavity detuning. The result of such measurement is presented in Fig.2.2, where the strength of the ESR lines of H atoms in a solid H_2 matrix is plotted as a function of the excitation frequency. The resonator frequency is adjusted at room temperature using a set of tuning screws which allow moving the top mirror within $\pm$1 mm. This ensures the tuning range $\sim$5 GHz and provides a possibility of selecting different resonator modes. In the current work, the TEM_{005} and TEM_{006} modes were used. The distribution of mm-wave field in the cavity can be probed by measuring the H-gas lines in a magnetic field gradient. The sample occupies the whole cell volume and each ESR maximum corresponds to a node of the standing wave (Fig.2.4). A high homogeneity of the static magnetic field in the sample cell was carefully ensured by accurate shimming. The currents in the shim coils were adjusted in order to achieve the smallest width of the ESR line of H atoms in the gas phase. We were able to decrease this width to about 100 mG which can also be considered as the upper limit for magnetic field inhomogeneity over the samples of H in H_2. Applying the magnetic field gradient we were also able to distinguish the signals from different mirrors of the Fabry-Perot cavity.

The quartz microbalance we used operates in the shear mode at the fundamental frequency $f \approx$10 MHz. The quartz disc has a diameter of 11 mm and a thickness of 0.5 mm. Two 400 nm thick gold electrodes were sputtered in order to excite acoustic oscillations in the crystal. We also sputtered thin ($\sim$15 nm thick) intermediate copper layers for providing better adhesion of gold to the quartz surface. The microbalance fundamental frequency reduced to $\simeq$9.7 MHz after sputtering of the electrodes. The thickness of the gold electrodes, 400 nm, was chosen to exceed the skin depth at 128 GHz, $\simeq$100 nm, and make the mirror opaque for the mm waves.

The QM oscillation frequency is related to the deposited mass through the Sauerbrey equation [62]:

$$\Delta f = \frac{2f^2}{n\sqrt{\rho_Q \mu_Q}} m_f ,$$

where Δf is the frequency change, n is the harmonic number, $\rho_Q=$2.65 g/cm^3, $\mu_Q=$2.947$\times 10^{11}$ g s^{-2}cm^{-1} is the quartz shear modulus, m_f is the surface density of the deposited substance. Depositing a monolayer of H_2, 9.2$\times 10^{14}$ molec cm^{-2}, shifts the QM frequency by $\simeq -$ 0.7 Hz (at the first harmonic). The QM operation was also checked at the third harmonic ($f \simeq$ 29.1 MHz) where the mass sensitivity is three times higher. The $Q-$factor of the microbalance was $\sim 10^4$ at the fundamental mode, and it did not change after depositing a 10 μm thick H_2 film,
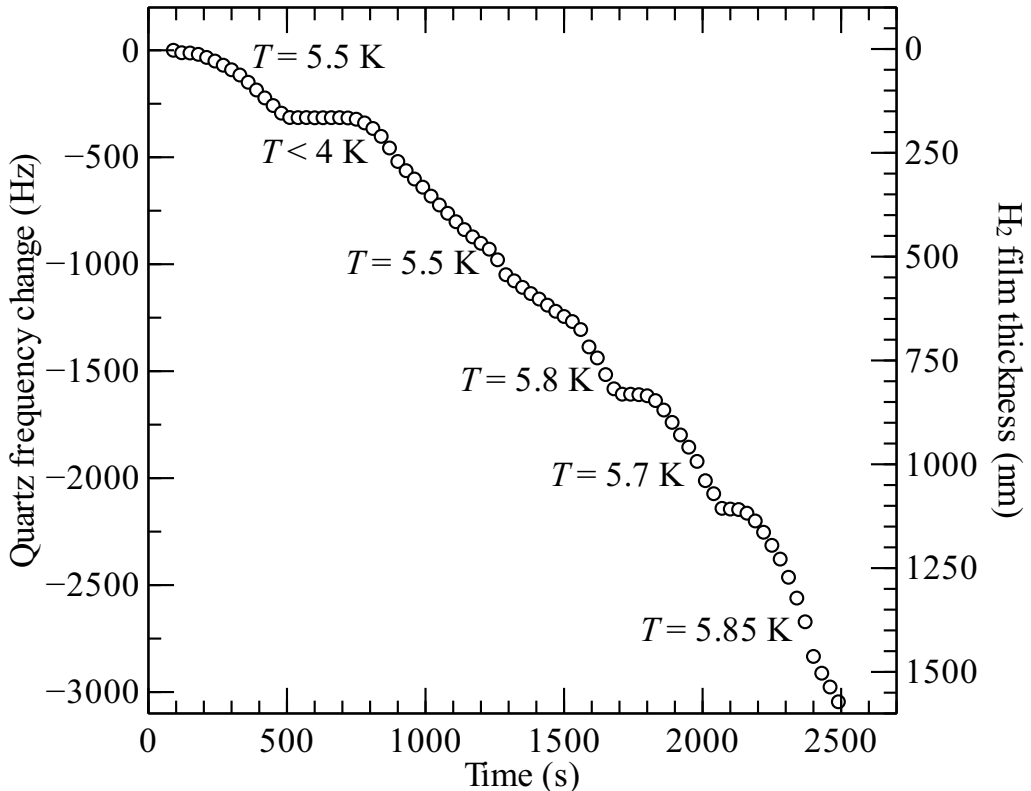
Figure 2.5: Dependence of the QM frequency on time at different temperatures of the sublimation source during H_2 deposition [P1].

the thickest film we studied. The QM mass sensitivity was estimated by measuring its frequency stability (Fig.2.3). Based on the short term stability (0.4Hz at the 3rd harmonic over three hours of measurement), we determine the QM mass sensitivity as $\simeq$0.2 monolayers of H_2.

Three additional resonators were installed near the QM to run the rf discharge in the cell and excite the NMR transitions of H, D and T atoms. Two of them are helical quarterwave resonators tuned to the $a - b$ transitions of H and T, f=910 MHz and 970 MHz respectively. They are inductively coupled to the coaxial line and grounded at one end. The third resonator is a Helmholtz-type coil tuned to $f \simeq$140 MHz, the $\alpha-\beta$ and $\beta - \gamma$ transitions of D atoms. The coil resonance frequency is adjusted using a varactor-tuned resonance circuit similar to that described in ref. [63].

We paid a special attention to assure a proper cooling of the QM during the film deposition. It becomes even more critical when working with solid tritium films where the heat released in β-decay may increase the sample temperature and stimulate recombination of atoms. A special volume was constructed under
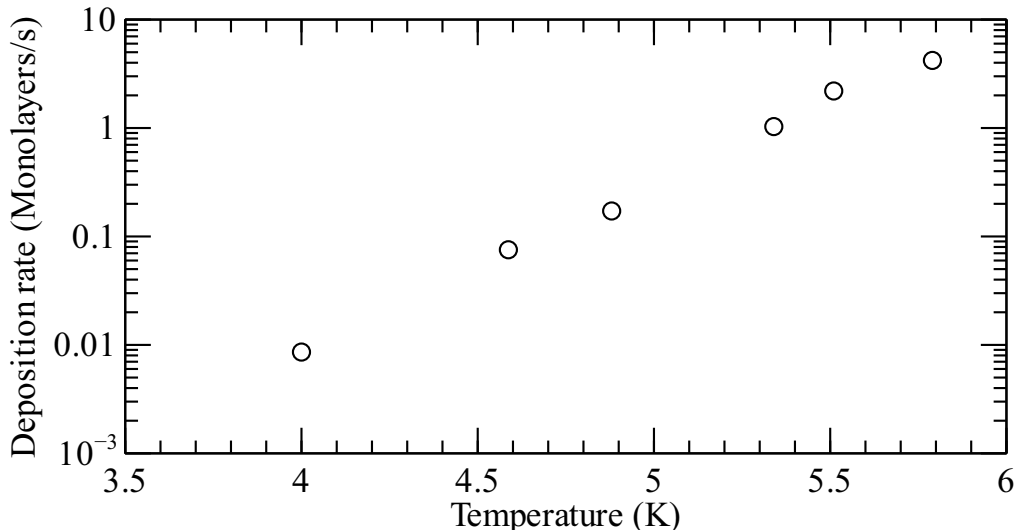
Figure 2.6: The rates of depositing H_2 as a function of the sublimation source temperature [P1].

the QM where a small amount, $\sim$mmol, of He was condensed in order to have a saturated superfluid film. The film flushes the quartz disc and removes the excess of heat from the sample.

A small amount of helium ($\sim 4\,\mu$mol) was condensed into the sample cell in order to start the rf discharge there. This method was initially developed for producing the gas of spin-polarized hydrogen [64] and used later by the Turku group for accumulating H atoms in solid H_2 [51]. The electrons produced during the discharge have energies $\sim 100\,$eV [51] which turned out to be sufficient to pierce the superfluid helium film and dissociate H_2 molecules in the film.

The performance of the sublimation source for condensing a solid H_2 film is shown in Figs.2.5 and 2.6. Heating the sources to temperatures 4-6 K for H_2 or 7-10 K for D_2 makes it possible to vary the condensing rate within $\sim$0.01-10 monolayers per second. The quartz microbalance temperature is kept at 0.7-1.5 K which assures the deposition of smooth and homogeneous hydrogen and deuterium films.

The calibration of an absolute number of spins in the samples was carried out by measuring the width and shift of the ESR lines of unpaired atoms in the films from the position of the H and D gas lines [23, 51]. The fluxes of spin-polarized hydrogen and deuterium gases were created by running the rf discharge in the sublimation sources. The second calibration method is based on finding a correspondence between the heat released in recombination of the atomic hydrogen gas and the decrease of the H↓ ESR line areas (see ref. [65] for details). It was found that both methods coincide within about 20%.
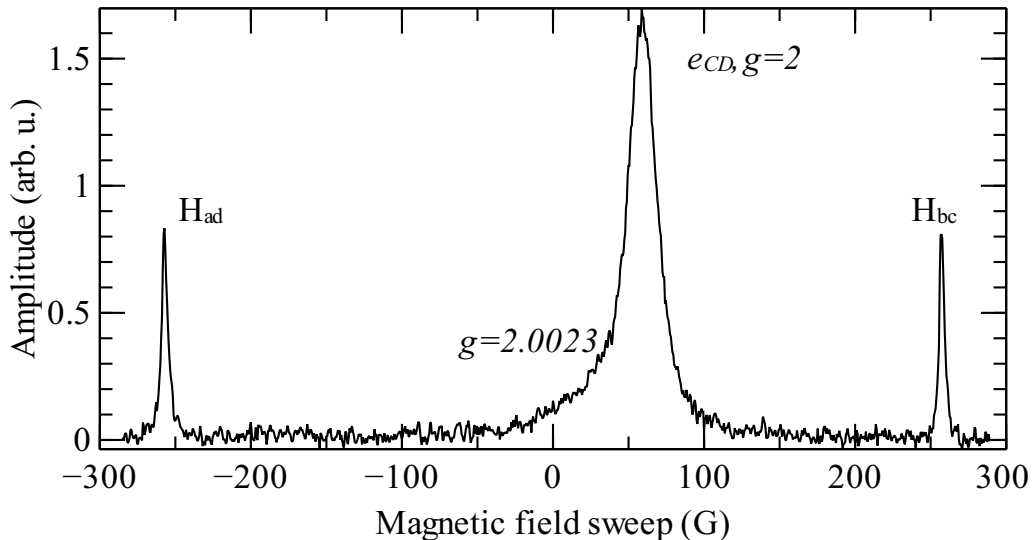
Figure 2.7: The ESR spectrum of H atoms in solid H_2 measured in the process of running the discharge in the sample cell. The cyclotron line of free electrons is labeled as e_{CD}.

2.2 H_2 dissociation in solid films by electron impact

Finding methods for increasing the concentrations of unpaired H atoms in solid hydrogen films was one of the main goals of this work. We tried different approaches for accumulating high concentrations of unpaired atoms in the matrices of hydrogen isotopes: running a cryogenic rf discharge in helium vapors and admixing β-radioactive tritium to the gas before condensing. An additional source of H atoms appears in solid mixtures of D_2 and H_2 (HD) where D atoms become converted into H due to the isotopic exchange reactions $D+H_2 \rightarrow HD+H$ and $D+HD \rightarrow D_2+H$, although the total concentration of unpaired atoms in the film, [H]+[D], is conserved.

Both methods, the discharge and admixing tritium gas, are based on dissociation of hydrogen molecules in the films by electron impact. The main difference is the mean energies of the electrons which dissociate the molecules. The energies of the electrons generated in the cryogenic rf discharge were previously estimated to be of the order of 100 eV [23], while the mean energy of the β-particles released in the decay of tritium is 5.7 keV. Direct dissociation of H_2 molecules into two atoms proceeds via exciting the molecules to the repulsive triplet state [66]. This process has a maximum cross-section at the electron energy $E=16.5$ eV and then rapidly decreases at higher energies [67]. At electron energies $\sim$keV, ionization of molecules, $H_2 \xrightarrow{e} H_2^+ + e$, is the most basic process. The H_2^+ ions are unstable and react with the H_2 molecules to form H_3^+ ions and unpaired H atoms,

Figure 2.8: The ESR signal increase as the function of the H_2 film thickness.

$H_2^+ + H_2 \rightarrow H_3^+ + H$. The latter ion is stable, but may recombine with an electron, $H_3^+ + e \rightarrow H_2^* + H \rightarrow 3H$ [34].

At the preliminary stage, we analyzed the efficiency of the accumulation of atoms by running the discharge as a function of the hydrogen layer thickness. An estimate of the penetration depth of electrons generated during the discharge was carried out in a few steps of depositing H_2 layers and accumulating H atoms. First we deposited a thin, 10 nm thick hydrogen film, created atoms there by running the discharge and then deposited a twice thicker film on the top of the existing film and the discharge was run once again (Fig.2.8). This procedure was repeated several times. The dependence of the ESR signal area as a function of the layer thickness is shown in Fig.2.8. The area of the ESR line of H in H_2 rose monotonically with the film thickness. We estimate the penetration depth of electrons generated by the discharge into H_2, $\lambda \sim 80$ nm. However, this measurement is influenced by a possible diffusion of H atoms during dissociation which may be stimulated by the phonons generated by the discharge. Taking into account possible diffusion we conclude that the value of λ reported should be considered as an upper limit estimate of the electron penetration depth. The 5.7 keV electrons released in tritium decay are expected to have a much larger penetration depth, $\simeq 3.5\,\mu$m [68].

Chapter 3

Hydrogen atoms in solid molecular matrices of hydrogen isotopes

The results of measuring the main spectroscopic parameters and the ESR line broadening and shift for H, D and T atoms in solid matrices of hydrogen isotopes will be discussed in this chapter. Our results on studying electrons trapped in the matrix are also surveyed. The results discussed in this chapter are published in papers [P1], [P3] and [P6].

3.1 Hyperfine constant change

The value of the hyperfine constant for a free hydrogen atom, A, (Table 1.1) is known with a high precision due to its special importance. The hydrogen maser operates at the low field $F = 1_{m_F=0} \to F = 0_{m_F=0}$ transition which frequency nearly coincides with the value of A for free atoms [69, 70]. This transition is also known as the 21 cm hydrogen line and it plays a special role in astronomy [71].

When a H atom is introduced into a solid matrix, interaction with the neighboring matrix molecules may modify both its hyperfine constant and the electron g-factor. The hyperfine interaction of the electron and nuclear spins of a hydrogen atom contains only the contact term and is defined by the probability of finding the electron at the nucleus. The interaction with the electron clouds of atoms of neighboring molecules may either increase or decrease this probability [72]. The former appears at short distances when the electron cloud of a H atom starts overlapping with the electron clouds of adjacent atoms. The Pauli repulsion in this case tends to contract the electron cloud of the H atom according to the exclusion principle. This increases the value of A for H atoms trapped in the matrix. At longer distances, the attractive van der Waals interaction slightly expands the electron cloud of unpaired atom and the A constant decreases. The former contribution

	Matrix	Our work		Literature		
		A (MHz)	$\Delta A/A$ (%)	A (MHz)	$\Delta A/A$ (%)	Ref.
H	H_2	1417.40(2)	-0.212	1417.34	-0.216	[51]
				1419.09	-0.093	[28, 51]
	D_2	1417.30(2)	-0.219			
	T_2	1417.18(2)	-0.227			
D	D_2	217.73(1)	-0.239	217.71	-0.250	[75]
				217.62	-0.291	[76]
T	T_2	1512.60(2)	-0.270	1515.3	-0.092	[49]
T	D-T			1532	1.009	[77]

Table 3.1: The values of the hyperfine constant A for H, D and T atoms in solid matrices of hydrogen isotopes measured in our work (para-H_2, ortho-D_2 and normal T_2 matrices) and in previous works (normal H_2 and D_2 matrices). D-T is a solid mixture of 50% DT, 25% D_2 and 25% T_2.

prevails when the atoms are stabilized in the matrix in the interstitial positions while the latter takes over for atoms occupying substitutional lattice sites. Thus, the sign of the hyperfine constant change depends on the trapping positions and becomes negative for the substitutional sites and positive for the interstitials [72]. There is no spin-orbit interaction associated either with the H atoms or with the H_2 molecules and stabilizing H atoms in H_2 matrices does not change the electron g-factor. However, such change may take place in matrices where the host particles have p electrons, for example solid argon [72]. Very small polarizabilities of H atoms and H_2 molecules which define the van der Waals contribution cause only a modest change in the hyperfine constant of H atoms in the hydrogen matrices.

Li and Voth showed [73] that hydrogen atoms cannot be stabilized in the interstitial sites of the H_2 matrix due to a so-called self-annealing effect which is caused by a strong repulsion between a H atom and a H_2 molecule at short distances. This repulsion exceeds a weak H_2-H_2 bond and causes a rearrangement of H_2 molecules around the H impurity which after all resides in a substitutional position. The short-distance repulsion is similar for all three H isotopes while the bond strength differs slightly for different molecular hydrogens. Therefore similar self-annealing effect should be expected for heavier hydrogen systems, such as D in D_2 and T in T_2. It also turned out that H atoms being stabilized in the substitutional positions push the surrounding matrix molecules by the distance of ~ 0.15 Å [74] due to a large amplitude of the zero-point oscillations.

We carried out accurate measurements of the hyperfine constants for all three hydrogen isotopes using the electron-nuclear double resonance (ENDOR) technique [78]. It is based on detecting the NMR transition frequency indirectly, by its influence on the ESR line intensity while sweeping the rf excitation in the vicinity of the NMR transition. The widths of the NMR transitions are a factor

of $\frac{g_e \mu_B}{g_N \mu_N}$ narrower than the ESR lines and it is possible to extract the values of A with almost three-order better accuracy compared to the estimate obtained from the ESR spectrum measuring the distance between the ESR lines.

We recorded the ENDOR spectra of H atoms using the lower, $a - b$, NMR transition. Prior to that, non-equal population of the lower hyperfine levels should be established. The first method of doing this is based on saturating the ESR line. This approach was employed in the original work of Feher [78] who used ENDOR for measuring the hyperfine constants of phosphorus donors in silicon. The second way, which we used in our work, relies on creating a large population difference between a and b levels via the Overhauser effect. The $a - b$ NMR transition frequency for H atoms:

$$f_{a-b} \simeq g_H \mu_H B + \frac{A}{2} \,. \tag{3.1}$$

The ENDOR spectra of H measured in different matrices of hydrogen isotopes are shown in Fig.3.1. In all cases we observed a negative shift of the ENDOR transition compared to the NMR frequency of free atoms, as expected for the substitutional positions of atoms in the matrix. It turned out that the hyperfine constant change of H atoms is slightly smaller in the lightest H_2 matrix compared to those in D_2 and T_2. The T_2 matrix has the smallest lattice constant and the smallest amplitude of the zero-point oscillations. The H_2 matrix has the largest lattice constant among the hydrogens and the H_2 molecules tend to push H atoms more efficiently due to the larger amplitude of the zero-point oscillations compared to D_2 and T_2 and A appears to be closer to that of free atoms. The values of the hyperfine constants, A, for H, D and T atoms in different solid matrices of hydrogen isotopes are summarized in Table 3.1.

The hyperfine constants were also measured for D atoms in solid D_2 and for T in T_2. For measuring the hyperfine constant of D atoms we created the population difference between all three lower hyperfine levels using the Overhauser effect in such a way that $D_\alpha < D_\beta < D_\gamma$. After that, we stopped the magnetic field sweep at the peak of the second ESR line of D corresponding to the $\beta - \epsilon$ transition. Then we applied an rf field to the NMR resonator tuned to the D resonance (see Fig.2.1), and swept its frequency around the expected resonance position (Fig.3.2). The frequencies of both NMR transitions for D atoms can be calculated as

$$f_{\alpha-\beta} \simeq g_D \mu_D B + \frac{A}{2} \tag{3.2}$$

$$f_{\beta-\gamma} \simeq g_D \mu_D B + \frac{A}{2} + \frac{9}{16} \frac{A^2}{(g_e \mu_B + g_D \mu_D)B} \,, \tag{3.3}$$

where g_D and μ_D are the $g-$factor and the magnetic moment of a D atom (Table 1.1). The ENDOR transition frequencies measured experimentally: 138.98 MHz and 139.16 MHz are smaller than the transition frequencies for free D atoms: D$_{\alpha-\beta}$=139.24 MHz and D$_{\beta-\gamma}$=139.43 MHz. We calculated the values of A_{DinD_2}
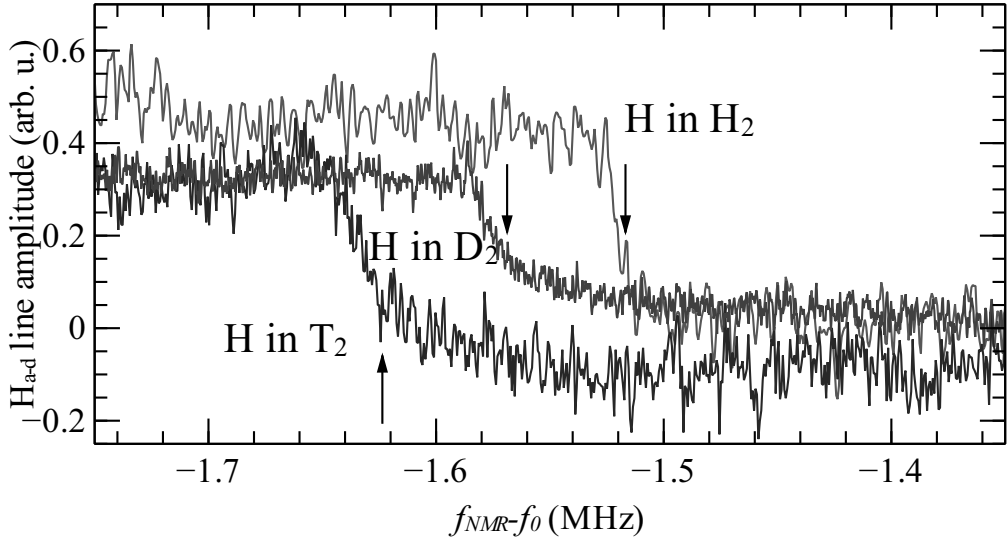
Figure 3.1: The ENDOR spectra of H atoms in different solid matrices of hydrogen isotopes. The $a - b$ transition frequency for free H atoms is labeled as f_0 [P6]. The resonance positions are marked by arrows.

from both transitions, A_{DinD_2}=217.737 MHz $(\alpha - \beta)$ and 217.733 MHz $(\beta - \gamma)$, which coincide within the measurement error. These results are in a good agreement with the values presented in literature [75]. The values of A_{DinD_2} extracted from both transitions differ only by $\leq$10 kHz which provides evidence that the transitions we observed correspond to atoms in the equal lattice sites. The mean value of the hyperfine constant of D atoms in solid D_2, A_{DinD_2} =217.73 MHz, is smaller compared to A =218.26 MHz for free D atoms (Table 1.1) which leads us to a conclusion that D atoms in solid D_2 reside in the substitutional lattice sites. The relative hyperfine constant change, $\Delta A_D \simeq -0.24\%$ is very similar to that of unpaired atoms of hydrogen isotopes in the other solid hydrogen matrices found experimentally in the present work and previously by other authors [46, 51, 75], and calculated theoretically by Adrian [72].

A similar study was also conducted for T atoms in a solid T_2 matrix (Fig.3.3). The frequency of the $a - b$ transition for tritium can be found using equation (3.1) as for hydrogen, but it is somewhat higher due to the larger hyperfine constant and gyromagnetic ratio of T atoms (Table 1.1). A large population difference between a and b levels $(a > b)$ in this case was also prepared by the Overhauser effect. The $a - b$ transition frequency appeared to be $\simeq$2.08 MHz lower than that calculated for free tritium atoms. Based on that we estimate the change of the hyperfine constant for T atom in solid T_2 as $\Delta A = -4.10$ MHz. A relative change, $\frac{\Delta A}{A} = -0.27\%$, is also in a good agreement with the other hydrogen matrices.

We observed only one ENDOR transition for all three hydrogen isotopes in all
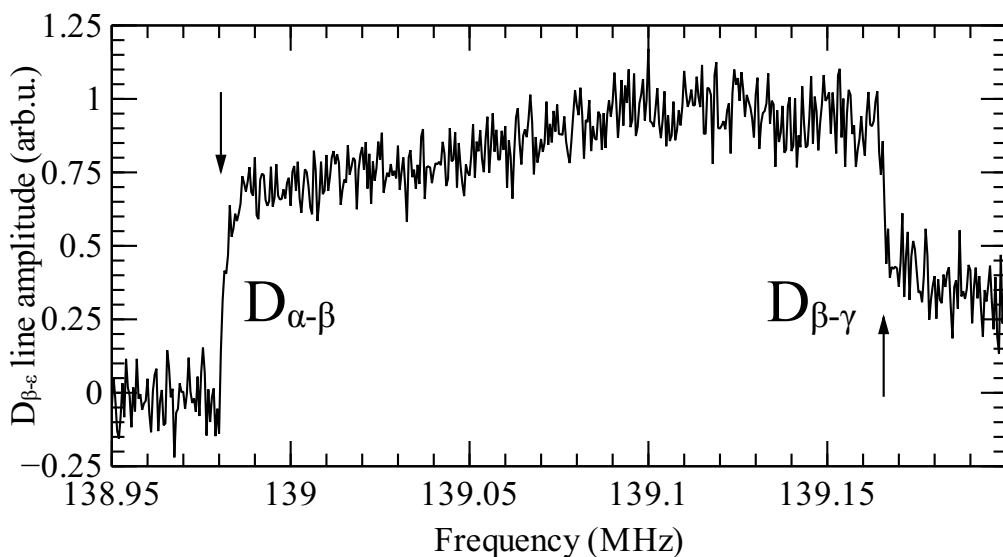
Figure 3.2: The ENDOR spectrum of D atoms in solid D_2. Two ENDOR features correspond to the $\alpha - \beta$ and β-γ transitions. The resonance positions are shown by arrows.
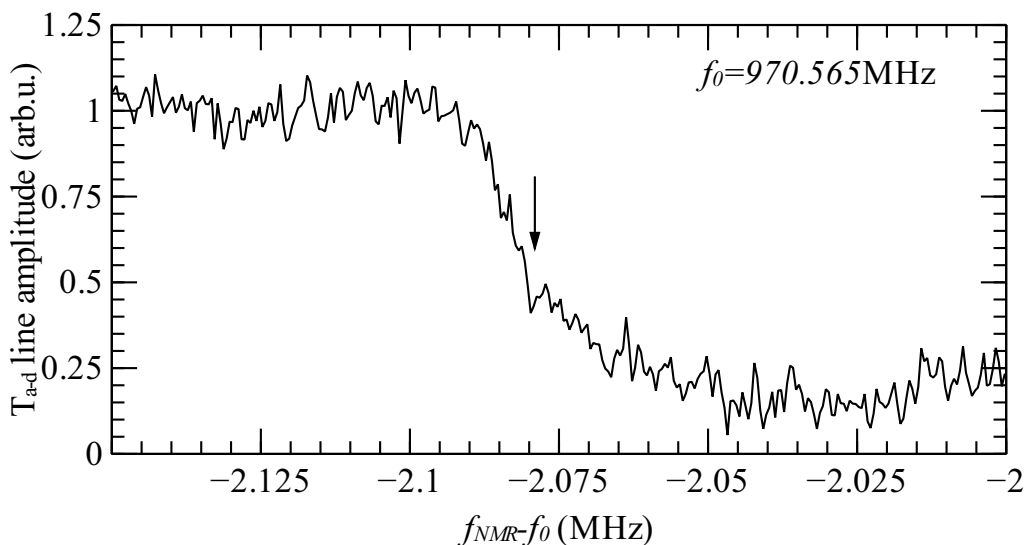

Figure 3.3: The ENDOR spectrum of T in solid T_2. The $a-b$ transition frequency for free T atoms is labeled as f_0 [P6]. The resonance position is marked by arrow.

Literature			Our work	
Matrix	Width (G)	Ref	Matrix	Width (G)
n-H_2	1.2	[79]	p-H_2	0.4(1)
p-H_2	0.34	[80]	o-D_2	1.3-2
p-H_2 (theory)	0.34	[73]	HD	2.9-3.4
n-D_2	1.3	[46, 80]	D_2:H_2 (3:1)	2.1(3)
HD	2.7-3.3	[79, 80]	D_2:HD (1:1)	2.5(3)
D-T	3.4-3.7	[79]	T_2:HT (5:1)	4.6(5)
T_2	2.4	[79]		

Table 3.2: The zero-concentration (matrix) widths of the ESR lines of unpaired atoms measured in solid matrices of hydrogen isotopes. D-T should be understood as a solid mixture of 25% D_2, 25%T_2, 50%DT.

hydrogen matrices we studied. Based on that we conclude that unpaired atoms of hydrogen isotopes occupy substitutional lattice sites in all solid hydrogen matrices. Two ENDOR transitions with the hyperfine constant change of H in $H_2 \simeq -1.5$ and $\simeq -3$ MHz were observed previously [51]. This difference may be caused by a different lattice structure of our films. We did not observe the ENDOR transitions which may indicate trapping of hydrogen atoms in the interstitial sites. This may be explained by the self-annealing effect which takes place for all three hydrogen isotopes.

3.2 ESR line shape and width

A careful analysis of the ESR line shape and width provides valuable information about the interactions in a spin system. In the limit of low temperatures and small concentrations of paramagnetic species where the spin-lattice and exchange interactions are of minor importance, the width and shape of the ESR lines are solely defined by the dipole-dipole interaction between the spins. In the case of unpaired hydrogen atoms in solid hydrogen matrices, one should distinguish the interaction of the electron spins of atoms with each other and with the magnetic moments of the molecules which form the matrix. The hamiltonian of the dipolar interaction between two spins, $\mathbf{I}$ and $\mathbf{S}$ is:

$$\hat{H} = \frac{g_S g_I \mu_S \mu_I}{4\pi r^3}[\mathbf{I} \cdot \mathbf{S} - \frac{3(\mathbf{r} \cdot \mathbf{I})(\mathbf{r} \cdot \mathbf{S})}{r^2}], \qquad (3.4)$$

where g_S and g_I are the corresponding g-factors, μ_S and μ_I are the magnetic moments and r is the distance between two dipoles.

Based on the van Vleck theory of moments [81], Kittel and Abrahams showed [82] that the ESR lines for dilute systems where a relative concentration of paramagnetic species c, $c = \frac{[H]}{[H_2]}$ for the case of H atoms trapped in solid H_2, is smaller

than 0.01 should possess a Lorentzian shape. The linebreadth becomes linearly proportional to the concentration c. The lineshape becomes Gaussian for a high concentration of electron spins, $c \gtrsim 0.1$, while the linewidth depends on the density as $\sqrt{c}$. Typical concentrations of unpaired atoms in the samples we studied are $\sim 3 \times 10^{19} \text{cm}^{-3}$ ($c \sim 0.001$) which ensures a Lorentzian lineshape.

An important distinction of the dipolar interaction between equivalent spins is that it leads to the homogeneously broadened ESR lines. The interaction between spins sustains a thermal equilibrium between them. A different situation appears when the linewidth is mainly contributed by the dipolar interaction of unlike spins, such as the electron spins and nuclear spins of the matrix molecules. The electron spins experience different local fields and precess with different Larmor frequencies and behave as a bundle of nearly non-interacting spin packets. Saturating only one spin packet will result in "burning a hole" in a such inhomogeneously broadened line. The ESR line becomes an envelope of a number of Lorenzian spin packets and has a Gaussian shape.

The ESR lines of unpaired atoms in magnetic hydrogen matrices have a Gaussian shape at small concentrations, $[\text{H}] \lesssim 10^{18} \text{cm}^{-3}$, when the observed linebreadth is caused mainly by paramagnetism of the matrix and the dipole-dipole interaction between the atoms is negligibly small. At higher concentrations, when the main source of broadening is the dipolar interaction between electron spins, the lines have a Lorentzian shape. The dipolar interaction between equivalent spins also results in a factor 1.5 greater broadening compared to unlike spins [83].

An interaction of the electron spin of an unpaired atom with the nuclear spin of matrix molecules in general may contain two terms: a contact term which is defined by the distribution of the electron cloud of an atom and the non-zero probability of finding it at the nucleus of a neighboring molecule and an anisotropic dipolar term. Although the contact term is small for hydrogen atoms due to their small size, it does not vanish to zero and defines the linewidth of H atoms in para-H_2 [73] which equals to $\simeq 0.3$ G (Table 3.2).

The contribution of the contact term is already negligibly small for D in D_2 due to a smaller magnetic moment of D nuclei compared to H [46]. The matrix linewidth of D atoms in a D_2 matrix is solely defined by the dipolar term. The zero-concentration or matrix width in the matrices constructed from heteronuclear molecules, such as HD and HT, turned out to be greater than that for D_2, ortho-H_2 or T_2. The dipolar field scales as μ_N/r^3 and the ESR linewidth is mostly defined by a presence of magnetic molecules in the closest neighborhood of unpaired atoms. However, the homonuclear molecules become converted within $\sim$10-30 s into their ground rotational state [84, 85] which is diamagnetic for T_2 and H_2 and only more distant neighbors may contribute to the matrix width. The heteronuclear molecules are not restricted by the ortho-para symmetry and the magnetic moments of atoms which form these molecules should be considered separately. We measured the matrix width of unpaired atoms in different hydrogen matrices and the results are summarized in Table 3.2. The largest width was observed in HD
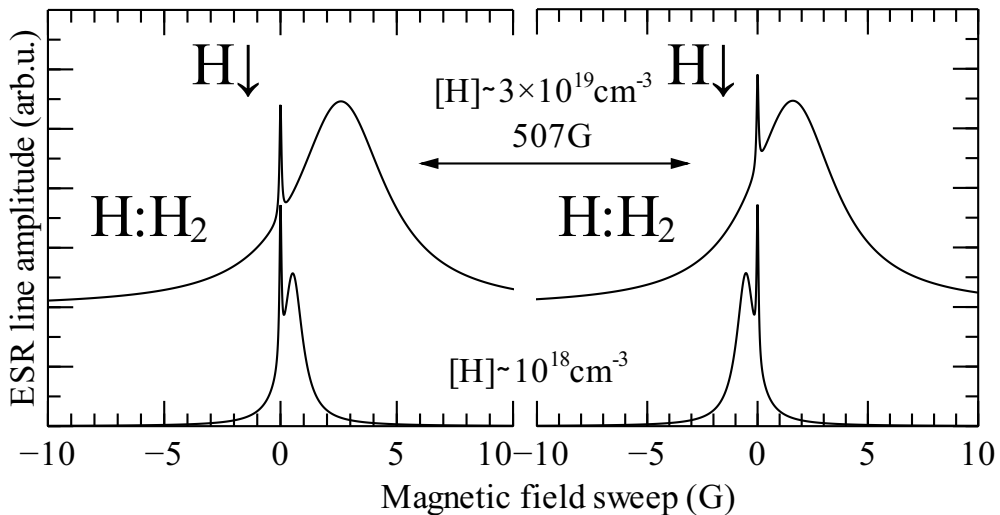
Figure 3.4: The schematic of a shift of the ESR line of H in solid H_2 due to the sample magnetization at $[H] \simeq 3 \times 10^{19}$ cm^{-3} measured relative to the H-gas lines (H↓) adapted from [51]. The lower traces correspond to [H] in solid H_2 $\sim 10^{18}$ cm^{-3}.

(2.9-3.4 G) and T_2 samples which contained $\simeq$15% of HT, 4.6 G. The matrix width in ortho-D_2 samples varied from 1.3 to about 2 G which might also be explained by the HD impurities in the films. The magnetic moment of a deuteron is much smaller compared to those of H and T (Table 1.1) and the matrix width of atoms in ortho-D_2 is small even though its ground rotational state has a non-zero magnetic moment.

For the samples with high densities of atoms ($> 10^{18}$cm^{-3}) the ESR lineshapes are usually a mixture of the inhomogeneous broadening due to the magnetic moments of the matrix molecules and the homogeneous broadening caused by the dipole-dipole interaction between electrons of the impurity atoms. A mixture of these effects can be well seen in the hole-burning experiment when the individual spin-packet of the electrons is saturated. This leads to a hole in the line having the width defined by the homogeneous broadening. This hole disappears with the characteristic time of the electron spin-lattice relaxation, which is of the order of $\sim$0.1 s at the conditions of our experiments.

In addition to the line broadening, unpaired atoms in the lattice also contribute to the sample magnetization. The magnetization is described by the Curie law

$$M = n\mu_B tanh(\frac{\mu_B B}{k_B T}), \tag{3.5}$$

where n is the concentrations of paramagnetic species, and becomes viable at the

lowest temperatures when the electron spins are polarized. The direction of the magnetization vector depends on the shape of the sample and its orientation in magnetic field. For the thin films studied in our experiments, the magnetization appears to be antiparallel to the static magnetic field. The schematic of the H lines in solid H_2 at two different concentrations adapted from [51] is shown in Fig.3.4. The lines of H in solid H_2 at low H concentrations are shifted from the reference H-gas lines due to a slight difference in the hyperfine constant A, and acquire an additional concentration-dependent shift due to magnetization. The lines of H in H_2 are shifted to a higher magnetic field which is required to compensate for the local field created by magnetization. Measuring the ESR line shift and width can be employed for determining the concentration of unpaired atoms in the sample [23, 51].

3.3   Satellite transitions

Along with excitation of allowed ESR transitions, there is a certain probability for a simultaneous flip of the electron spin of an unpaired atom and the nuclear spin of a neighboring magnetic molecule, a so-called satellite transition. The satellite transitions are shifted in the spectrum from the position of the main ESR transition by a distance $\Delta B = g_N \mu_N B$, where g_N is the nuclear g-factor and μ_N is the nuclear magnetic moment. Coupling between the electron spin of the atom and the nuclear spin of the molecule mixes their states and makes such transitions slightly allowed, whereas they are forbidden for non-interacting spins. For H atoms in the magnetic hydrogen matrices (ortho-H_2 or ortho-D_2) such coupling is dipolar and the mixing factor $\epsilon(r)$ [32] is

$$\epsilon(r) \sim (\frac{\mu_B \mu_N}{r^3})/\mu_N B. \qquad (3.6)$$

The probability of exciting the satellite transitions is proportional to ϵ^2 and detecting them in high fields is challenging. However, the satellite transitions were observed in ortho-H_2 and HD matrices in low fields [75, 86, 87, 88].

The satellite transition cannot occur with the change of the total nuclear spin of the molecule. In the case of H_2, this would lead to the ortho-para conversion which requires $\simeq 170$ K of energy. Therefore, the magnetic quantum number of the nucleus is changed by 1 in the satellite transition together with the change of the electron spin projection.

We did not observe the satellite transitions directly as the lines in the ESR spectra. However, we were able to detect them indirectly by pumping their positions, $\pm g_N \mu_N B$, from the ESR lines, for 10 min-1 h. This resulted in a formation of long-living holes in the ESR lines. The result of pumping the satellite transitions of H and D atoms in a D_2 matrix is shown in Fig.3.5. The holes in the main ESR lines appeared ~ 11 G shifted from the pumping position. Similar holes were observed after pumping the H satellites in the normal H_2 samples $\simeq 70$ G aside
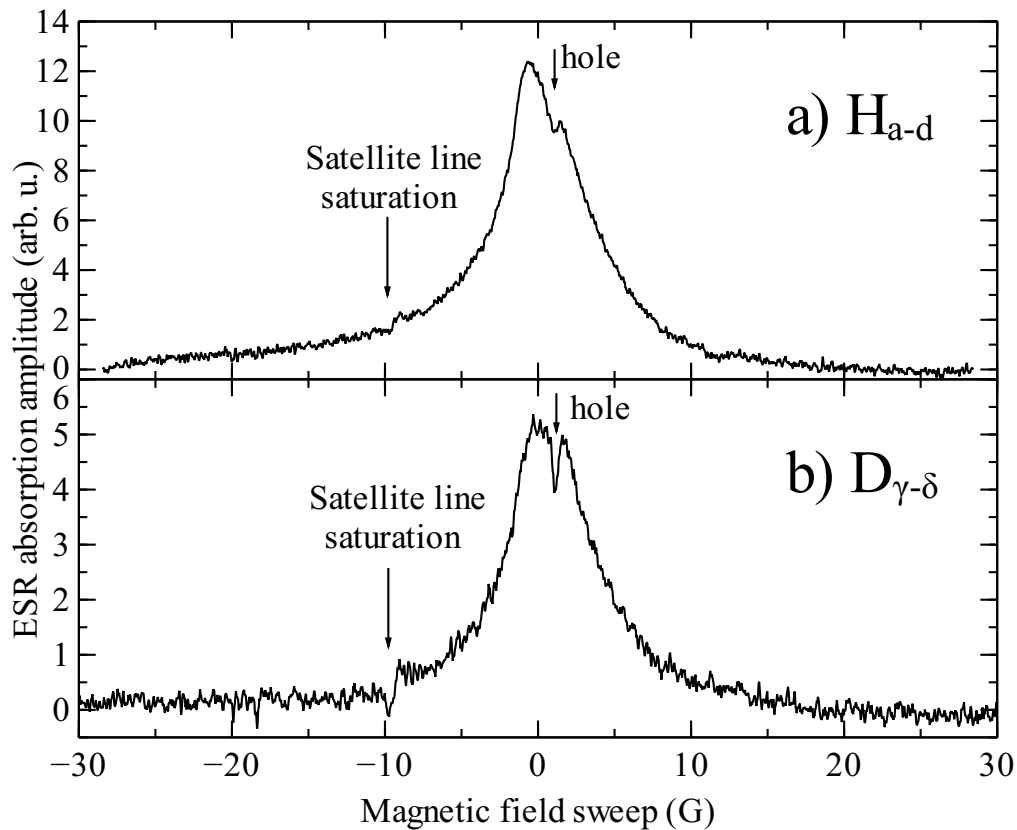
Figure 3.5: "Burning holes" in the ESR lines of H_{a-d} (a) and $D_{\gamma-\delta}$ (b) in solid D_2 after saturating the satellite transitions.

Matrix	Matrix width (G)	Electron line width (G)	n_e (cm^{-3})
H$_2$:1%T$_2$	0.9(1)	1.0(1)	7(3)×10^{16}
HD	3.1(2)	2.1(2)	10(5)×10^{16}
D$_2$:H$_2$(5:1)	2.1(2)	1.3(1)	3(1)×10^{17}
T$_2$:4%H$_2$	5.5(3)	2.3(2)	13(6)×10^{16}

Table 3.3: The ESR linewidths and concentrations of trapped electrons in different matrices of hydrogen isotopes.

from the ESR lines. The holes obtained after pumping the satellite transitions result from the nuclear spin flips of the molecules, which have a very long relaxation time. Therefore, unlike the holes created by pumping the ESR lines, they lived for several hours.

The ratios of the main ESR and satellite lines are derived in refs. [32, 89]. The dipolar field decreases as r^{-3} which makes the probability for flipping a neighboring nuclear spin along with the electron spin to be proportional to r^{-6} for a single nuclear spin and r^{-12} for two nuclear spins. This makes the satellite transitions a useful tool for probing a neighborhood of unpaired atoms.

3.4 Electrons trapped in hydrogen solids.

Producing unpaired atoms in hydrogen films by electron impact dissociation may also result in generating a large number of defects and formation of other species in the matrix, such as electrons and ions. A number of authors reported on a possibility of observing trapped electrons in solid hydrogens where they are expected to form bubbles due to the large amplitudes of the zero-point oscillations. The signals associated with the trapped electrons were observed in different hydrogen matrices where the unpaired atoms were produced by various methods: γ-irradiation [90], irradiation by a high-energy electron beam [50], admixing β-radioactive tritium [91]. Along with the trapped electrons, a number of other species in solid hydrogen matrices were observed. Among them are H$_6^+$ and H$_2^+$ ions [92, 93, 94, 95]. However, the most stable of the hydrogen ions, H$^+$ and H$_3^+$ have a zero electron spin and cannot be observed by ESR.

In the course of the experiments described here we observed three different lines in the spectra which are caused by unbound electrons. First of all, a strong and broad cyclotron resonance line e$_{CD}$ (Fig.3.3) due to the electrons in the volume between the FPR mirrors which appears upon running the discharge. The intensity of this line was strongly dependent on the discharge power. Sometimes the cyclotron signal from the free electrons in the bulk of the SC could be seen several hours and days after turning off the discharge. We concluded that in this case the electrons were trapped in the Penning type traps created by tiny stray electric fields occurring due to residual charges on the parts of the sample cell.
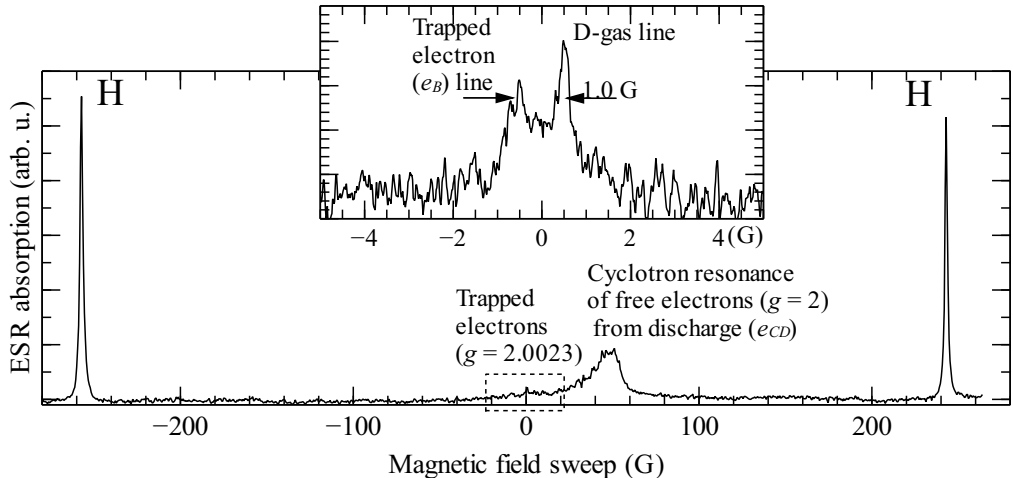
Figure 3.6: The ESR spectrum of H in H_2. Two lines in the center are the ESR line of trapped electrons (e_B) and the cyclotron line of free electrons due to running the discharge in the sample cell. The inset: the line of the trapped electrons in the D_2:H_2 sample and the reference $D_{\beta-\epsilon}$ gas -phase line [P3].

Cyclotron resonance is more sensitive than the spin resonance because the transitions are driven by the electric dipole moment. The ratio of the sensitivities, P_C/P_S, for two methods assuming that the amplitudes of magnetic and electric fields in the resonator are of the same order can be estimated as [96]

$$P_C/P_S \simeq (e \cdot r)^2 c^2/(\mu_B)^2, \tag{3.7}$$

where $r = \frac{\sqrt{2E/m^*}}{\omega_C}$ is the radius of the electron cyclotron orbit, ω_C is the cyclotron angular frequency, E is the energy corresponding to the spacing between the Landau levels, m^* is the electron effective mass, c is the speed of light. The P_C/P_S ratio for our experimental conditions is of the order of 10^9 and therefore even several tens of electrons may provide a quite strong cyclotron line.

In addition to the cyclotron line, a narrow singlet line, e_B, in the center of the ESR spectra was also observed in nearly all samples we studied (Fig.3.6). In our field, the two lines are separated by $51\,\mathrm{G}$ and are well resolved. The e_B line did not have hyperfine satellites which rules out a possibility that it originates from any of hydrogen ion species. We attributed this line to the electrons trapped in the matrix. The e_B line appeared very quickly after starting accumulation of unpaired atoms in the films and lived for about 5 days (in H_2) and could be regenerated by running the discharge in the sample cell. A different behavior was observed in solid T_2 where the line disappeared much faster, within a few hours. A strong signal of the $D_{\beta-\epsilon}$ line obscured the e_B line in the samples containing D_2 which made it impossible to track the line evolution after about 1 day of running the

discharge.

The e_B line turned out to be shifted $\simeq 0.3(1)\,$G from the position of spin-resonance of free electrons in all matrices we studied and had a g-factor $g=2.00233(5)$, very close to that of free electrons$-$ $g_e = 2.0023193$. This shift was accurately measured relatively to the position of the D$_{\beta-\epsilon}$ line of spin-polarized deuterium gas which has a g-factor $-$ $g = 2.002284$ (Table 1.1) (Fig.3.6).

Comparing the ratios of the areas of the e_B line and the lines of H and D atoms, we estimated the concentrations of electrons trapped in the samples (Table 3.3). It turned out that we reached the highest concentrations of the trapped electrons in the D$_2$:H$_2$ sample where one expects a larger number of voids and vacancies suitable for trapping electrons. Moreover the D$_2$ matrix should provide a more stable trapping site for the electrons because of smaller amplitudes of the zero-point oscillations of D$_2$ molecules compared to hydrogen [97]. Similar behavior should also be expected for the tritium samples. However, the heat released in the recombination of unpaired atoms raises the temperature of the matrix and makes electrons more mobile and easier recombining with positively charged species.

We tried to influence the e_B line observed in the D$_2$:H$_2$ mixture sample by applying DC voltage to the top electrode of the quartz microbalance. The voltages $V=\pm 250\,$V did not affect the e_B line. The trapped-electron line was easily saturated and recording it required substantial reducing the ESR mm-wave power. The widths of the e_B lines appeared to be somewhat smaller than the matrix width varying slightly in different hydrogen matrices (Table 3.3). Electrons being extremely light, and having a large amplitude of the zero-point oscillations, are able to push the neighboring matrix molecules and form bubbles. The bubble radii can be estimated by comparing the matrix widths of the lines of unpaired atoms to the widths of the e_B lines. The width of the electron line within the limit of the zero concentration of unpaired atoms below saturation should be solely defined by the dipolar interaction with the nuclear spins of neighboring molecules. Considering the r^{-3} dependence of the dipolar field on distance, we estimated the bubble radius in D$_2$:H$_2$ (5:1) matrix $r_b \simeq 5\,$Å. This value is in a good agreement with the results of Brooks. et. al. [98] who estimated the size of the electron bubble in D$_2$ as $r_b=5.1\,$Å.

It also turned out that the breadths of the electron lines did not depend on the concentration of unpaired atoms in the films within the precision of our linewidth measurement. In order to verify this we compared the time evolution of the H and e_B lines in a $300\,$nm thick T$_2$:H$_2$(2:1) mixture film (Fig.3.7). This observation is in a stark contrast to the ESR lines of unpaired atoms in the films which acquired an extra width $\sim 1.2\,$G per 10^{19} cm^{-3} in addition to the matrix broadening [51]. We suggest that the electrons not only form bubbles but also push unpaired atoms and become trapped in the regions free of atoms. Moreover they distort the lattice which precludes trapping unpaired atoms in the vicinity of the electron bubbles.

The evolution of the line of trapped electrons in the D$_2$:H$_2$ sample where we observed the highest concentration of these species is shown in Fig.3.8. The line

Figure 3.7: The widths of the trapped electron line, e_B, (open circles) and of H (filled circles) in T_2:H_2 (2:1) solid mixture film as a function of time.

Figure 3.8: The evolution of ESR spectra for D_2:H_2 sample. 1. Beginning of accumulation, after running the discharge for 10 min. 2. After running the discharge for 30 min. 3. After accumulating 48 h the middle deuterium line has obscured the electron line. 4. After heating the sample above 1 K the cyclotron resonance line appears. Notice that spectra are scaled for fitting the screen. The scaling factors are specified above each spectrum [P3].

Figure 3.9: Temperature dependence of the e_{CS} line area plotted in Arrhenius coordinates [P3].

appeared about 10 minutes after starting the discharge (trace 1). The D lines did not appear yet due to D-to-H conversion in the film caused by the isotopic exchange reactions D+H$_2$ →HD+D and D+HD→D$_2$+H. The second spectrum (trace 2) was recorded ≃30 min after starting the discharge when the small D lines appeared. The e_B line became obscured by the D signal in the process of running the discharge (spectrum 3). One more feature related with unbound electrons was obs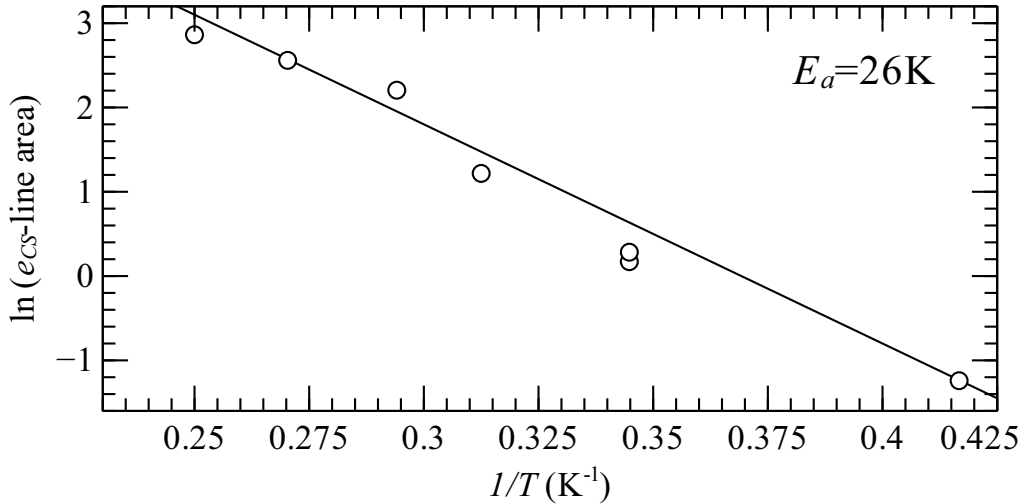erved in the D$_2$:H$_2$ samples. As described above, we run the rf discharge for ≃2 days for getting the highest density of unpaired atoms. Then the discharge was stopped, the sample cell heated to 4 K and a helium film, present during the discharge, was evacuated. A broad line at the position of cyclotron resonance of free electrons, e_{CS}, appeared (spectrum 4) when all helium was removed from the cell.

The area of the e_{CS} line had a strong dependence on temperature and it vanished after cooling the sample below about 1 K. The line was completely destroyed after condensing He to the cell and small positive and negative voltages, ±1 V, applied to the QM completely suppressed the line. We were unable to split the e_{CS} line by applying a magnetic field gradient. Based on these arguments, we attributed the e_{CS} line to the surface bound electrons which diffuse from the bulk to the sample surface.

The activation energy, $E_a = 26$ K, of this process was estimated by plotting the e_{CS} line area as a function of temperature in Arrhenius coordinates (Fig.3.9). We think that the electrons captured in the bulk of the film are released to the surface from which they escape into the space above the film and eventually disappear at

the other cell surfaces. The activation energy, $E_a = 26\,\mathrm{K}$, measured in Fig.3.9 is the difference in the chemical potential of the electrons captured in the bulk and on the surface of the hydrogen film.

The cyclotron line of electrons on the surface of solid H_2 was previously observed by Edel'man and Faley [99]. The widths reported there, $\sim\mathrm{kG}$, are much larger than those observed in our experiments, 10-30 G. The cyclotron linewidth should be strongly dependent on the film roughness which influences the effective mass of the surface electrons. A much smaller linewidth of the e_{CS} line in our experiments may be explained by much smoother film surfaces. The study of the electrons bound to the surface of a hydrogen film is an interesting topic which may be the subject of future experiments.

Chapter 4

Isotopic exchange reactions and recombination of H and D atoms

The results on studying isotopic exchange reaction of hydrogen and deuterium, D+HD→D$_2$+H, will be discussed in this section. The temperature range below 1 K was not probed in experiments of this type before and we provide evidence of the first experimental observation of this reaction at temperatures down to 130 mK. We discuss two different regimes: a pure reaction when no diffusion stage is needed and when the reactants need to diffuse a distance of several lattice constants before taking part in the reaction. The results discussed in this section are published in paper [P4].

4.1 Introduction

The mechanisms of chemical kinetics change significantly upon lowering temperature. Reaction rates at high temperatures follow a classical Arrhenius dependence when reactants possess enough energy to surmount the reaction barrier. At lower temperatures when their thermal energy decreases substantially, the effects of tunneling start playing a decisive role, especially for lighter species (Fig.4.1). In contrast to a classical case of high temperatures, tunneling reactions are characterized by a strong isotope effect and a weak dependence of their rates on temperature. For the mixtures of hydrogen and deuterium, we will mainly concern the following reactions:

$$H+H_2 \rightarrow H_2+H \qquad (4.1)$$

$$D+D_2 \rightarrow D_2+D \qquad (4.2)$$

$$D+H_2 \rightarrow HD + H \qquad (4.3)$$

$$W \sim exp(-V/k_B T)$$

$$V \quad W \sim exp\left[-2\left(\frac{2m(V-E)}{\hbar^2}\right)^{1/2} a\right]$$

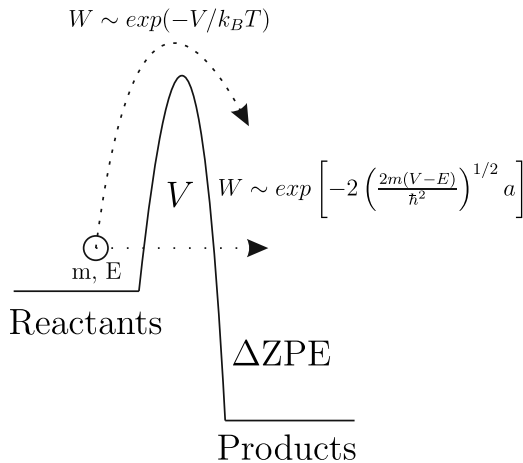m, E

Reactants

ΔZPE

Products

Figure 4.1: A schematic of the reaction kinetics presented in the reaction coordinates. The activation mechanism dominates at high temperatures while the tunneling contribution prevails at low temperatures. The width and height of the reaction barrier are labeled as a and V, respectively.

$$D+HD \rightarrow D_2+H. \qquad (4.4)$$

First two reactions are equivalent to a replacement of the atom with the molecule and effectively lead to the diffusive motion of the atomic impurity along the crystal. Exchange reactions (4.1)-(4.4) are the simplest among chemical reactions. Due to the simplicity of the reactants, these reactions play a special role in the field of chemical kinetics where they serve as a perfect object for theoretical models [100, 101]. In addition to that, exchange reactions (4.3) and (4.4) are of a great significance in interstellar chemistry where they govern dynamics of deuterium in the primordial gas [14, 15]. Studying reactions (4.1) and (4.2) in the gas phase experimentally is challenging due to a number of practical difficulties [102]. Reactions (4.3) and (4.4) are more accessible from the experimental point of view and their rates are measured for a great variety of systems [13, 103] including solid mixtures of hydrogen isotopes.

A striking difference in the yields of H and D atoms in quench condensed hydrogen-deuterium solid mixtures where H and D atoms were created by bremsstrahlung irradiation was first pointed out by Solem and Rebka [104]. A preferential production of H atoms in D_2:H_2, HD samples was explained 15 years later nearly simultaneously by the groups at Nagoya [105], Chernogolovka [47] and Moscow [106] who suggested that D atoms become converted into H during the course of the isotopic exchange reactions (4.3) and (4.4).

The exchange reactions (4.1) and (4.2) are thermoneutral while reactions (4.3) and (4.4) are exothermic. They have an activation barrier $\simeq 4600\,\mathrm{K}$ and proceed at $T \sim 1\,\mathrm{K}$ exclusively by tunneling. The classical time constant of these reactions

at $T \sim 1\,\text{K}$ estimated theoretically exceeds the life-time of the Universe [94]. The Gibbs free energy, $\sim 300\,\text{K}$, appears from the difference in the zero-point energies of the products and reactants. A large isotope effect results in much smaller rates of the reverse reactions. Moreover, they are endothermic and cannot proceed at sufficiently low temperatures. This explains a preferential production of H atoms in expense of D in HD and $D_2:H_2$ solids. The isotope effect becomes of minor importance at high temperatures when it causes a difference in the heights of the activation barriers for the direct and reverse reactions. The reaction barrier is larger for the deuterated reactants due to their smaller zero-point energies [11]. The classical rates of the direct and reverse reactions (4.1)-(4.4) are collected in ref. [14].

Reactions (4.1)-(4.4) were intensively studied in solid hydrogens at temperatures 1.9-6.5 K [107, 108, 109, 110, 111, 112] and it turned out that the rate of reaction (4.4) does not depend on temperature below $4\,\text{K}$. Due to the larger zero-point energies of the reactants, reaction (4.3) proceeds ~ 2 orders of magnitude faster than reaction (4.4) and its rate was measured only recently [48]. The rates of reactions (4.1)-(4.4) within the approach of a gas-phase reaction model were calculated by Takayanagi et al. [113, 114, 115] and Hancock et al. [116].

The recombination reaction of hydrogen atoms $H+H\rightarrow H_2$ in solid H_2 is always a two stage process: diffusion which ensures approaching of two H atoms by the distance of a lattice constant followed by the recombination reaction itself. The diffusion of H atoms in solid H_2 and of D in solid D_2 at temperatures below $\sim 4\,\text{K}$ proceeds in a repetition of the tunneling chemical reactions (4.1) and (4.2) [12]. The exchange reaction and diffusive motion slow down significantly when the atom is located near another impurity or defect due to the energy level mismatch. Therefore it is important to distinguish pure spatial diffusion when a single H atom moves in a perfect H_2 crystal and the real case of diffusion towards another H atom which decelerates when two H atoms approach each other. The former case is idealistic and the rate of a pure diffusion of H in solid H_2 has not been measured experimentally. The measurements of the diffusion coefficient of H atoms in solid H_2 based on their recombination are always biased due to the energy level mismatch. The mismatch can be compensated by phonons and the recombination rates acquire a characteristic dependence on temperature. The recombination of H in H_2 slows down significantly below $1\,\text{K}$ and becomes immeasurably small at $T=150\,\text{mK}$ [28] when no phonons are available to compensate for the level mismatch and enhance tunneling.

4.2   Experimental results

4.2.1   Experimental procedures

We measured the rates of reaction (4.4) in a temperature range 0.13-1.5 K in two types of matrices: pure HD and D_2 with a small, 0.23%, admixture of HD

(D_2:0.23% HD). These kinds of samples made it possible to probe the reaction rates for two different regimes: studying pure isotopic exchange reaction (4.4) in solid HD and reaction (4.4) limited by the diffusion of D atoms.

The HD gas we used contained 3% of H_2 and D_2 as impurities, while our D_2 gas with 0.23% HD turned out to be the purest deuterium gas commercially available (Linde AG). 200 nm thick films were deposited onto the quartz microbalance directly from a room temperature reservoir. Prior to condensing, the D_2 gas was converted to the $J = 0$ state in a para-ortho converter [2]. Accumulation of unpaired atoms in the films was carried out by running the rf discharge in the sample cell similar to that described in Chapter 2.

4.2.2 Pure HD

The evolution of H and D concentrations in the HD sample while running the discharge and after turning it off is shown in Fig.4.2. The concentrations of H and D approached 2×10^{19}cm^{-3} and 2×10^{18}cm^{-3}, respectively. The H concentration continued to grow even after the discharge switch-off while the D signal rapidly decreased after this point. The discharge was typically run for 5-12 h which was sufficient to reach the D signal saturation, i.e $\frac{d[D]}{dt} \to 0$.

After the maximum concentrations of D atoms were reached, the discharge was stopped and the sample cell was stabilized at a desired temperature. The polarization of D nuclei was negligibly small even at the lowest experimental temperature, $T = 130$ mK and the decay of D atom concentration was measured by recording only the $D_{\alpha-\zeta}$ ESR line. A line of the trapped electrons, similar to those discussed in Chapter 3, was also observed in the center of the ESR spectrum near the $D_{\beta-\epsilon}$ line. This line persisted in the spectrum after the $D_{\beta-\epsilon}$ line vanished in noise.

The cell temperature increased to about 0.7 K while running the discharge and it took $\sim$2 hours to cool it to the lowest temperature, 130 mK, studied in this work (Fig.4.3). The D concentration significantly decreased during such cool-down and a special attention was paid to improve the signal-to-noise ratio for measuring the ESR line of D atoms at this temperature. Typically, the ESR lines were measured using the mm-wave power far below the saturation threshold where the dispersion and absorption signals are equal. In order to measure the evolution of D signal at 130 mK, high mm-power was used and the [D] kinetics was analyzed by following the D-line dispersion instead of the absorption which was heavily saturated. The amplitude of the dispersion signal remained proportional to the mm-wave power and was not saturated [59].

In order to have the same initial conditions and avoid a possible influence of the history of the sample on the measured kinetics, each new measurement was started with re-accumulation of atoms by running the rf discharge for the same duration of time. Reproducibility of the starting conditions was confirmed by comparing several identical measurements at the same temperature of 200 mK.

The evolution of the D atom density at different temperatures caused by the
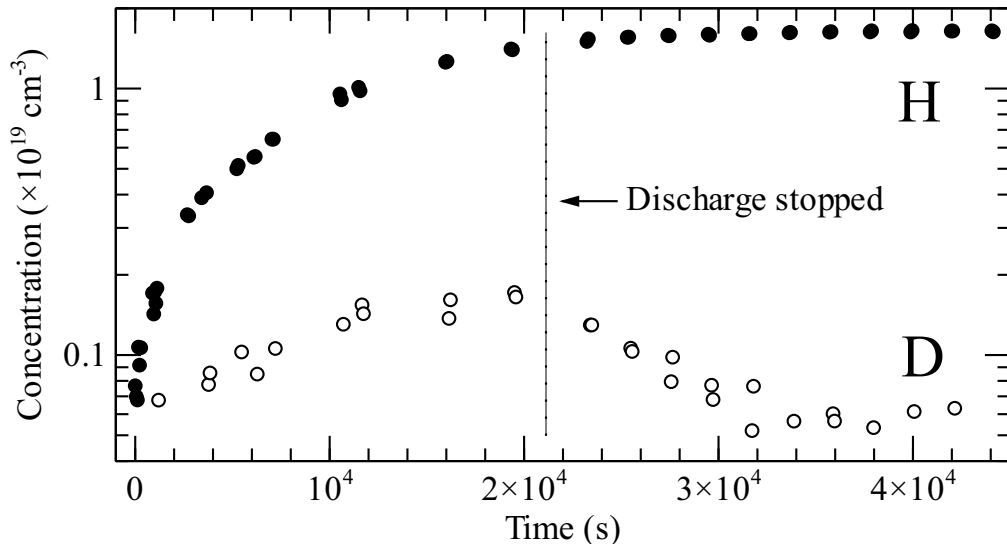
Figure 4.2: Dependence of the H and D concentrations in solid HD on time during accumulation and after stopping the discharge [P4].

isotopic exchange reaction (4.4) is shown in Fig.4.3. The total concentration of [H]+[D] did not change after the discharge switch-off which indicates the absence of atomic recombination. The rate of exchange reaction (4.4) in the absence of recombination can be found by solving the differential equation:

$$\frac{d[D]}{dt} = -k^{ex}[D][HD],\tag{4.5}$$

where k^{ex} is the second-order rate of reaction (4.4). The HD concentration can be recalculated from the molar volume at zero temperature (see Table 1.2). The HD concentration greatly exceeds the concentration of D atoms, [HD]≫[D], which gives a possibility to consider the decay of D atoms due to reaction (4.4) as a pseudo-first order process. The reaction rates, k^{ex}, were extracted by fitting the experimental points in the semi-logarithmic coordinates with the exponential functions (Fig.4.3). The rate of a pseudo-first order chemical reaction does not depend on the concentration of a less abundant reactant and the reaction rates we found are not biased by any possible error in the absolute calibration of the ESR signals, which are estimated to be ≃20%. A weak dependence of the reaction rates on temperature in the range 0.13-1.5 K agrees with the results obtained at higher temperatures [107, 111, 117] and supports the tunneling nature of the isotopic exchange reaction (4.4) and provides evidence that it may proceed with a substantial rate down to the absolute zero of temperature.
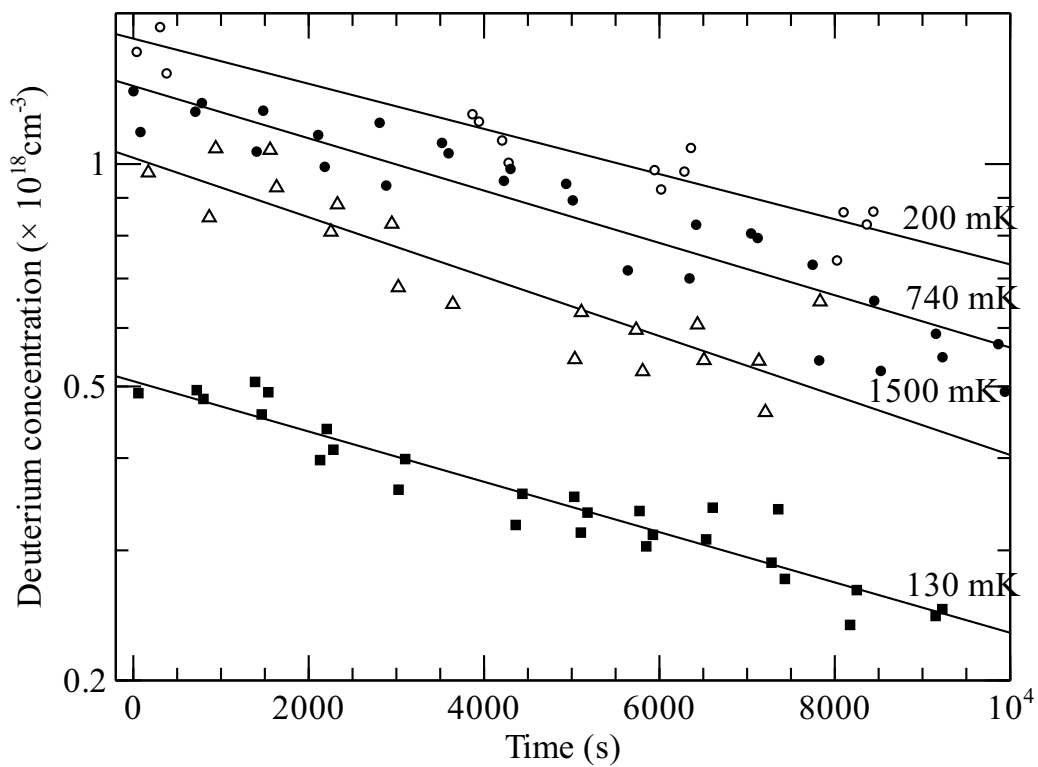
Figure 4.3: The decay of the D atom concentration in solid HD at different temperatures [P4].

4.2.3   D$_2$:0.23% HD

A similar measurement was also carried out in solid D$_2$ with a 0.23% admixture of HD. Here only a small fraction of D atoms, $(1 - 0.9977)^{12} \simeq 2.7\%$, has a HD molecule as one of its 12 closest neighbors. Therefore, a majority of D atoms should first diffuse the distance of several lattice constants before participating in reaction (4.4).

The evolution of H and D partial concentrations and the total concentration of atoms, [H]+[D], in this sample stored at 150 mK are shown in Fig.4.4. The concentration of H atoms in the end of this measurement approached 2.2×10^{18}cm^{-3} which is much larger than that expected from direct dissociation of molecules. The D:H atomic ratio in this case should be $\simeq$1700:1. The 10:1 ratio observed experimentally provides clear evidence that the vast majority of H atoms are indeed generated in exchange reaction (4.4) after diffusion of D atoms (4.2). The total, [H]+[D], concentration of atoms remained constant in the course of this measurement which indicates that the exchange reaction proceeds sufficiently well whereas the recombination is suppressed.

The concentrations of reactants in this sample, [D]$\simeq$2.5$\times10^{19}$cm^{-3} and [HD]$\simeq$ 6.9$\times10^{19}$cm^{-3}, are comparable to each other and reaction (4.4) should be treated as a true second-order process. The solution of the differential equation (4.5) for a second-order reaction can be presented as [118]:

$$k^{ex}t = \frac{1}{[HD]_0 - [D]_0} \times ln\frac{[HD][D]_0}{[D][HD]_0} , \qquad (4.6)$$

where [HD]$_0$ and [D]$_0$ are the concentrations in the beginning of measurement and [HD] and [D] are the time-dependent concentrations of reactants in the course of measurement. The concentrations of D atoms were determined from the areas of the ESR signals and the HD concentration, [HD]=[HD]$_0$−[H], was estimated assuming that exchange reaction (4.4) is the only process which influences the concentration of HD. The second-order reaction rate, $k^{ex}_{D_2} = 9(4) \times 10^{-28}$ cm^{3}s^{-1}, is ∼4 times smaller than the reaction rates measured in pure HD.

A similar measurement was then carried out at $T = 1.35$ K. Unfortunately, the long-term stability of the ESR spectrometer degraded at temperatures above 1 K and it was not sufficient for accurate monitoring the concentrations of H and D. Therefore, we present the fractional concentrations of H and D obtained in this measurement which were not affected by the slow drifts of the spectrometer sensitivity. The reaction rate measured at this temperature, $k^{ex}_{D_2} = 8(4) \times 10^{-28}$ cm^{3}s^{-1} turned out to be the same as measured at 150 mK. The time evolution of the partial concentrations of H and D in these two measurements are compared in Fig.4.4. The evolution of H and D ratios appears nearly parallel and was not influenced by raising the SC temperature from 150 mK to 1.35 K. Based on that we concluded that the spatial diffusion of D or HD reactants in the D$_2$ crystal is a pure tunneling process (4.4) unlike the recombination of H atoms in solid H$_2$ below 1 K where the

Figure 4.4: The time evolution of the H and D partial concentrations at $T = 150\,\mathrm{mK}$ (gray diamonds) and $T = 1.5\,\mathrm{K}$ (open circles) in D_2:0.23%HD. The dependence of the total [H]+[D] concentration on time in this sample at $T=150\,\mathrm{mK}$ is shown by black circles. The "ratio" axis is broken to emphasize the growth of H atoms. The "concentration" axis corresponds only to the points of total [H]+[D] concentration [P4].

approaching of H atoms towards each other requires phonon assistance in order to compensate for the energy level mismatch [23, 28].

The recombination rates of H in H_2 and D in D_2, k^r, and the rates of exchange reaction (4.4), k^{ex}, collected from the literature and measured in this work are summarized in Fig.4.5. An upper limit for the recombination rate of D in D_2 at 150 mK was estimated by analyzing the total concentrations of H and D atoms, [H]+[D], which remained constant (Fig.4.4). The differential equations for the evolution of the H and D concentrations when the rf discharge is turned off can be written in a following way:

$$\frac{d[D]}{dt} = -k^{ex}[D][HD] - k^r[D]^2 - k^{r'}[D][H] \tag{4.7}$$

$$\frac{d[H]}{dt} = k^{ex}[D][HD] - k^{r'}[D][H] - k^{r''}[H]^2. \tag{4.8}$$

The concentration of H atoms in the sample was ten times smaller than that of D and the terms which correspond to D-H and H-H recombination can be neglected. Hydrogen atoms cannot diffuse in solid D_2 at temperatures ~1 K and are localized. Their diffusion via the repetition of the isotopic exchange reaction H+D_2 →HD+D is endothermic and is completely suppressed at these temperatures. The H atoms become more mobile above helium temperatures when diffusion related to the formation of vacancies should take over. Therefore, equations (4.7) and (4.8) can be modified as the following:

$$\frac{d[D]}{dt} = -k^{ex}[D][HD] - k^r[D]^2 \tag{4.9}$$

$$\frac{d[H]}{dt} = k^{ex}[D][HD]. \tag{4.10}$$

The upper limit for recombination constant of D in D_2, $k^r_{D_2}$ at 150 mK was estimated from the fit of the total [H]+[D] concentration in Fig.4.4: $k^r_{D_2} \simeq 3(2) \times 10^{-28} \mathrm{cm^3 s^{-1}}$. This value is $\simeq 2$ orders of magnitude smaller than those reported in literature at 1.3 K [112] and 4.2 K [52]. Such a small value of the D recombination rate resembles a strong suppression of the recombination rate of H in H_2 below 1 K when less and less phonons are available to compensate for the energy level mismatch. The recombination rates measured experimentally should also be sensitive to the method used to create the sample. Lattice defects and irregularities efficiently localize the atoms and preclude their recombination.

The fact that recombination of D atoms in D_2:0.23% HD becomes immeasurably small while exchange reaction (4.4) proceeds with a high-enough rate indicates a much faster diffusion stage in the latter case. Here one may distinguish two different contributions: diffusion of D atoms by a repetition of exchange reactions (4.2) and physical diffusion of HD molecules in an ortho-D_2 matrix. Being heavier, HD molecules should produce smaller perturbation of the periodic potential of the
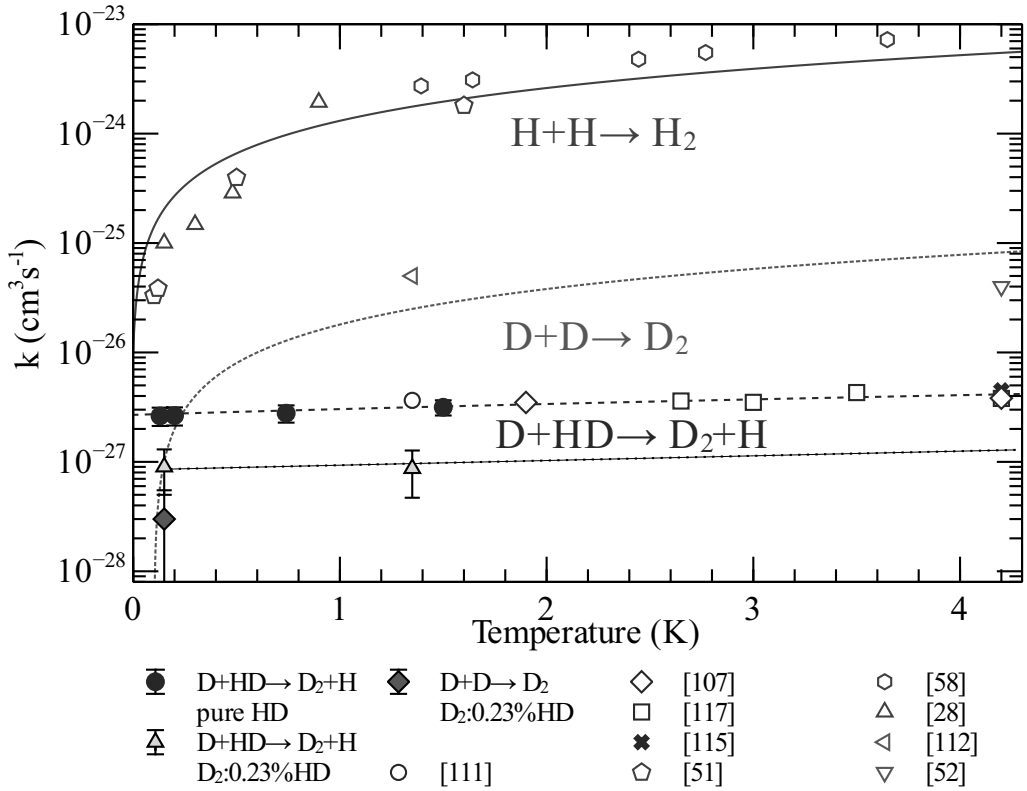
Figure 4.5: The rates of the exchange reaction (4.4) and the H and D recombination rates in H_2 and D_2 as the functions of temperature. The lines are drawn as a guide [P4].

matrix compared to unpaired D atoms. A smaller mass difference between HD and the host D_2 molecules compared to that of D atoms and D_2 molecules should also result in a smaller level mismatch and more efficient diffusion of D atoms towards HD molecules. The second possible scenario is diffusion of HD molecules through the D_2 matrix [9].

The rate of reaction (4.4) in the D_2:0.23%HD sample, $k^{ex} = 9(4) \times 10^{-28} \mathrm{cm^3 s^{-1}}$, is about 4 times smaller than that measured in a pure HD matrix, $\simeq 3 \times 10^{-27} \mathrm{cm^3 s^{-1}}$. Assuming random positions of D in the HD lattice, one can expect a 12 times smaller rate for the D_2:0.23% HD matrix. Moreover, in contrast to the recombination reactions which are barrierless, the exchange reaction (4.4) has a large activation barrier $V \simeq 4600\,\mathrm{K}$. This means that reaction (4.4) in D_2:0.23% HD should proceed only in a fraction of cases when a D atom and a HD molecule occupy neighboring lattice sites. The exchange reaction in a HD matrix will lead to the formation of two lattice defects compared to only one defect in solid D_2. This can be visualized in a simplified way as a 1D chain HD-D-HD-HD$\rightarrow$HD-D_2-H-HD. In contrast to that, two lattice defects are converted to one in the D_2 matrix: D_2-HD-D-$D_2\rightarrow D_2$-D_2-H-D_2. Creating an additional defect in the lattice should require additional energy and may cause a mismatch between the initial and final tunneling state.

The rate of the reaction (4.4) has no clear temperature dependence while the recombination rates of H and D atom diminish significantly at temperatures below $1\,\mathrm{K}$. The independence of the reaction rate (4.4) on temperature in pure HD provides evidence that the exchange reactions (4.1) and (4.2) also take place in H_2 and D_2. The suppression of H and D atom recombination is caused by the energy level mismatch emerging when two H and D atoms approach each other.

Chapter 5

Dynamic nuclear polarization

In this chapter, we discuss the mechanisms of spin relaxation and dynamic nuclear polarization (DNP) for H and D atoms trapped in solid matrices of hydrogen isotopes. We review the main factors which influence the efficiency of relaxation and DNP of H atoms in different matrices. Prior to the experiments with solid hydrogen-deuterium mixtures, we did not expect any significant differences in DNP for H atoms in H_2 and D_2. However, several distinct features of samples containing deuterium were observed already during the first experiments. Among them are much higher efficiency of pumping the forbidden transitions of H atoms and a faster nuclear and cross-relaxation in the samples containing unpaired deuterium atoms. However the most intriguing feature of these samples was the build-up of the H nuclear polarization after pumping the center of the ESR spectrum. The experimental results presented in this chapter are published in papers [P2] and [P5].

5.1 Introduction

A straightforward way for polarizing the spins is to cool them in a magnetic field to low temperatures. Electron spins obtain a close-to-unity polarization already in magnetic fields $\sim 1\,\mathrm{T}$ and at temperatures close to $1\,\mathrm{K}$. Nuclear magnetic moments are much smaller and polarizing them requires much higher fields and much lower temperatures. There are four main methods for polarizing nuclei dynamically by transferring high polarization of electron spins to unpolarized nuclei: the Overhauser effect, the Solid effect, the Cross effect and the thermal mixing. The Overhauser effect was initially proposed for metals where nuclear spins relax through the hyperfine coupling to conduction electrons [119]. Pumping the ESR line of the conduction electrons polarizes nuclear spins and causes a substantial enhancement of the NMR signal [120]. Nuclear polarization in this case emerges from the difference in the flip-flop and flip-flip cross-relaxation rates. The Overhauser effect also works for the nuclei which have a hyperfine coupling to their
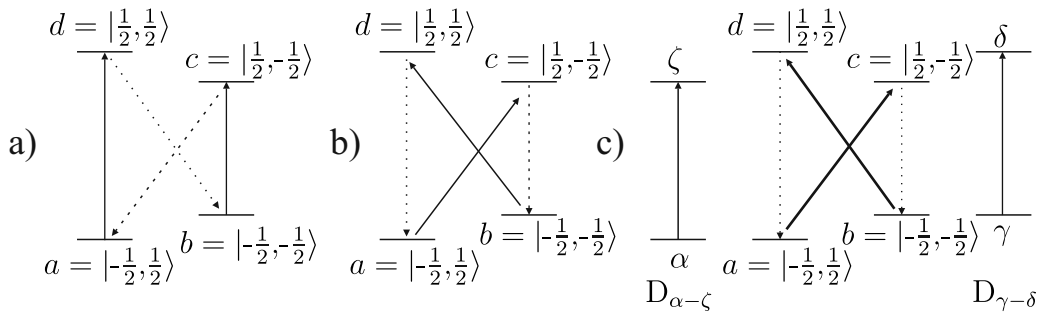
Figure 5.1: Formation of nuclear polarization of H atoms by a) Overhauser effect. The allowed transitions, $a-d$ or $b-c$ are saturated and the nuclear polarization appears due to cross-relaxation through the forbidden transitions $b-d$ or $a-c$, respectively. b) Solid effect. Saturation of the forbidden transitions, $b-d$ or $a-c$, is followed by the electronic relaxation $a-d$ and $b-c$, respectively. c) Cross effect. Pumping the forbidden transitions of H atoms, $b-d$ and $a-c$ is accompanied by a simultaneous saturation of the allowed transitions of D atoms, $\gamma-\delta$ and $\alpha-\zeta$, respectively.

own electrons [121]. The main requirement, therefore, is a non-zero component of the oscillating field which stimulates cross-relaxation. It can be either due to lattice vibrations in solids, or modulation of hyperfine coupling due to the Brownian motion in liquids or conduction electrons.

In contrast to the Overhauser effect which relies on saturating allowed transitions, the Solid effect is based on saturating the forbidden ESR transitions which correspond to a simultaneous flip of an electron and nuclear spin. The probability for exciting forbidden transitions is defined by the mixing factor of the electron and nuclear states, $\kappa^2 = (\frac{A}{B})^2$, for the flip-flop and $\kappa^2 = (\frac{B_{dip}}{B})^2$ for the flip-flip transition, where A is the hyperfine constant, B_{dip} is the dipolar component of the electron-nucleus interaction and B is the static magnetic field. The flip-flip transition is completely forbidden for the free hydrogen atoms but becomes partially allowed when they are stabilized in solids where dipolar interaction mixes all four energy states. The mixing factor scales as B^{-2} and the efficiency of the Solid effect significantly decreases in high fields.

Both Overhauser and Solid effects are two-spin phenomena and involve an electron-nucleus pair coupled by either the contact or dipolar interaction. The Cross effect and the thermal mixing are the three-spin phenomena. They require two electron spins coupled together by the dipolar interaction and a nuclear spin which has either a dipolar or scalar coupling to one of the electrons. The Cross effect may be realized when the ESR frequencies of two electrons differ by the Larmor frequency of the nucleus involved [122, 123]:

$$\omega_{1e} = \omega_{2e} + \omega_N. \tag{5.1}$$

Saturation of the allowed ESR transition for the first electron will also excite a forbidden transition for the second electron. Flipping the spin of the first electron is compensated by a simultaneous flip of the nuclear spin and the spin of the second electron. The energy during such three-spin flips is conserved and this process does not involve an interaction with the lattice. The mechanism of the thermal mixing is similar to that of the Cross effect. The main difference is that the energy equal to the nuclear Larmor frequency is allocated by the reservoir of the electron dipole-dipole interaction in contrast to the Cross effect where it is compensated by the nuclear Zeeman reservoir. A schematic of the Overhauser, the Solid and the Cross effects for H atoms is shown in Fig.5.1.

5.2 Experimental results

5.2.1 Relaxation

We studied relaxation and dynamic nuclear polarization of H and D in several different solid matrices: para-H_2, ortho-D_2, HD and D_2:2%HD. The ortho-D_2 samples also contained a small natural impurity of HD and H_2. The samples, $\simeq 250$ nm thick, were deposited directly from the room temperature gas handling system. Unpaired H and D atoms were created by running the rf discharge in the sample cell similar to that explained in Chapter 2. Typical concentrations of unpaired atoms we concerned with in these experiments were $\sim 3 \times 10^{19} \text{cm}^{-3}$ and the H:D ratio varied from sample to sample. The concentration of D atoms in the HD sample was an order of magnitude smaller, $\sim 3 \times 10^{18}$ cm^{-3}, due to fast conversion of D atoms into H in the course of isotopic exchange reaction D+HD→D_2+H. The D lines rapidly decayed after stopping the discharge and vanished in noise within about 3 hours. We were also able to create substantial concentrations of H and D atoms in the gas phase by running the discharge in the sublimation source. The lines of a spin-polarized deuterium gas were used as the field markers to find an exact location of the forbidden transitions of hydrogen in those samples where we did not have the lines of D atoms trapped in the matrix.

The electron spin-lattice relaxation was measured using the saturation-recovery technique: first the ESR line was saturated by applying mm-wave power of the order of a μW, then the ESR excitation was decreased by 30 dB and the line recovery was recorded. The T_{1e} times were ~ 0.1 s for all samples we studied. We did not observe any substantial dependence of the T_{1e} times on temperature. They decreased only by a factor of 2 after raising the sample cell temperature from 0.15 to 1.5 K.

The nuclear relaxation times were measured in a similar way. First a large population difference between the lower hyperfine levels was created using the Overhauser effect and then the recovery of the nuclear polarization was measured. The T_{1N} times at temperatures below about 0.7 K followed a weak, close to linear dependence on temperature. The only exception was the H:D_2−HD sample where

the T_{1N} times had a strong temperature dependence even below $0.7\,\text{K}$. The nuclear relaxation times in all samples decreased significantly after raising the sample cell temperature above $\sim 0.7 - 1\,\text{K}$. It also turned out that the relaxation rates of H in D_2 were faster compared to those of H in H_2 and D in D_2 at the same temperatures. These results are summarized in Fig.5.2.

In addition to that, we measured the cross-relaxation times, T_{ca} and T_{bd}, using the Overhauser effect. We saturated the allowed ESR transitions, $b - c$ or $a - d$, and recorded the evolution of both ESR lines as a function of the pumping time. We were able to create a substantial nuclear polarization of H atoms using the Overhauser effect by saturating the $b - c$ transition in all samples. However, the cross-relaxation times for H atoms differed significantly from sample to sample. The fastest $c - a$ cross-relaxation, $\sim 10\,\text{s}$, was observed in the D_2 and D_2-HD samples. The cross-relaxation time, T_{ca}, for H atoms in the pure para-H_2 matrix was two orders of magnitude slower, $\sim 10^3$s. A peculiar behavior was observed for cross-relaxation of H atoms in solid HD. It turned out that the T_{ca} cross-relaxation time measured immediately after stopping the discharge, $\sim 300\,\text{s}$, was about six times smaller than that measured after about $4\,\text{days}$ of sample storage. The cross-relaxation through the $b - d$ transition for H in D_2 had a characteristic time $\sim 10^3$s. We did not observe cross-relaxation via the flip-flip transition in other samples.

5.2.2 Discussion

Spin-lattice relaxation in solids at low temperature is stimulated by phonons and its rate is defined by the number of phonons which are in resonance with the transitions between the energy levels in the spin system. Due to the scarcity of phonons "on speaking terms" with the spins, electron spins relax through the direct process when a single phonon is either absorbed or emitted. The relaxation rate in this case is either independent of temperature when the phonon emission occurs spontaneously or increases linearly with temperature which is defined by the low-frequency part of the phonon spectrum. Another distinct feature of the direct process is a strong, $\frac{1}{T_{1e}} \sim B^4$, dependence of the relaxation rate on magnetic field [124, 125, 126]. The electron spin-lattice relaxation times were measured previously in a number of works at 0.3 T [76], 0.86 T [49] and 4.6 T [127]. The T_{1e} reported there have a scatter within 1-2 orders of magnitude. However, a weak temperature dependence observed in our experiments leads us to a conclusion that the electron relaxation is indeed governed by the direct process.

The nuclear spin-lattice relaxation through the direct process is a factor of $(\omega_e/\omega_n)^3$ less efficient compared to the electron relaxation. As temperature is raised, the nuclear Orbach mechanism takes over [125]. The nuclear relaxation in this case proceeds via excitation to the upper hyperfine levels followed by the cross-relaxation through the forbidden transitions:
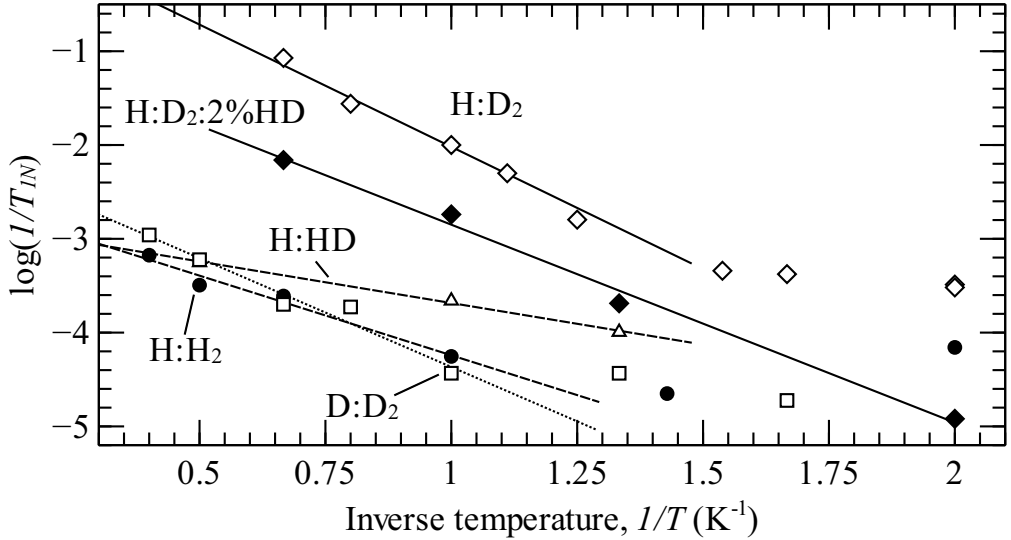
Figure 5.2: The inverse T_{1N} times of H and D plotted in Arrhenius coordinates and fitted by exponential functions (straight lines in a semi-log plot) [P5].

$$\frac{1}{T_{1n}} = (\frac{1}{T_{ca}} + \frac{1}{T_{bd}}) \times exp(-\frac{2\mu_B B}{k_B T}). \tag{5.2}$$

A strong temperature dependence given by the Boltzmann factor in eq. (5.2) is a characteristic feature of the nuclear Orbach relaxation. A more efficient cross-relaxation for H atoms in D_2 compared to H in para-H_2 and D in D_2 also leads to the shorter T_{1N} times.

In order to check the contribution of the nuclear Orbach process to nuclear relaxation, we plotted the experimental points measured at temperatures above $0.5\,K$ in the Arrhenius coordinates (Fig.5.2). The points are fitted by the exponential functions which appear in a semi-log plot as straight lines with the slopes equal to the activation energy.

The slopes appear to be nearly parallel for H in D_2, H:D_2-HD and D:D_2. The activation energy, $E_a \simeq 5.5\,K$, obtained from this analysis is in a fair agreement with the Zeeman energy level splitting in our field, $E_{Zeeman} \simeq 6.3\,K$. This allows us to conclude that the nuclear spin-lattice relaxation in these samples is governed mainly by the nuclear Orbach process. The slopes are somewhat different for H in H_2 and H in HD which may be caused by a contribution of other processes to the relaxation, e.g. the direct process.

Comparing our results with the previous works, we recall that a different behavior was observed in thin, $\simeq 50\,nm$ thick, solid H_2 films [28] where both unpaired H atoms and the host H_2 matrix were created in the course of three-body recom-

bination of the spin-polarized atomic hydrogen gas:

$$H+H+H \rightarrow H_2^* + H. \tag{5.3}$$

The distinct features of these samples were a long electron spin-lattice relaxation time, $T_{1e} = 2.5\,s$, and a very fast cross-relaxation, $T_{ca} \sim 10\,s$. In addition to that, the H nuclear spins relaxed to a much higher polarization than expected from the Boltzmann occupation of the hyperfine sub-levels. We did not observe such effects in the present experiments. We suggest that the behavior observed in [28] might be caused by the influence of the Mylar substrate or a different structure of these films.

5.3   Dynamic nuclear polarization of H atoms

We studied dynamic nuclear polarization of H atoms in several matrices described in the previous section: para-H_2, ortho-D_2, D_2-HD and pure HD. A common observation for all samples was that a large positive polarization of H atoms could be created using the Overhauser effect by pumping the high-field, $b - c$, line. Using this method we reached polarization of nuclear spins ~ 0.8 in para-H_2 and it approached unity for H in D_2. We were also able to create a substantial nuclear polarization of H atoms by pumping the forbidden transitions for all samples containing atomic deuterium. The only way of polarizing nuclear spins of H in para-H_2 was the Overhauser effect by pumping the $b - c$ transition.

We reached a large negative, $p \rightarrow -1$, polarization of H in D_2 by pumping the $a - c$ forbidden transition and a clear positive polarization, $p \simeq 0.25$, by pumping the second, $b - d$, forbidden transition. Both forbidden transitions of H atoms in our field nearly match the position of the ESR lines of atomic deuterium and pumping the forbidden transitions of H atoms also led to build-up of polarization of D atoms by the Overhauser effect. The most intriguing result was that pumping the center of the ESR spectrum which coincides with the $D_{\beta-\epsilon}$ line in addition to the formation of a positive polarization of D atoms, also resulted in a substantial negative nuclear polarization, $p \simeq -0.5$, of H atoms.

We carefully measured the enhancement of H DNP as a function of the pumping position in a range $\pm 110\,G$ from the center of the ESR spectrum (Fig.5.3). This range includes the forbidden transitions of H atoms and both forbidden and allowed transitions of D atoms. The lines of H and D atoms in the D_2 matrix had the contributions from the effects of both homogeneous and inhomogeneous broadening and we did ESR pumping using the frequency modulation with a 5 MHz frequency deviation. Each experimental point corresponds to pumping for 1 hour applying the maximum mm-wave power, $\sim 1\,\mu W$. After each measurement, the H lines were returned to their equilibrium polarization. The enhancement of DNP of H atoms in solid D_2 as a function of the pumping positions measured at $300\,mK$ is shown in Fig.5.3. The H DNP pattern has three peaks around the H forbidden
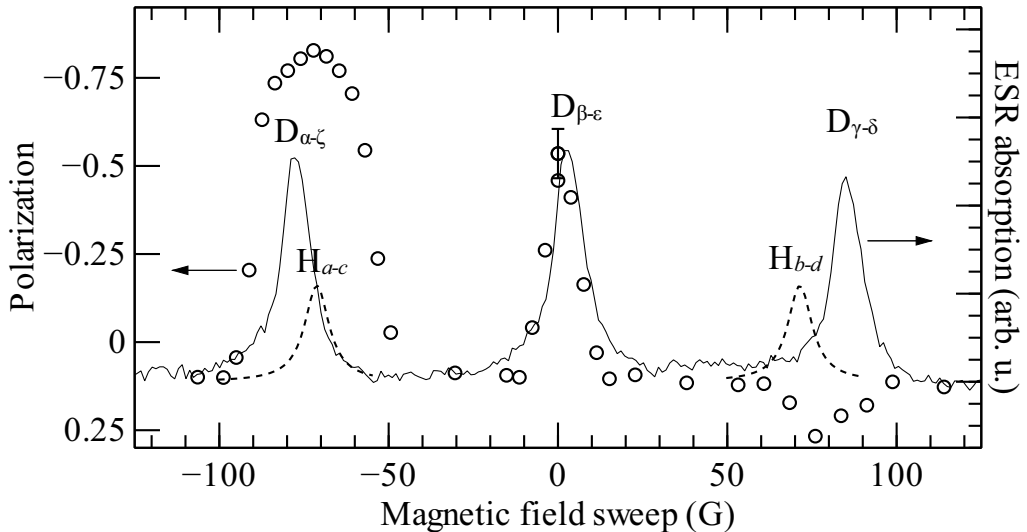
Figure 5.3: Enhancement of H polarization in solid D_2 as a function of the pumping position. Each point corresponds to ESR pumping for 1 h. Note that the polarization axis is inverted [P2].

transition and in the center of the ESR spectrum. The peak in the vicinity of the $D_{\alpha-\zeta}$ line is much broader than the other two which may be explained by a too long pumping time and a partial saturation of the DNP effect.

We performed an additional study aiming on clarification of the shapes of the H DNP peaks and comparing them to the lineshapes of atomic deuterium. We adjusted the ESR pumping times in order to avoid saturation of the DNP effect: 1.7 min for points in the vicinity of the $D_{\alpha-\zeta}$ line, 10 min for points around the $D_{\beta-\epsilon}$ line and 1 h per point near the $D_{\gamma-\delta}$ line. We used frequency modulation with a smaller deviation, 1.1 MHz, in order to study the DNP enhancement within the D lines more accurately. The results of these measurements are summarized in Fig.5.4. The shape of the DNP enhancement patterns matched the shapes of the $D_{\alpha-\zeta}$ and $D_{\beta-\epsilon}$ lines, while it was slightly shifted towards position of the $b-d$ forbidden transition in the case of the $D_{\gamma-\delta}$ line.

We also studied H DNP build-up after pumping the center of the ESR spectrum as a function of time. It should be emphasized that there are neither allowed nor forbidden transitions for isolated H atoms in the center of the ESR spectrum. The evolution of H and D ESR lines in D_2 and the efficiency of transferring H atoms from the a to b state as a function of time is shown in Fig.5.5. The time evolution of transferring deuterium atoms from the β state to the α state due to the Overhauser effect is shown for comparison.

The most peculiar behavior was observed in the pure HD sample where the H DNP enhancement was dependent on a time period the sample was stored. It
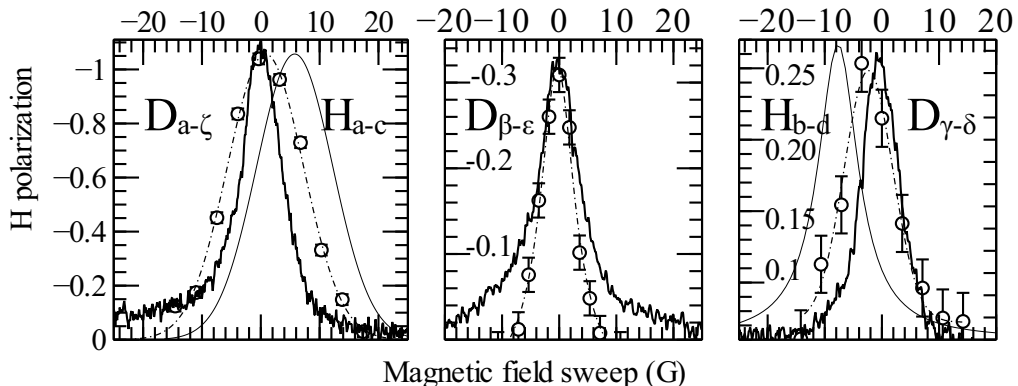
Figure 5.4: The H DNP enhancement as a function of the pumping position in the vicinity of the ESR lines of atomic deuterium (open circles). The positions of the H forbidden transitions are shown as a reference. The ESR pumping times are 1.7 min (left), 10 min (central) and 1 h (right). The equilibrium polarization is subtracted for convenience. Note that the polarization axes for $D_{\alpha-\zeta}$ and $D_{\beta-\epsilon}$ transition figures are inverted [P5].

was possible to create a substantial negative polarization of H atoms by pumping both forbidden transitions and the center of the ESR spectrum immediately after stopping the discharge. However, these effects disappeared after storing the sample for 3-4 days. In addition to that, sample storage also resulted in increasing the cross-relaxation times of H and HD by a factor of 6. The concentration of D atoms in HD was one order of magnitude smaller than that of H atoms. The D signals rapidly vanished in the noise within ∼3-4 h after turning off the discharge. However, we anticipate that a substantial amount of D atoms still remained in the film even though their signals lie below our sensitivity threshold. This observation also agrees with the enhancement of the cross-relaxation times for H atoms in the samples containing deuterium (Fig.5.2). Therefore we concluded that the presence of unpaired D atoms is essential for polarizing nuclear spins of H atoms by pumping both forbidden transitions and the center of the ESR spectrum.

Build-up of the H nuclear polarization after pumping the forbidden transitions may be caused by either the Solid or the Cross effect. The Solid effect involves only the electron and nuclear spins of H atom and its efficiency should not depend on concentration of D atoms in the sample. In contrast to that, the Cross effect requires two electron spins which fulfill requirement (5.1). This condition is satisfied for both forbidden transitions of H atoms which have a significant overlap with the ESR lines of atomic deuterium (Figs.5.3 and 5.4). Cross-relaxation proceeds through the three-spin flips when a simultaneous flip of electron and nuclear spins of a hydrogen atom is compensated by a reversal of a single electron spin
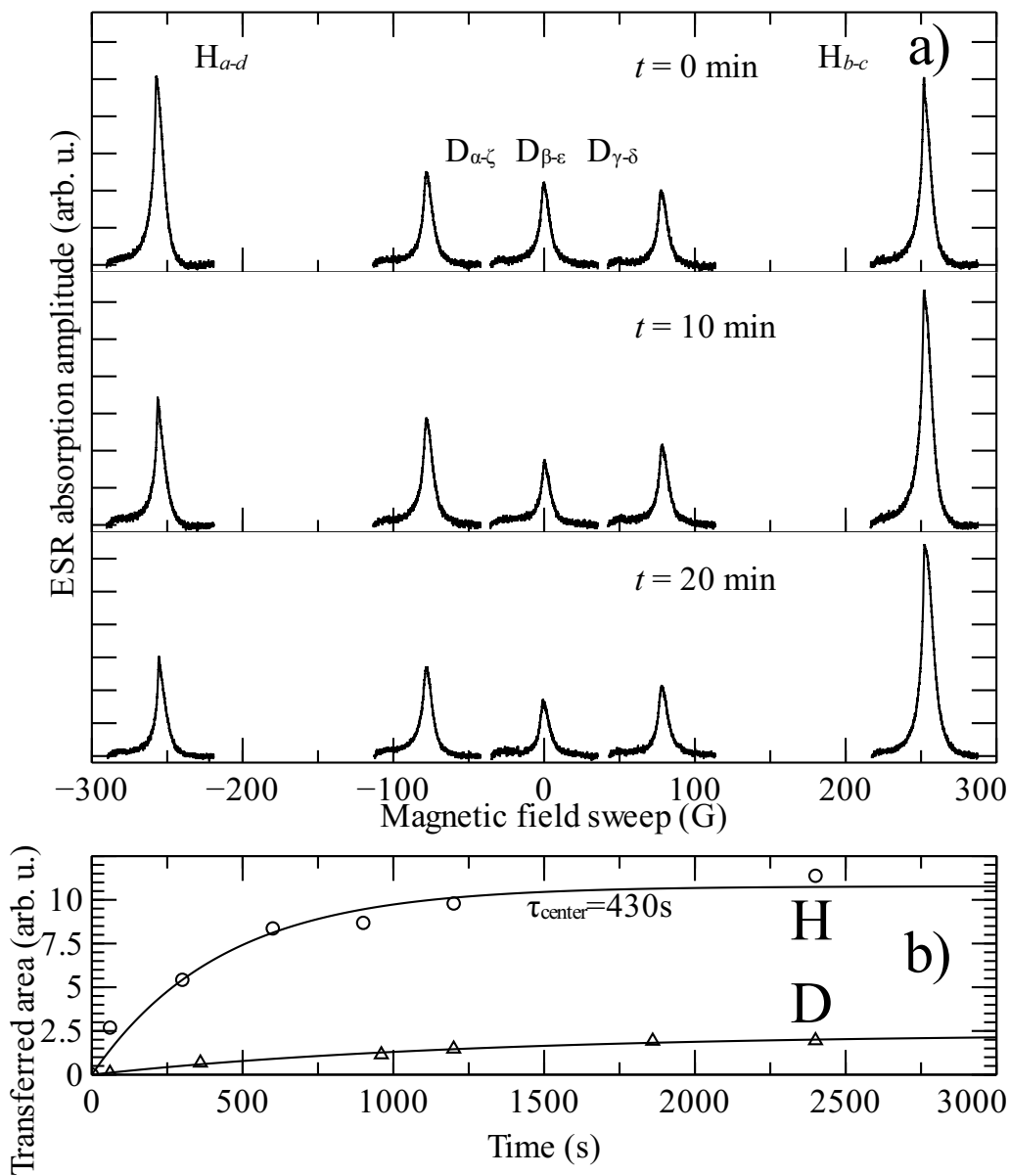
Figure 5.5: a) Time evolution of H and D lines during ESR pumping of the center of the spectrum. b) Transfer of the H (circles) and D (triangles) ESR line areas as a function of the pumping time plotted for the same measurement as in (a) [P2].
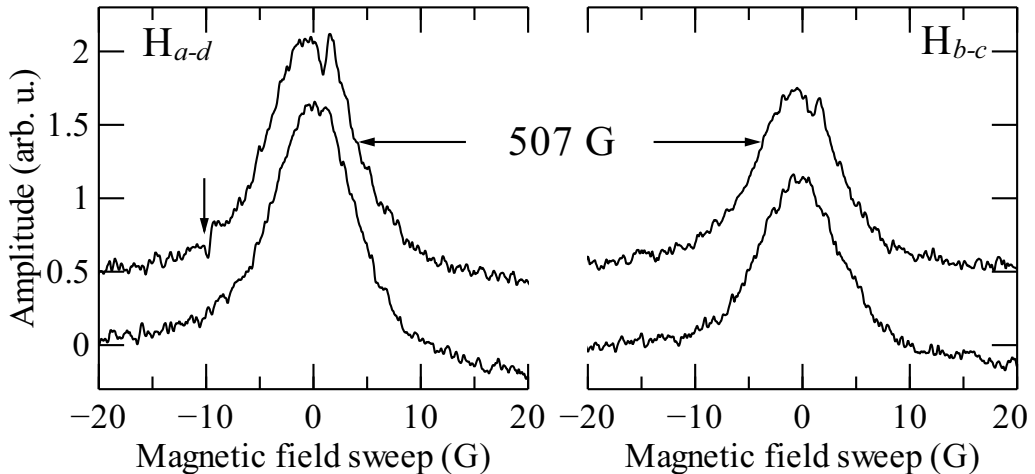
Figure 5.6: The ESR lines of H after pumping the satellite transitions for H in D_2. The hole also appears in the partner ESR line after saturating the satellite transition only at one line. The position of pumping of the satellite transition is shown by the arrow [P2].

of a deuterium atom. A similar effect, enhancement of the nuclear spin-lattice relaxation, was observed previously in hydrated copper salts [128] where matching requirement (5.1) significantly shortened the T_{1N} times.

Both Solid and Cross effects should result in a nuclear polarization of the same sign and distinguishing between them is challenging [129]. However, a dependence of the H DNP efficiency on concentration of D atoms in solid HD leads us to a conclusion that the Cross effect is at least one of the DNP mechanisms involved. The efficiency of the Solid effects scales as κ^2 (eq. 1.7) and it decreases with magnetic field as B^{-2}. In contrast to other observations of the Cross effect reported in literature, it is well resolved in our case and can be effectively used for making DNP.

The most intriguing result is the formation of the H DNP after pumping the center of the ESR spectrum. There are no either allowed or forbidden transitions for unpaired hydrogen atoms and the DNP build-up cannot be explained by the Solid or Cross effect of unpaired H atoms. However, such a transition appears for the pairs of closely residing atoms when there is an appreciable exchange interaction between their electron clouds. A large number of such pairs should be generated during the course of the isotopic exchange reactions $D+H_2 \rightarrow HD+H$ and $D+HD \rightarrow D_2+H$. The H atoms should be extremely stable in D_2 because their diffusion is completely suppressed at low temperatures. Formation of such pairs was also observed in semiconductors, such as phosphorus doped silicon, Si:P [130, 131]. The ESR line of the exchange coupled P pairs appears in the spectrum at the phosphorus concentration $\sim 6\times 10^{16} cm^{-3}$ [130]. The size of a hydrogen atom is much

smaller than that of a phosphorus donor and much higher concentrations of atoms are required in order to observe this transition. The distance between such H or D atoms, two lattice constants, (Table 1.2) is too large for having a strong enough direct exchange interaction [2] and the superexchange may be responsible. We are unable to detect the ESR signal of the pairs directly due to their scarcity. However, the build-up of H DNP after pumping the center of the spectrum supports this suggestion.

Formation of the stable atomic pairs was confirmed indirectly in the experiments with ESR pumping of the satellite transitions of H atoms in solid D_2 (see Chapter 3). It turned out that saturating a satellite transition of one of the H ESR lines leads to burning holes in both ESR lines. No holes were observed in the lines of atomic deuterium.

This observation may be explained assuming that a certain fraction of H atoms are separated from each other by a distance of two lattice constants and share same D_2 molecules. A hole in the partner ESR line may appear for the pairs formed by atoms of different hyperfine states, H_a and H_b. Considering unpolarized ESR lines, the depth of a hole in the H_b line after saturating the satellite transition at the H_a line should be a factor of $3/2$ smaller which also agrees with that observed experimentally (Fig.5.6). The exchange coupled radical pairs may also be identified by a signal at half magnetic field which corresponds to the $\Delta m_S = \pm 2$. The half-field transitions of the H and D radical pairs stabilized in solid rare gas matrices were directly observed by X-band ESR by the group of L. Knight [132, 133]. The amplitude of these transitions are of the order of 10^4 smaller compared to the hyperfine lines of the isolated atoms which requires samples with a large absolute number of spins. The films studied in our work, $\sim 100\,\text{nm}$, are much thinner than typical samples in the matrix isolation experiments, $\sim\text{mm}$, which does not allow us to observe the half-field transitions directly.

Further studies may provide more evidence for better understanding of these effects.

Chapter 6

Experiments with tritium

Accumulation of atoms by β-decay of tritium may lead to the highest concentrations of unpaired atoms in solid hydrogen matrices compared to other methods. It was demonstrated [29, 134] that lowering the temperature of the tritiated matrix below $1\,\mathrm{K}$ may allow storing substantially larger densities of atoms. However, no quantitative experimental studies were performed in this temperature range. Motivated by that, we carried out a series of experiments with pure solid T_2 and T_2:H_2 mixtures in order to clarify optimal conditions for reaching the highest concentrations of hydrogen atoms in solid matrices of hydrogen isotopes. In this chapter, we present a survey of our experiments with solid hydrogen matrices where unpaired atoms were accumulated due to β-decay of tritium. The main results discussed in this chapter are published in paper [P6].

6.1 Introduction

There is a number of methods for accumulating unpaired hydrogen atoms in solid matrices of hydrogen isotopes. Among them are condensing products of discharge onto a liquid-helium cooled substrate (flash condensing) [46, 58] or directly into superfluid helium (impurity-helium condensates) [47, 110], bombardment of a solid hydrogen sample by high-energy electrons [50], γ-ray radiolysis [11], depositing products of 3-body recombination of H atoms in the gas phase, *in situ* cryogenic rf discharge [23, 51], admixing β-radioactive tritium to the gas mixture prior to deposition [54]. The highest concentrations of H atoms in pure H_2 are achieved so far using the method of cryogenic discharge, $\sim 3.5 \times 10^{19} \mathrm{cm}^{-3}$ [51]. Accumulation of H atoms H_2 by tritium decay led to somewhat lower concentrations, $\simeq 5 \times 10^{18} \mathrm{cm}^{-3}$ [79], however concentrations of T atoms, $\sim 10^{20} \mathrm{cm}^{-3}$, were reached while storing pure solid T_2 samples [79] (Table 6.1).

Employing β-decay of tritium for generating unpaired atoms in molecular matrices was pioneered by Lambe [136] who studied radiation induced defects in solids and by Sharnoff and Pound [49] who admixed tritium for producing D atoms in

Method	[H] (cm^{-3})	T (K)	Ref.
Flash condensing	1(18)	1.3	[52]
Radiolysis	8(16)	4.2	[108]
Impurity He condensates*	1(19)	1.3	[135]
Electron bombardment	1(19)	1.4	[50]
3-body recombination	1(18)	0.3	[28]
Cryogenic rf discharge	3(19)	0.7	[51]
Tritium β-decay **	1(20)	2.1	[79]

Table 6.1: Comparison of the maximum concentrations of unpaired H atoms obtained in solid matrices of hydrogen isotopes by different dissociation methods. *: in solid krypton, **: for T in T_2.

a solid D_2 matrix at T=4.2 K. Webeler [29] studied bulk samples of H_2:0.02% T_2 calorimetrically at temperatures 0.2-1 K and reported both spontaneous and stimulated spikes of the sample cell temperature which were attributed to instantaneous recombination of a large number of unpaired atoms in the matrix. The concentrations of H atoms reached in this experiment were estimated indirectly as $\simeq 5 \times 10^{17} \text{cm}^{-3}$. Collins et al. [30] carried out a quantitative study of tritiated hydrogen hosts using ESR as a detecting tool and confirmed that the sample cell temperature spikes are accompanied by a sudden decrease of the concentration of unpaired atoms in the matrix. Later Mapoles et al. [137] reported that the heat bursts also produce $\simeq 1$ ms long light flashes. Zeleznik [138] and Rosen [134] modeled the development of such thermal explosions in tritiated H_2 and predicted that lowering the storage temperature should significantly increase the concentrations of unpaired atoms. This was confirmed by Collins et al. [79] who achieved higher concentrations of T atoms in solid T_2 samples upon lowering temperature and finally reached [T]$\simeq 10^{20} \text{cm}^{-3}$ at T=2.1 K.

In the course of our experiments with solid HD and D_2:HD mixtures (Chapter 4) we observed a high efficiency of isotopic exchange reaction D+HD$\rightarrow D_2$+H at temperatures $\sim$100 mK. We also expected that the isotopic exchange reactions of tritium and hydrogen in T_2:H_2 mixtures should lead to an efficient T-to-H conversion:

$$\text{T}+\text{H}_2 \rightarrow \text{TH} + \text{H} \tag{6.1}$$

$$\text{T}+\text{TH} \rightarrow \text{T}_2+\text{H}. \tag{6.2}$$

The rates of reaction (6.1) were calculated for a wide temperature range by Truhlar et al. [139] and Aratono et al. [140] who predicted a high reaction rate, k^{ex}=1.4$\times 10^{-25} \text{cm}^3\text{s}^{-1}$, at T=1.3 K. The rates of reaction (6.2) at low temperatures are expected to be few orders of magnitude lower in analogy to the isotopic exchange reactions of deuterium atoms with H_2 and HD molecules. The only experimental observation of reaction (6.1) at low temperatures was reported so

far by Aratono et al. [141] who produced tritium atoms in liquid helium *in situ* by neutron bombardment. The authors were unable to deduce the rates of reaction (6.1) but reported on a large isotope effect for reactions $T+H_2 \rightarrow TH+H$ and $T+D_2 \rightarrow TD+D$, $k_{H_2}^{ex}/k_{D_2}^{ex} \approx 150$. A low efficiency of the isotopic exchange reactions of T with D_2 molecules agrees with the conclusions of Collins et al. [77] who reported on the absence of T-to-D conversion in their D-T (25% T_2, 25%D_2, 50% DT) samples stored at 2.1 K.

In our experiments, we studied different possibilities for reaching the highest concentrations of unpaired atoms in the hydrogen films: both in the pure T_2 samples and in the T_2:H_2 solid mixtures where a large fraction of T atoms was expected to be converted into H due to isotopic exchange reaction (6.1).

6.2 Experimental details

6.2.1 Experimental cell

The schematic of the sample cell used in the experiments with tritium is shown in Fig.6.1. The SC design is similar to that described in Section 2. The T_2 and T_2:H_2 mixture films were deposited on the surface of the quartz microbalance directly from the room temperature gas handling system. We preferred this method to the deposition from the sublimation source described in Chapter 2 in order to avoid uncertainties with the isotopic composition of the films. Condensing the gas via the heated capillary from room temperature provided an efficient way to clean the gas from all heavy impurities, such as air or tritiated water. The only concern in this case is the admixture of other hydrogen isotopes. Therefore we did not pay much attention to the chemical purity of the tritium gas and used the cheapest source available. The T_2 gas used in our experiments was extracted from the commercially available tritium vials used as luminescent fishing floats. Each vial contained 5-10 μmol of the T_2 gas which was enough for creating 2-3 samples. However, working with such small amounts of tritium made it difficult to prepare the T_2:H_2 mixtures with the accurately known small admixtures of H_2.

A Ru-oxide bolometer was arranged in a close proximity to the QM for studying the dynamics of explosive recombination of atoms in the films. The bolometer was suspended on fine superconducting wires which assured only a weak thermal coupling to the sample cell walls. The bolometer has a much smaller heat capacity compared to the SC which makes it more suitable for studying the process of thermal explosions. The bolometer thermal time constant, $\tau = R_{th}C$ where C is its heat capacity and R_{th} is the thermal resistance, is much smaller than that of the SC and even tiny amounts of heat may substantially increase its temperature above the environment.

The composition of the gas extracted from the vials was carefully studied with a mass spectrometer. The tritium gas cleaned from ^{3}He contained $\sim$15% of HT as the main impurity. Typically, the main impurity in the T_2 gas immediately after
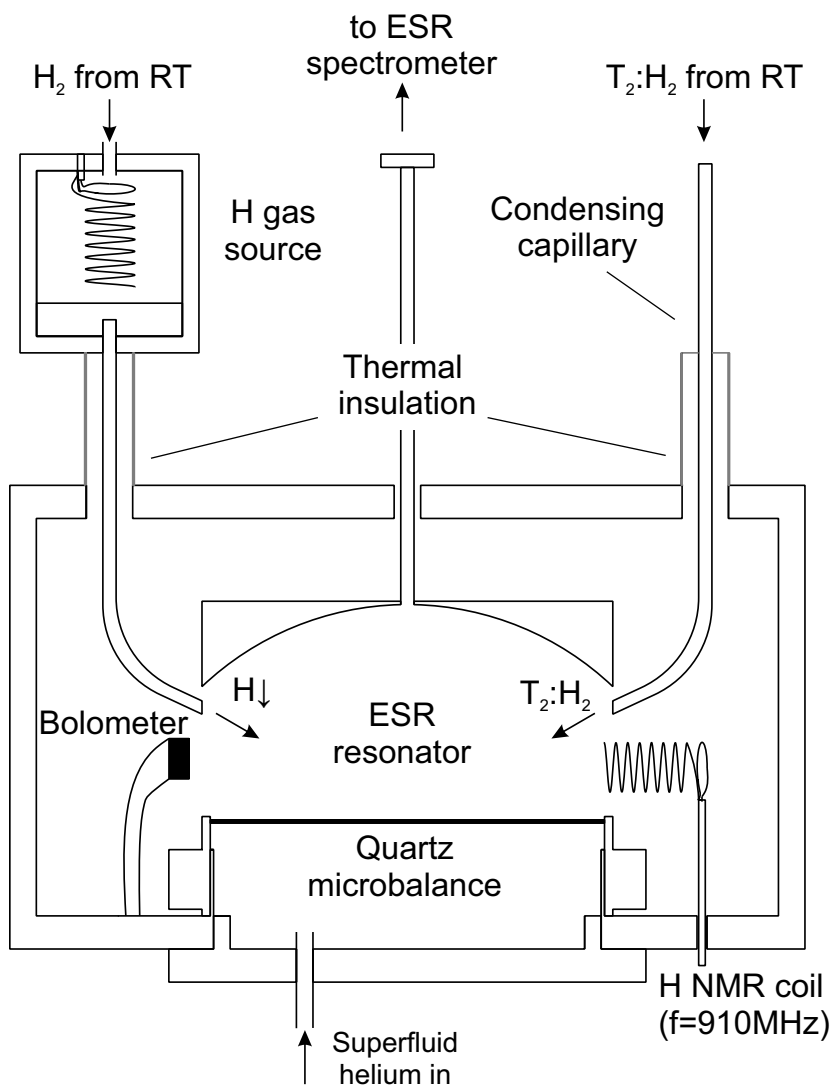
Figure 6.1: Schematic of the sample cell used in our experiments with solid tritium. The rf resonator used to measure the ENDOR spectra of H atoms is labeled as HNMR. Similar coils were also mounted for the T and D ENDOR experiments (not shown on the picture) [P6].

#	s, nm	Composition,%			$n \times 10^{19}$ cm^{-3}			H/(T+H)	
		T$_2$	H$_2$	HT	T	H	total	observed	expected
1.	1000	1	99	-	-	1.0	1.0	1.00	0.99
2.	250	85	-	15	15	2.5	18	0.14	0.08
3.	35	85	-	15	10	1.0	11	0.09	0.08
4.	80	81	4	14	4.2	4.5	8.7	0.53	0.11
5.	300	60	29	11	0.5	10.5	11	0.95	0.35
6.	250	4	95	1	-	2.5	2.5	1.00	0.96

Table 6.2: A summary table for the samples studied in this work. The film thickness is labeled as s. Expected ratios for H and T were calculated from the molecular compositions of the films and considering equal dissociation probability for all molecules of hydrogen isotopes [P6].

production is DT, however a significant HT contamination may appear during storage especially in steel containers [34]. We also observed that the tritium gas purity degraded by $\sim$20% during three months of storage and therefore we used only the fresh T$_2$ gas for creating our samples.

6.2.2 Samples

The main motivation of our experiments with solid tritium was to obtain the maximum concentrations of unpaired H and T atoms. Aimed on that we tried to vary both the thickness and the T$_2$:H$_2$ ratio in our samples. Varying the thickness we tried to reach a compromise between better cooling expected for thinner films and a more efficient production of unpaired atoms in thicker samples. Adjusting the T$_2$:H$_2$ content we aimed on increasing the concentration of H atoms due to isotopic exchange reactions (6.1) and (6.2) which were expected to proceed in the T$_2$:H$_2$ solid mixtures. We studied six samples of different thickness (30-300 nm) and T$_2$:H$_2$ composition (0-99% of H$_2$) (Table 6.2) in order to find a condition where the maximum concentrations of H and T atoms could be achieved.

First we studied a 1000 nm para-H$_2$ sample with a 1% admixture of T$_2$. The sample was stored at $T = 150$ mK for about two weeks. The maximum concentration of H atoms reached there approached $\sim$10^{19}cm^{-3}. We did not observe any signatures of explosive recombination of H atoms during storage even though the H concentration in this sample exceeded more than an order of magnitude that of experiments of Webeler [29] who observed explosive recombination of atoms in bulk H$_2$ samples at [H]$\simeq$5$\times$10^{17}cm^{-3}. Our samples are much better cooled due to a larger surface-to-volume ratio compared to bulk samples studied before which allows us to achieve higher concentrations of unpaired atoms.

A different behavior was observed in Sample 2, a 250 nm "pure" tritium film where we have not added any H$_2$ prior to deposition. In this sample, we observed collective recombination of T and H atoms both being stimulated by the magnetic

field sweeps and appearing spontaneously. The presence of a substantial amount of tritium limited the minimum attainable storage temperatures to 160 mK. Periodic explosive recombination of atoms in the film raised the cell temperature to $\simeq 0.25$ K (Fig.6.6).

We did not observe explosive recombination in a 35 nm pure tritium film (Sample 3). Depositing thinner tritium films also allowed us to cool the SC to 70 mK. However, the maximum concentrations of atoms in this sample were nearly two times smaller than in Sample 2 (Table 6.2). That can be explained by a less efficient use of the kinetic energy of the emitted β-particles which have a penetration depth ($\simeq 3.5\,\mu$m) [68] much larger than a typical thickness of our samples.

In addition to "pure" tritium samples we studied three mixture samples with different T_2:H_2 ratios: 80 nm T_2:4% H_2 (Sample 4), Sample 5: 300 nm T_2:$\simeq 30\%$ H_2 and Sample 6: 250 nm H_2:4% T_2. The total concentrations of atoms reached in these samples were at least 2 times smaller compared to Sample 2. However, we were able to reach the maximum concentration of H atoms in Sample 5 ($\simeq 1 \times 10^{20}$cm^{-3}). The H:T ratios in these samples were much larger than those expected from direct dissociation molecules which provides clear evidence of isotopic exchange reaction (6.1). We did not observe explosive recombination in these samples.

6.2.3   ESR spectra

Depending on the T_2:H_2 content in our samples we observed different ratios of the T and H ESR lines. An ESR spectrum measured in Sample 4 is shown in Fig.6.2. The spectrum contains two doublets corresponding to the H and T lines with the splitting equal to the values of the hyperfine constants: $\simeq 541$ G and $\simeq 507$ G for T and H, respectively (Table 1.1). The dipolar interaction between the electron spins of unpaired atoms influences both the width and the position of the H and T ESR lines. The large concentrations of polarized electron spins lead to a formation of the substantial sample magnetization which alters the local field felt by the atoms (see Chapter 3). The shift and width of the ESR lines as a function of concentration of unpaired atoms in the film measured in Sample 2 are presented in Fig.6.3. The linewidth is linearly proportional to the concentration of atoms which is in accordance with the theory of the dipolar line broadening of Kittel and Abrahams [82]. The positions of the ESR lines of H and T differ by 17 G due to the difference in the values of the hyperfine constants A, and the lines can be easily separated at low concentrations of atoms. Resolving them at concentrations of H and T $\simeq 10^{20}$ cm^{-3} becomes challenging and required an accurate fitting of the ESR spectra. (Inset of Fig.6.3).

For films thicker than ~ 350 nm and high concentration of atoms, the linewidth was influenced by an additional broadening mechanism, radiation damping, which occurs for the spin systems strongly coupled to the ESR resonator. Radiation damping is caused by spontaneous and coherent radiation of energy stored in the
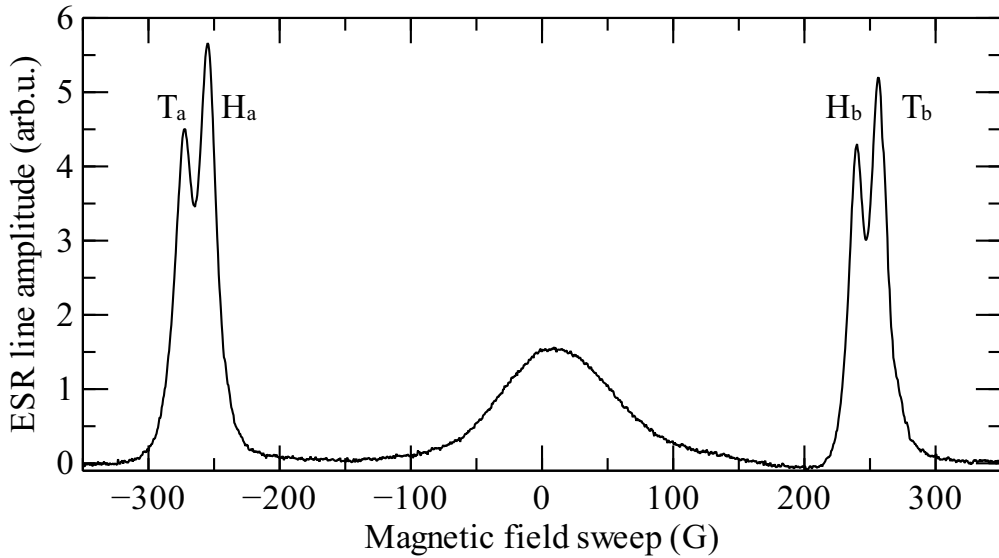
Figure 6.2: An ESR spectrum of H and T atoms measured in the T_2:H_2 mixture (Sample 4). A line of an unknown origin persists in the center of the ESR spectrum [P6].
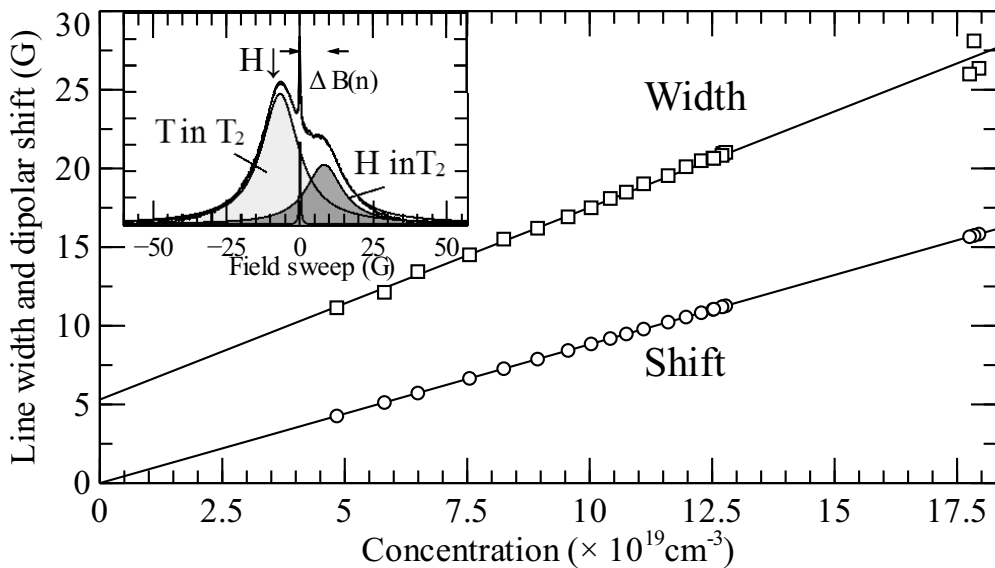

Figure 6.3: The width and shifts of the ESR lines of H and T as a function of concentration of unpaired atoms measured in Sample 2. Inset: a typical ESR spectrum of a low-field $(a - d)$ T and H lines fitted by three Lorentzian curves. The H-gas line used as a reference is labeled as H↓ [P6].

spin system at the spin Larmor frequency [142, 143]. In other terms, the spin system works as a maser [69]. The probability for spins to relax by emitting a photon at frequencies ∼GHz spontaneously is negligibly small, however this probability enhances enormously when the spin system is placed in a high-quality resonator [144]. This can be considered similar to increasing the density of radiating oscillators at a certain frequency over the equilibrium values of the Planck distribution. The radiation damping effects were also observed previously in the high field ESR work with atomic hydrogen in the gas phase [145]. The effects of radiation damping start influencing the ESR linewidth when the spin-spin relaxation time becomes comparable to spin-relaxation due to radiation damping:

$$1/T_2^* = 1/T_2 + 1/T_{rad}. \tag{6.3}$$

The relative line broadening due to radiation damping is greater for narrower ESR lines. The relaxation time due to radiation damping can be estimated as [142]

$$T_{rad} = (2\pi M_0 Q\eta)^{-1}, \tag{6.4}$$

where M_0 is the sample magnetization, Q is the cavity quality factor, η is the resonator filling factor. Substantial broadening from radiation damping was observed in Sample 1. The natural (dipolar) linewidth, $\simeq 2$ G, increased to $\simeq 6$ G due to radiation damping. The effect of radiation damping can be eliminated by detuning the ESR frequency from the frequency of the Fabry-Perot resonator (Fig.6.4). The contribution of the effects of radiation damping was verified for all samples we studied.

A broad, ∼100 G wide line of an unknown nature was observed for all samples containing tritium (Fig.6.2). The line remained in the spectrum after warming the sample cell to $T \simeq 20$ K when the hydrogen films were completely removed from the QM and the cell was evacuated for several hours before creating a new sample. However, this line disappeared after warming the setup to room temperature and cooling again for the next experimental run. Based on these observations we concluded that the unknown signal is of the species in the metallic mirrors of the Fabry-Perot resonator. The large line area also implies large concentrations of these species which should be comparable to those of T and H atoms in the films. The broad central line is reminiscent of the signal of phosphorus donor pairs in silicon coupled by the strong exchange interaction [130, 146] which appears in the ESR spectrum at $[P] \simeq 5 \times 10^{16} \text{cm}^{-3}$. Therefore we think that it can be caused by the clusters of atomic tritium penetrated inside the metallic substrate [147]. A strong exchange interaction of the atoms in these clusters leads to an averaging of the hyperfine interaction, and like in metals, the doublet of the ESR lines merges into a single broad line in the center of the ESR spectrum. Additional work is required to understand better the nature of this line.
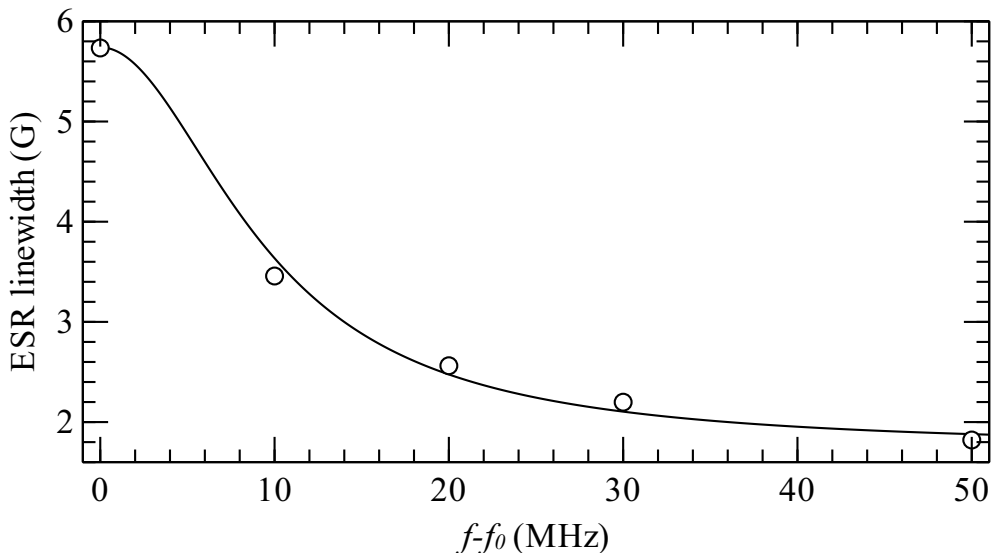
Figure 6.4: The width of the ESR line of H in H_2 (Sample 1) as a function of detuning, f, from the resonance frequency of the Fabry-Perot cavity, f_0. The solid line is shown as a guide for the eye.

6.3   Experimental results

"Pure" tritium films

Accumulation of atoms in the "pure" tritium Sample 2 is shown in Figs.6.5 and 6.6. The ESR lines of T and H in this sample appeared $\simeq$10 minutes after the deposition of the film with a width of $\sim$5 G and grew monotonously. Accumulation of atoms in the film was periodically interrupted by explosive recombination upon reaching total concentrations [T]+[H]$\simeq$1.8$\times$10^{20}cm^{-3}. The thermal explosions were initiated both by the magnetic field sweeps when the sample cell temperatures increased to $\simeq$180 mK and occurred spontaneously. Typically $\sim$1/4 of atoms recombined in the thermal explosion which also led to sublimation of $\simeq$5% of molecules from the QM surface (Fig.6.6).

We did not observe explosive recombination in a similar experiment with a thinner, 35 nm T_2 film (Sample 3). The total [H]+[T] concentration of atoms in this sample, $\simeq$1.2$\times$10^{20}cm^{-3}, was smaller than in Sample 2 (Table 6.2). Smaller concentration of unpaired atoms in the film may be explained by a reduced efficiency of dissociation of atoms in thinner samples. The estimated penetration depth for 5.7 keV is $\simeq$3.5 μm [68] and the emitted β-particles dissociate less molecules in the film before escaping.

Adding helium to the sample cell resulted in accumulation of a weak line of H atoms in the gas phase. The atoms produced in dissociation of molecules by β-particles acquire substantial kinetic energies and travel a distance of the order of
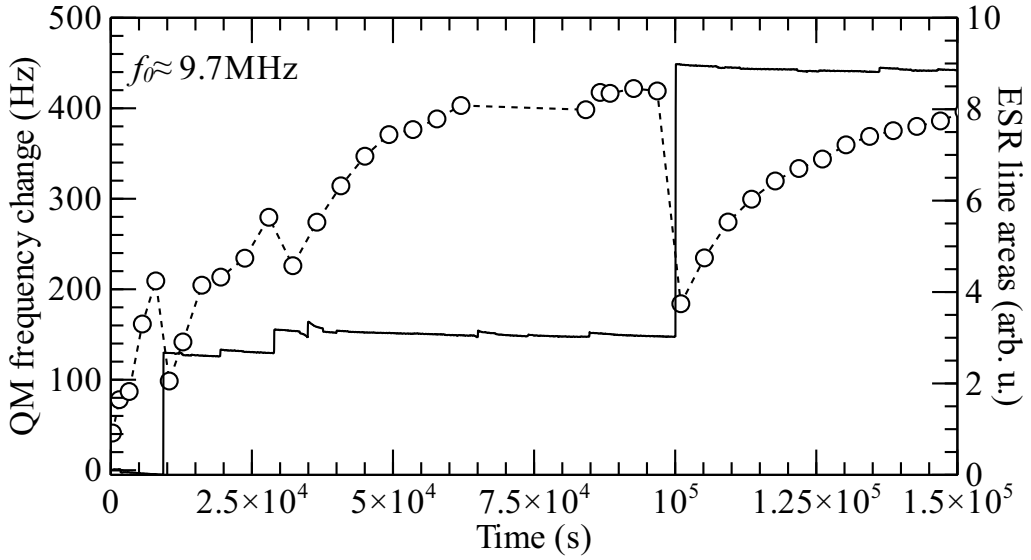
Figure 6.5: Evolution of the ESR line areas of H+T and the QM response to explosive recombination of atoms in Sample 2 [P6].
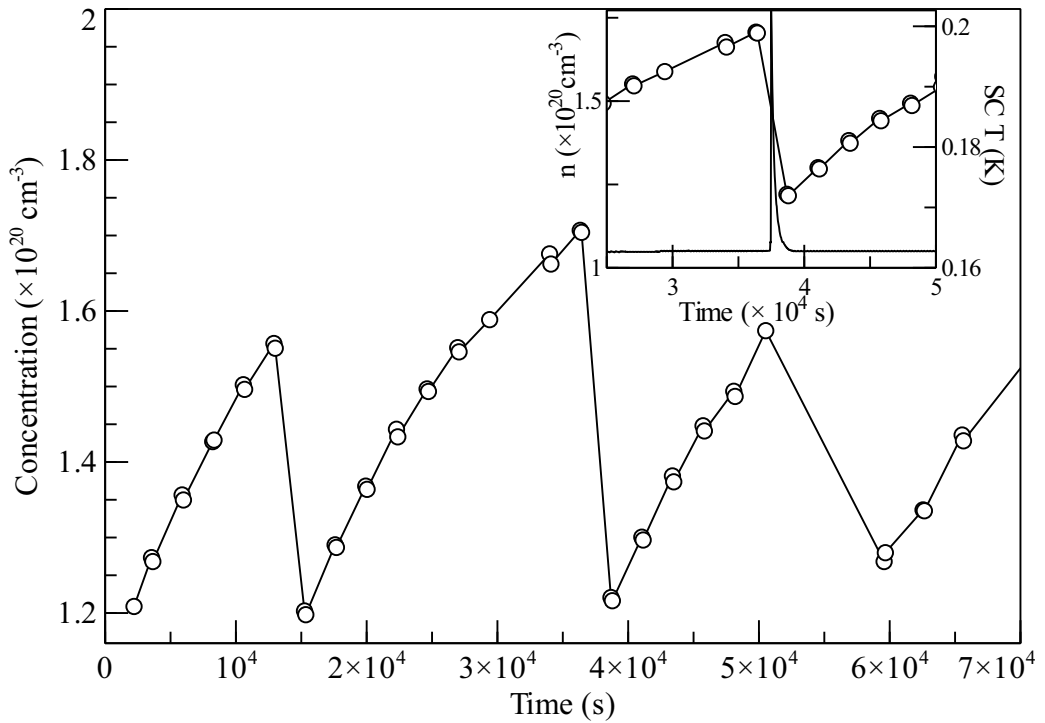

Figure 6.6: Time evolution of the total H+T concentrations in Sample 2. Inset: a sudden increase of the sample cell temperature due to explosive recombination of atoms in the film [P6].
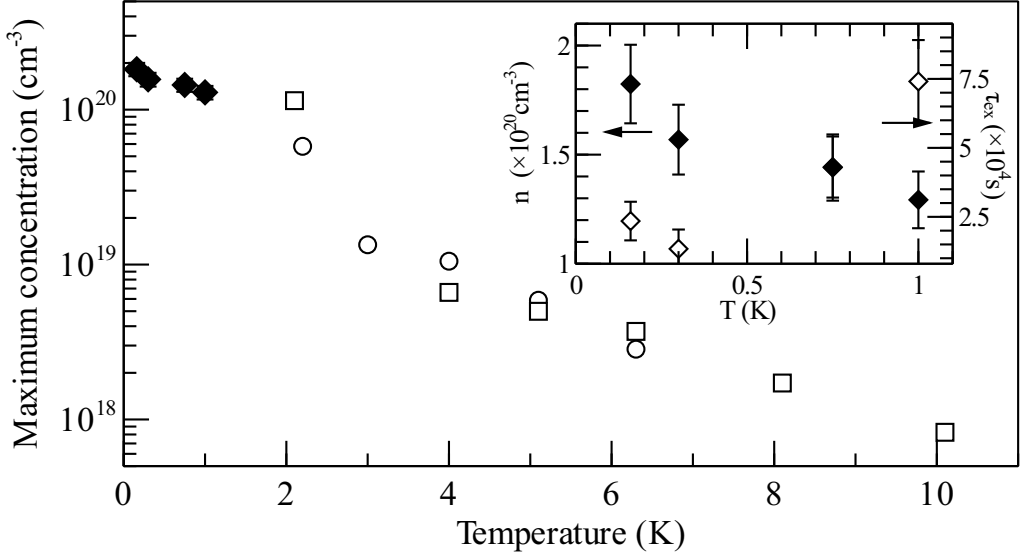
Figure 6.7: Maximum concentrations of unpaired atoms achieved in Sample 2 at different storage temperatures (filled diamonds). The open points are the results of Collins et al. [79] measured for T in T_2 (open squares) and D and T in D-T (25% T_2, 25% D_2, 50% DT) (open circles) in bulk samples. The inset: the maximum concentrations (filled diamonds) and the periodicity of the thermal explosions measured in Sample 2 (open diamonds) [P6].

several lattice constants before being thermalized and trapped in the matrix [50]. Some of these atoms may escape from the film and remain in the gas phase when the surface recombination of atoms is suppressed. However, we have not observed the ESR lines from the T atoms in the gas phase. Two-body surface recombination for T atoms should be much faster than that for H [148]. Moreover, the chemical potential for dissolving T atom in liquid ^{4}He is only slightly positive and T atoms might sink in ^{4}He, which may explain why we were unable to accumulate a measurable amount of the spin-polarized tritium gas [149, 150].

The T:H ratios in "pure" tritium samples (Samples 2 and 3) were ~6 for Sample 2 and ~10 for Sample 3. These ratios differ only by a factor of ~1.5 from the ratios expected from direct dissociation of molecules in the films assuming that our "pure" tritium films contained 15% of HT. The T:H ratios we observed provide evidence of a very low efficiency of the isotopic exchange reaction (6.2).

The matrix width of T and H atoms in the "pure" T_2 films, $\simeq 5$ G, is much larger than that in para-H_2 and normal (75% ortho, 25% para) H_2 matrices. It is unlikely that it is caused by the magnetic moments of ortho-T_2 because large concentrations of unpaired atoms efficiently catalyze the ortho-para conversion of tritium molecules. The nearest molecules should be converted within ~10 s and the conversion time for the sample as a whole is ~1000 s [84].

The matrix width of T atoms in pure T_2 measured in ref. [77] (Table 3.2) is much smaller than that in the present work. Therefore we suggest that the main contribution to the matrix width in our samples appears due to a presence of a large number of HT molecules in a close neighborhood to unpaired T and H atoms. Similar to other hydrogen matrices, we observed weak signals from electrons trapped in the matrix [P3], however these lines were seen for a short time after the film deposition and disappeared from the spectrum within a few hours. We did not detect any ionic species, such as H_2^+ or H_2^- (T_2^+ or T_2^-) which may be explained by a much smaller yield compared to unpaired atoms [94]. The most stable ionic species, such as H^+ and H_3^+ (T^+, T_3^+) have zero electron spins and cannot be detected by ESR.

Accumulation of atoms due to β-decay of tritium obeys the differential equation:

$$\frac{d[T]}{dt} = k([T_2] + \frac{1}{2}[HT]) - k^r[T]^2,\tag{6.5}$$

where k is the accumulation rate due to β-decay of tritium, k^r is the recombination constant. Fitting the experimental points of accumulation in Sample 2, we extracted the value of the accumulation rate k, from which it follows that each β-particle produces about 50 unpaired atoms. This value is close to the estimate of Sharnoff and Pound: 22 atoms per β-particle [49].

Thermal explosions

In our study of the effect of storage temperatures on the atomic concentrations and appearance of explosive recombination, we stored Sample 2 at four different temperatures: $160, 300, 750$ mK and 1 K. Increasing the storage temperature led to smaller concentrations of atoms reached. In addition to that, we observed longer time delays between the thermal explosions at higher temperatures. These results are presented in Fig.6.7. The results reported by Collins et al. [77] are also added to the plot for the sake of comparison. The explosion periodicity as the function of temperature is shown in the inset.

We attempted to study the dynamics of the thermal explosions using a bolometer. However, the events of explosive recombination developed too fast to resolve them reliably with the bolometer. A typical response of the bolometer to an explosion event is shown in Fig.6.8. The time interval which corresponds to the occurrence of the explosion is magnified in the figure inset. The bolometer temperature increases within about 0.2 s which is limited by its intrinsic response time. This is much larger than the duration of the flashes observed by Mapoles et al. [137], ≤ 1 ms.

We also simulated the heating effect of a typical thermal explosion by applying a current pulse to the heater installed on the sample cell body. The result of applying a 17 ms long $P = 22$ mW ($P = I^2R$) pulse and the result of a thermal explosion are shown in Fig.6.9. We found that the thermal explosion shown in
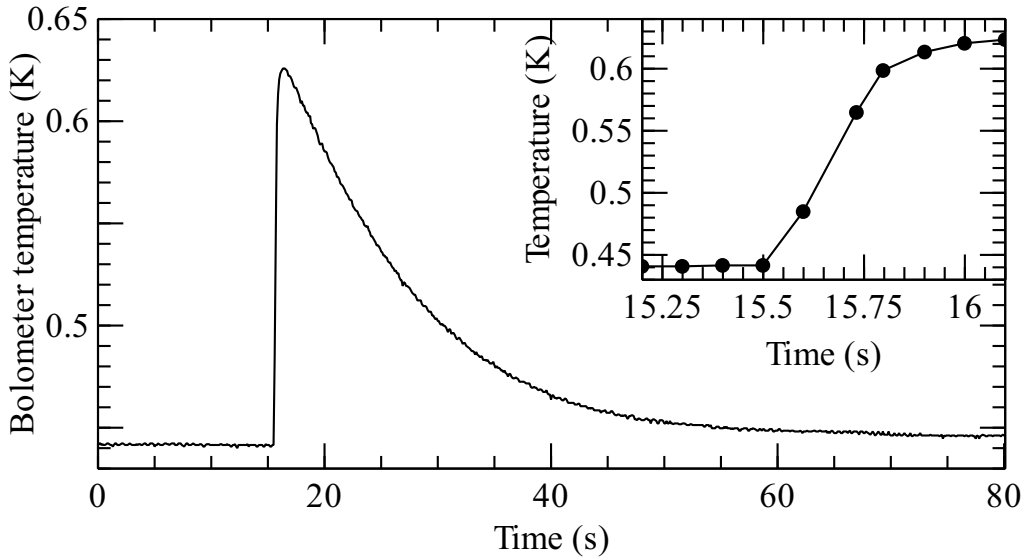
Figure 6.8: Bolometer response to explosive recombination of atoms in Sample 2. The sudden increase of the bolometer temperature due to the explosion is magnified in the inset [P6].
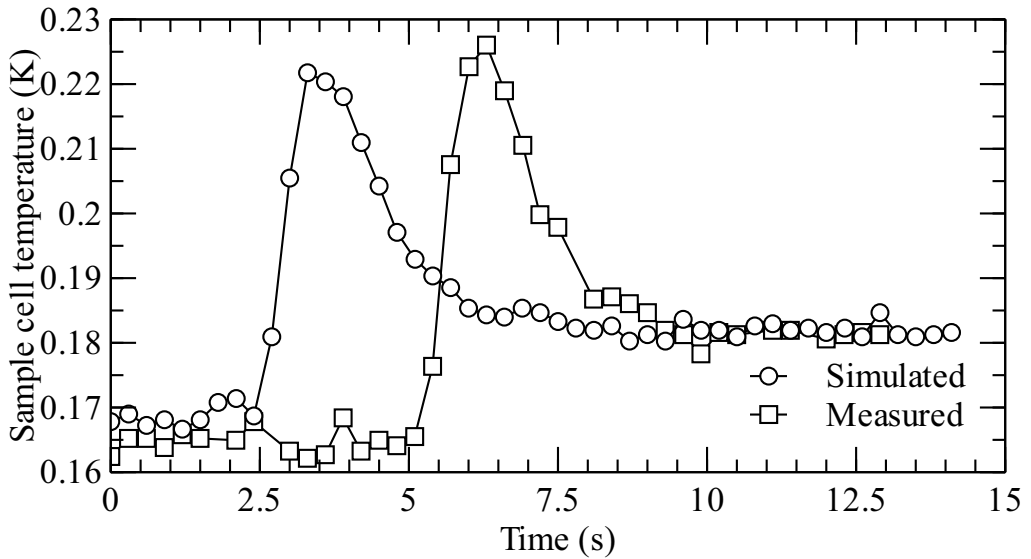

Figure 6.9: Evolution of the sample cell temperature during a thermal explosion (squares) and after applying a heat pulse using the SC electric heater (circles).
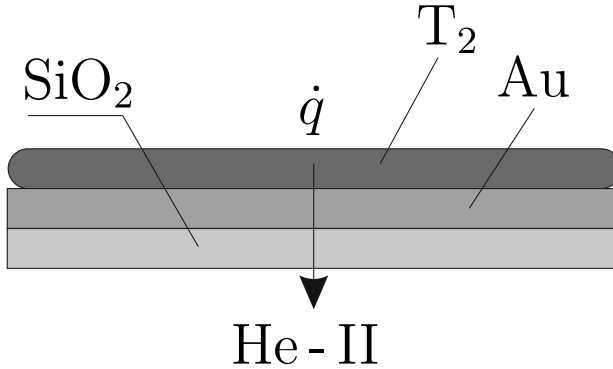
Figure 6.10: Schematic of the heat conductance from the T_2 film to superfluid helium below the QM. The bottom gold electrode has a key-hole shape, it covers only a fraction of the quartz disc and was omitted from the analysis.

Fig.6.6 is caused by the collective recombination of $\simeq 1 \times 10^{15}$ atoms. This value is in a good agreement with that estimated from the decrease of the ESR line area.

The heat released in explosive recombination of atoms can be removed from the sample either by sublimation of molecules or conducted from the tritium film to superfluid helium below the QM via several interfaces: T_2 film-gold film-quartz-superfluid helium (Fig.6.10). Considering that the recombination heat is released during a certain duration of time, τ_{ex}, long enough to ensure a steady flow of heat through all these interfaces. For evaluating the energy E_{ex} released in the explosion we considered a typical burst where 10^{15} atoms recombine and 5% of the film becomes sublimated due to that. Assuming the sublimation heat of T_2 molecules, $J_{subT_2} \simeq 1400\,\text{J/mol}$ [34], about 2/3 of the released energy should be removed by heat conductance to superfluid helium. Then, taking the steady heat flux during the explosion, $\dot{q} = E_{ex}/\tau_{ex}$, we calculate the tritium film overheating as a function of the time τ_{ex}. We use a simple heat balance model similar to that discussed by Wyatt [151]:

$$\dot{q} = AG_{ij}(T_i^n - T_j^n), \tag{6.6}$$

where $\dot{q}$ is the power released during collective recombination of atoms, A is the QM surface area ($1\,\text{cm}^2$), G_{ij} is the boundary Kapitza conductance between the interfaces, T_{ij} are the temperatures of the different layers, n is the integer, $n = 4$ for the solid-solid interface, $n = 5$ for the interface between solid and superfluid helium. The bottleneck of the heat transfer is the interface between tritium film and the gold top QM electrode. Equation (6.6) can be modified using the expression for a phonon flux from layer i to layer j through the interface [152]:

$$\dot{q} = A\frac{\pi^2 k_B^4 \rho_i v_i}{30\hbar^3 \rho_j v_j^3}(T_i^4 - T_j^4), \tag{6.7}$$

where ρ are the densities of two media and v are the transverse sound velocities
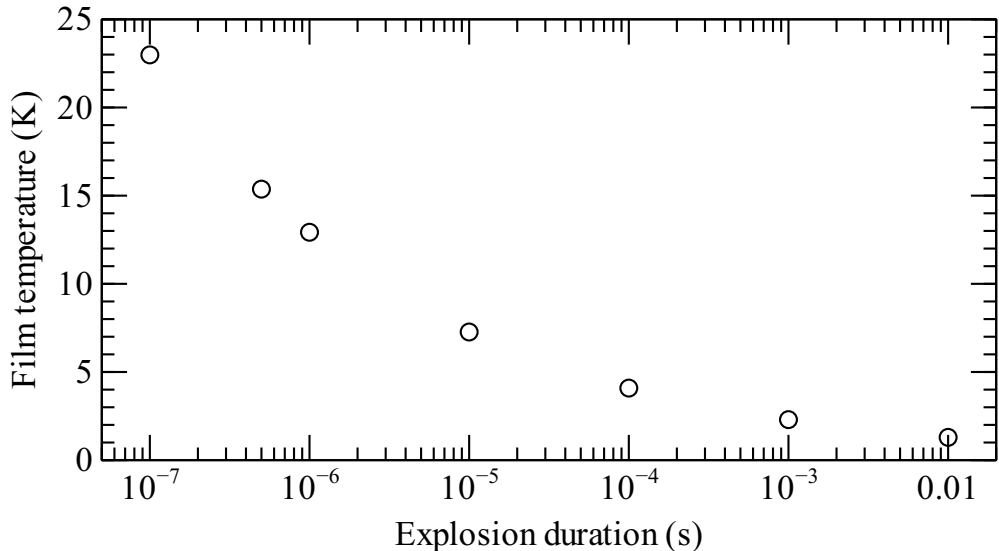
Figure 6.11: Sample temperature as a function of the burst duration based on model (6.6).

[153]. The sample temperature as a function of the duration of the recombination event calculated by the model (6.6) is shown in Fig.6.11. Assuming that the sublimation of the tritium film starts at temperatures $\geq 10\,\mathrm{K}$, the duration of the recombination event must be of the order of $\tau_{ex} \sim 10^{-6}\,\mathrm{s}$. The model does not take into account the heat losses due to the finite heat capacities of the film and quartz disc and the heat conduction through the copper wires glued to the QM electrodes.

T_2:H_2 mixture films

We studied three T_2:H_2 mixture samples: Samples 4, 5, 6 (Table 6.2). The maximum total concentrations were achieved in Sample 5: $\simeq 1.1 \times 10^{20}\mathrm{cm}^{-3}$ while only the modest concentrations were reached in Samples 4 and 6: $8.7 \times 10^{19}\mathrm{cm}^{-3}$ and $2.5 \times 10^{19}\mathrm{cm}^{-3}$, respectively. The maximum concentration of H atoms was also obtained in Sample 5: $1.05 \times 10^{20}\mathrm{cm}^{-3}$. The main distinct feature of the samples containing H_2 is the much larger ratios of the ESR lines of H and T than those expected from direct dissociation of H_2 and T_2 molecules by the β-particles. This provides evidence of T-to-H conversion due to isotopic exchange reaction (6.1).

The time evolution of H, T and total [H]+[T] concentrations in 80 nm T_2:4% H_2 film (Sample 4) stored at 70 mK is shown in Fig.6.12. The T:H ratio remained nearly 1:1 during the whole measurement. The total concentrations of atoms stopped increasing at $t = 80000\,\mathrm{s}$ but the H signal continued to grow even after this point. We suggest that this may be explained by a contribution from the slower reaction (6.2).
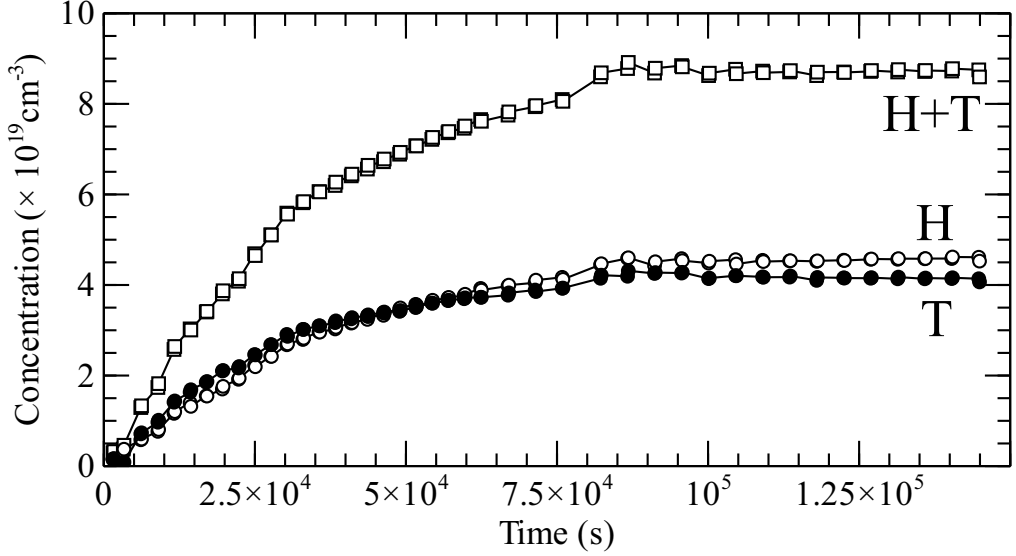
76

Figure 6.12: Time evolution of the T (filled circles), H (open circles) and total T+H (open squares) concentrations in Sample 4 stored at $70\,\text{mK}$ [P6].

Curve	k $(\text{cm}^{-3}\text{s}^{-1})$	$k^{ex}/[\text{H}_2]$ $(\text{cm}^3\text{s}^{-1})$	k^r $(\text{cm}^3\text{s}^{-1})$
dotted	3×10^{14}	3.4×10^{-26}	1.1×10^{-24}
dashed	5×10^{14}	2.2×10^{-26}	8.8×10^{-25}
solid	7×10^{14}	1.0×10^{-26}	6.4×10^{-25}

Table 6.3: Parameters used to fit the experimental data presented in Fig.6.12.

The evolution of the T and H concentrations follows differential equations

$$\frac{d[\text{T}]}{dt} = 2F([\text{T}_2] + \frac{1}{2}[\text{HT}]) - K^{ex}[\text{T}][\text{H}_2] - K^r_T[\text{T}]^2 - K^r_H[\text{T}][\text{H}] \qquad (6.8)$$

$$\frac{d[\text{H}]}{dt} = 2F([\text{H}_2] + \frac{1}{2}[\text{HT}]) + K^{ex}[\text{T}][\text{H}_2] - K^r_H[\text{H}]^2 - K^r_{TH}[\text{T}][\text{H}] \qquad (6.9)$$

where K^{ex} is the second-order rate constant of reaction (6.1), K^r are recombination constants. In this analysis, we neglected the contribution from the isotopic exchange reaction (6.2) which appeared to be rather inefficient. It turned out that the T and H lines appeared in the spectrum nearly equal which provides evidence of the very fast rate of the isotopic exchange reaction (6.1). The life-time of a D atom near a H_2 molecule was estimated in ref. [48] as $\sim60\,\text{s}$. The 1:1 ratio of T:H lines from the very beginning of the measurement provides evidence of a similar life-time of the T atom near a H_2 molecule.

Having [H]=[T] during the course of measurement, the [H] growth rate, $\frac{d[H]}{dt}$, can be fitted by the parabolic function $f(x) = k + k^{ex}x - k^r x^2$, where $x = [\text{T}], [\text{H}],$
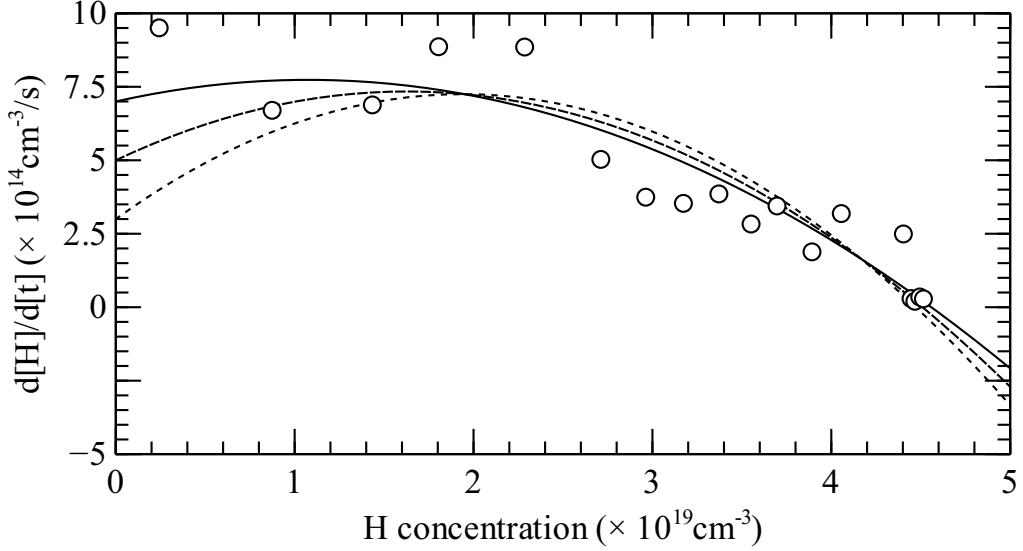
Figure 6.13: Fitting of experimental data by rate equation 6.8. See Table 6.3 for the fitting parameter.

$k = 2F([\mathrm{T}_2] + \frac{1}{2}[\mathrm{HT}])$, $k^{ex} = K^{ex}[\mathrm{H}_2]$ and $k^r = K_{TH} + K_H$ is the effective recombination constant. The experimental points were fitted by three different parabolic functions where k was adjusted as a parameter. It was constrained between $3 \times 10^{14} \mathrm{cm}^{-3} \mathrm{s}^{-1}$ and $7 \times 10^{14} \mathrm{cm}^{-3} \mathrm{s}^{-1}$. These limits were estimated from the comparison of with the constant accumulation rate of tritium measured in Samples 3 and 5 taking into account the T_2 and H_2 and HT content. The lower limit comes from the assumption that Sample 4 contains 4% of H_2 and 14% of HT (Table 6.2). The parameters used in fitting presented in Fig.6.13 are also collected in Table 6.3.

From experimental points shown in Fig.6.12 we extracted the values for $K^{ex} = 3(2) \times 10^{-26} \mathrm{cm}^3 \mathrm{s}^{-1}$ and $k^r = K_{TH} + K_H = 10(5) \times 10^{-25} \mathrm{cm}^3 \mathrm{s}^{-1}$. The large error margins are caused by an uncertainty in the H_2 admixture in the film. The rate of exchange reaction (6.1) found in this work is smaller than that calculated by Aratono et al. [140] for $T = 1.3 \, \mathrm{K}$ ($1.4 \times 10^{-25} \mathrm{cm}^3 \mathrm{s}^{-1}$). The recombination rates are however in a good agreement with that of T in pure T_2 at $2.1 \, \mathrm{K}$ reported by Collins et al. [77]. Estimating the rate of reaction (6.2) is more challenging and requires more sophisticated analysis. Also a longer measurement may be required.

6.4 Discussion

Similar to recombination of H and D atoms in the H_2 and D_2 matrices, recombination of tritium atoms also proceeds in two stages: approaching of two atoms towards each other by a distance equal to the lattice constant and the recombina-

tion reaction itself. Diffusion of D and H atoms in the D_2 and H_2 solids at temperatures below $\simeq 4\,K$ proceeds by the repetition of tunneling exchange reactions $H+H_2 \rightarrow H_2+H$ and $D+D_2 \rightarrow D_2+D$. A similar exchange reaction, $T+T_2 \rightarrow T_2+T$ may also be expected to proceed in a solid T_2 matrix. The recombination rates of H in H_2 fairly coincide with the rates of reaction $H+H_2 \rightarrow H_2+H$, $k \sim 10^{-25} cm^3 s^{-1}$, calculated for low temperatures within the gas-phase model [115]. The recombination rates of T in T_2 measured in this work: $K^r \sim 10^{-25} - 10^{-24} cm^3 s^{-1}$ are much larger than the expected rates of the exchange reaction $T+T_2 \rightarrow T_2+T$. The recombination rates measured experimentally may be somewhat constrained by the energy level mismatch and the pure rates may be even higher.

Based on these arguments we suggest that the fast motion of atoms in the samples created by β-decay of tritium is caused by their physical diffusion related to the formation of vacancies in the lattice. β-decay of tritium may result in a generation of a large number of non-equilibrium vacancies and phonons which may significantly enhance physical diffusion of H and T atoms. Ebner and Sung showed [53] that such diffusion may proceed either through tunneling or hopping to a vacant site. The phonons may not only compensate for the energy level mismatch but also help the atoms to surmount the diffusion barrier. Recombination of atoms brings extra heat to the lattice which enhances diffusion and recombination of atoms. This process has a positive feedback and it finally ends up in a rapid acceleration of recombination and the thermal explosion of the samples.

The fact that only a fraction of atoms recombines in the thermal explosions we observed may be explained by higher stability of atoms residing more close to the substrate while the atoms at the top of the film recombine preferentially. This also explains the absence of thermal explosions in thin films and suppression of spontaneous explosive recombination after adding helium to the sample cell. Helium provides better cooling for the upper surface of the film and stabilizes unpaired atoms.

Conclusions and future prospects

In this thesis we presented the results of an experimental study of H, D and T atoms stabilized in solid matrices of hydrogen isotopes at temperatures down to 70 mK. We employed different techniques for dissociating matrix molecules: a cryogenic rf discharge and dissociation by high-energy electrons released in β-decay of tritium. The maximum concentrations of H atoms we reached using the first method approached $\sim 4 \times 10^{19} \text{cm}^{-3}$. Even higher concentrations of unpaired atoms were achieved using the second technique: $[\text{T}] \simeq 1.8 \times 10^{20} \text{ cm}^{-3}$ in pure T_2 samples and $[\text{H}] \simeq 1.0 \times 10^{20} \text{cm}^{-3}$ in solid mixtures of T_2 and H_2. However these concentrations turned out to be still insufficient for the observation of quantum phenomena related with the BEC or superfluidity of trapped hydrogen atoms.

Studying solid mixtures of hydrogen and deuterium (H_2, HD and D_2) we observed a high efficiency of the isotopic exchange reactions $\text{D} + \text{H}_2 \rightarrow \text{HD} + \text{H}$ and $\text{D} + \text{HD} \rightarrow \text{D}_2 + \text{H}$. We were also able to measure the rate of the latter reaction in pure HD, $k^{ex} \sim 3 \times 10^{-27} \text{ cm}^3 \text{s}^{-1}$, which did not change within the temperature range 0.13-1.5 K. This measurement supports the quantum-tunneling nature of this reaction and suggests that it may proceed with a high enough rate down to the absolute zero of temperature. The reaction has a 4 times smaller rate, $k^{ex}_{D_2} = 9(4) \times 10^{-28} \text{cm}^3 \text{s}^{-1}$, in solid D_2:0.23%HD where its rate did not change after raising temperature to 1.35 K. This observation suggests that the observed rate is not limited by diffusion of the reactants but by the reaction itself.

Similar exchange reaction $\text{T} + \text{H}_2 \rightarrow \text{HT} + \text{H}$ was observed in solid T_2:H_2 mixtures. The second reaction $\text{T} + \text{HT} \rightarrow \text{T}_2 + \text{H}$ was found to be much less efficient. We also provide our estimate for the rate of the former reaction, $k^{ex} = 3(2) \times 10^{-26} \text{cm}^3 \text{s}^{-1}$. The maximum concentrations of H and T atoms in the samples of solid T_2 and T_2:H_2 were limited by the recombination of atoms which was stimulated by phonons due to β-decay of tritium. Depending on the storage conditions, the recombination of atoms also appeared in an explosive manner. We also suggest that the main mechanism of atomic diffusion is related to the formation of vacancies in contrast to isotopic exchange reactions $\text{H} + \text{H}_2 \rightarrow \text{H}_2 + \text{H}$ and $\text{D} + \text{D}_2 \rightarrow \text{D}_2 + \text{D}$ in samples where unpaired atoms are created by different dissociation techniques.

New and unexpected results were observed while studying relaxation and dynamic nuclear polarization (DNP) of H atoms in solid D_2 with a small admixture of H_2 and HD. The nuclear spins of H atoms could be easily polarized by pumping

both forbidden transitions in contrast to the pure para-H_2 samples. The forbidden transitions of H atoms in our field overlap with the ESR lines of D atoms and therefore both well-resolved Solid and Cross effect may result in the formation of DNP of H atoms. However the most intriguing result was observed after pumping the center of the ESR spectra which also caused a significant negative polarization of H atoms. We suggest that this effect may be related to the formation of the H-H or H-D radical pairs with a strong exchange interaction which possess an allowed transition there in contrast to unpaired H atoms.

A certain work can still be done on increasing the concentrations of unpaired atoms in solid hydrogen films. Optimizing the energy of bombarding electrons may lower the heat dissipated in the matrix and reduce the recombination of atoms. Also the local concentrations of H atoms could be increased by stabilizing them in matrices of solidified inert gases, such as Kr. The H atoms could occupy interstitial sites there which may lead to the more pronounced exchange effects.

In this thesis, we also reported an observation of a strong broad line in the center of the ESR spectra during the experiments with solid tritium. We suggested that this line may be related to the species trapped in the metallic mirrors of our ESR resonator. A further study may provide more evidence on the origin of this signal.

Bibliography

[1] Isaac F. Silvera and J. T. M. Walraven, Phys. Rev. Lett. **44**, 164 (1980).

[2] Isaac F. Silvera, Rev. Mod. Phys. **52**, 393 (1980).

[3] M. H. Anderson, J. R. Ensher, M. R. Matthews, Wieman C. E., and E. A. Cornell, Science **269**, 198 (1995).

[4] K. B. Davis, M. O. Mewes, M. R. Andrews, N. J. van Druten, D. S. Durfee, D. M. Kurn, and W. Ketterle, Phys. Rev. Lett. **75**, 3969 (1995).

[5] Dale G. Fried, Thomas C. Killian, Lorenz Willmann, David Landhuis, Stephen C. Moss, Daniel Kleppner, and Thomas J. Greytak, Phys. Rev. Lett. **81**, 3811 (1998).

[6] A. I. Safonov, S. A. Vasilyev, I. S. Yasnikov, I. I. Lukashevich, and S. Jaakkola, Phys. Rev. Lett. **81**, 4545 (1998).

[7] A. P. Bass and H. P. Broida, *Formation and Trapping of Free Radicals* (Academic Press, New York and London, 1960).

[8] D. Zhou, C. M. Edwards, and N. S. Sullivan, Phys. Rev. Lett. **62**, 1528 (1989).

[9] E. G. Kisvarsanyi and N. S. Sullivan, Phys. Rev. B **51**, 3462 (1995).

[10] J. Kranendonk, *Solid Hydrogen: Theory of the Properties of Solid H2, HD, and*, no. pt. 2 (Springer US, 2012).

[11] Tetsuo Miyazaki, Kwang Pill Lee, Kenji Fueki, and Akira Takeuchi, J. Phys. Chem. **88**, 4959 (1984).

[12] Takayuki Kumada, Phys. Rev. B **68**, 052301 (2003).

[13] Steven L. Mielke, Kirk A. Peterson, David W. Schwenke, Bruce C. Garrett, Donald G. Truhlar, Joe V. Michael, Meng-Chih Su, and James W. Sutherland, Phys. Rev. Lett. **91**, 063201 (2003).

[14] P. C. Stancil, S. Lepp, and A. Dalgarno, Astrophys. J. **509**, 1 (1998).

[15] C. D. Gay, P. C. Stancil, S. Lepp, and A. Dalgarno, Astrophys. J. **737**, 44 (2011).

[16] A. F. Andreev and I. M. Lifshitz, Sov. Phys. JETP **29**, 1107 (1969).

[17] G. V. Chester, Phys. Rev. A **2**, 256 (1970).

[18] A. J. Leggett, Phys. Rev. Lett. **25**, 1543 (1970).

[19] E. Kim and M. H. W. Chan, Nature **427**, 225 (2004).

[20] Duk Y. Kim and Moses H. W. Chan, Phys. Rev. Lett. **109**, 155301 (2012).

[21] I. F. Silvera and J. T. M. Walraven, *Spin-polarized atomic hydrogen*, in *Prog. in Low Temp. Phys.*, edited by D. F. Brewer (North-Holland, Amsterdam, 1986), vol. X, p. 139.

[22] Yu. Kagan, J. Low Temp. Phys. **87**, 525 (1992).

[23] J. Ahokas, O. Vainio, J. Järvinen, V. V. Khmelenko, D. M. Lee, and S. Vasiliev, Phys. Rev. B **79**, 220505(R) (2009).

[24] E. Wigner and H. B. Huntington, J. Chem. Phys. **3**, 764 (1935).

[25] M. I. Eremets and I. A. Troyan, Nat. Mater. **10**, 927 (2011).

[26] Phillip Dalladay-Simpson, Ross T. Howie, and Eugene Gregoryanz, Nature **529**, 63 (2016).

[27] R. Dias and I. Silvera, arXiv:1610.01634v1 (2016).

[28] J. Ahokas, J. Järvinen, V. V. Khmelenko, D. M. Lee, and S. Vasiliev, Phys. Rev. Lett. **97**, 095301 (2006).

[29] R. W. H. Webeler, J. Chem. Phys. **64**, 2253 (1976).

[30] G. W. Collins, E. M. Fearon, J. L. Maienschein, E. R. Mapoles, R. T. Tsugawa, P. C. Souers, and J. R. Gaines, Phys. Rev. Lett. **65**, 444 (1990).

[31] P. Ehrenfest and J. R. Oppenheimer, Phys. Rev. **37**, 333 (1931).

[32] C. P. Poole and H. A. Farach, *The theory of magnetic resonance*, A Wiley-Interscience publication (John Wiley & Sons Canada, Limited, 1972).

[33] W. A. Barker, Rev. Mod. Phys. **34**, 173 (1962).

[34] P. C. Souers, *Hydrogen Properties for Fusion Energy* (University of California Press, 1986).

[35] L. I. Bodine, D. S. Parno, and R. G. H. Robertson, Phys. Rev. C **91**, 035505 (2015).

[36] National Institute of Science and Technology, The NIST reference on constants, units and uncertainty, http://www.physics.nist.gov/cuu/index.html. Accessed: 2016-11-13.

[37] J. Vanier and C. Audoin, *The quantum physics of atomic frequency standards*, no. v. 2 in The Quantum Physics of Atomic Frequency Standards (A. Hilger, 1989).

[38] J. De Boer, Physica **14**, 139 (1948).

[39] J. O. Hirschfelder, C. F. Curtiss, and R. B. Bird, *Molecular theory of gases and liquids* (Wiley, 1954).

[40] Felix Fernandez-Alonso, Carlos Cabrillo, Ricardo Fernández-Perea, Francisco J. Bermejo, Miguel A. González, Claudia Mondelli, and Emmanuel Farhi, Phys. Rev. B **86**, 144524 (2012).

[41] Robert G. Mortimer, *Physical Chemistry (Second Edition)* (Academic Press, Burlington, 2000).

[42] B. I. Verkin and A. F. Prikhotko, *Cryocrystals* (Naukova Dumka, 1983). (in Russian).

[43] Uwe Albrecht, Peter Evers, and Paul Leiderer, Surf. Sci. **283**, 419 (1993).

[44] U. Albrecht, H. Dilger, P. Leiderer, and K. Kono, Physica B **165-166, Part 2**, 841 (1990).

[45] C. K. Jen, S. N. Foner, E. L. Cochran, and V. A. Bowers, Phys. Rev. **104**, 846 (1956).

[46] Yu. A. Dmitriev, J. Low Temp. Phys. **180**, 284 (2015).

[47] E. B. Gordon, A. A. Pel'menev, O. F. Pugachev, and V. V. Khmelenko, JETP Lett. **37**, 282 (1983).

[48] Takayuki Kumada, J. Chem. Phys. **124**, (2006).

[49] Mark Sharnoff and R. V. Pound, Phys. Rev. **132**, 1003 (1963).

[50] R. K. Leach, A paramagnetic resonance study of hydrogen atom production and recombination in solid H_2 from 1.4 to 8 K, Ph.D. thesis, University of Wisconsin (1972).

[51] J. Ahokas, O. Vainio, S. Novotny, J. Järvinen, V. V. Khmelenko, D. M. Lee, and S. Vasiliev, Phys. Rev. B **81**, 104516 (2010).

[52] A. S. Iskovskikh, A. Ya. Katunin, I. I. Lukashevich, V. V. Sklyarevskii, V. V. Suraev, V. V. Filippov, N. I. Filippov, and V. A. Shevtsov, JETP **64**, 1085 (1986).

[53] C. Ebner and C. C. Sung, Phys. Rev. A **5**, 2625 (1972).

[54] James R. Gaines, P. C. Souers, Evelyn M. Fearon, James D. Sater, and Evan R. Mapoles, Phys. Rev. B **39**, 3943 (1989).

[55] B. N. Esel'son, V. A. Mikheev, V. N. Grigor'ev, and N. P. Mikhin, JETP **74**, 2311 (1978).

[56] Yu. Kagan, L. A. Maksimov, and N. V. Prokof'ev, JETP Lett. **36**, 253 (1982).

[57] Yu. Kagan and L. A. Maksimov, Sov. Phys JETP **57**, 459 (1983).

[58] A. V. Ivliev, A. Ya. Katunin, I. I. Lukashevich, V. V. Sklyarevskii, V. V. Suraev, V. V. Filippov, N. I. Filippov, and V. A. Shevtsov, JETP Lett. **36**, 472 (1982).

[59] C. P. Poole, *Electron Spin Resonance: A Comprehensive Treatise on Experimental Techniques*, Dover books on physics (Dover Publications, 1996).

[60] G. Feher, Bell Syst. Tech. J. **36**, 449 (1957).

[61] Sergei Vasilyev, Jarno Järvinen, Esa Tjukanoff, Alexander Kharitonov, and Simo Jaakkola, Rev. Sci. Instrum. **75**, 94 (2004).

[62] Günter Sauerbrey, Z. Phys. **155**, 206 (1959).

[63] Jonathan F. Reichert and Norman C. Jarosik, Phys. Rev. B **27**, 2710 (1983).

[64] R. van Roijen, J. J. Berkhout, B. Hebral, and J. T. M. Walraven, A cryogenic dissociator for atomic hydrogen, unpublished.

[65] J. M. Ahokas, Magnetic resonance experiments with atomic hydrogen, Ph.D. thesis, University of Turku (2010).

[66] Sunggi Chung, Chun C. Lin, and Edward T. P. Lee, Phys. Rev. A **12**, 1340 (1975).

[67] S. J. B. Corrigan, J. Chem. Phys. **43**, 4381 (1965).

[68] J. Schou and H. Sørensen, J. Appl. Phys. **49**, 816 (1978).

[69] H. M. Goldenberg, D. Kleppner, and N. F. Ramsey, Phys. Rev. Lett. **5**, 361 (1960).

[70] Daniel Kleppner, H. Mark Goldenberg, and Norman F. Ramsey, Phys. Rev. **126**, 603 (1962).

[71] H. I. Eiwen and E. M. Purcell, Nature **168**, 356 (1951).

[72] F. J. Adrian, J. Chem. Phys. **32**, 972 (1960).

[73] Daohui Li and Gregory A. Voth, J. Chem. Phys. **100**, 1785 (1994).

[74] Takayuki Kumada, Tomoyoshi Noda, Jun Kumagai, Yasuyuki Aratono, and Tetsuo Miyazaki, J. Chem. Phys. **111**, 10974 (1999).

[75] C. K. Jen, S. N. Foner, E. L. Cochran, and V. A. Bowers, Phys. Rev. **112**, 1169 (1958).

[76] E. P. Bernard, R. E. Boltnev, V. V. Khmelenko, V. Kiryukhin, S. I. Kiselev, and D. M. Lee, Phys. Rev. B **69**, 104201 (2004).

[77] G. W. Collins, P. C. Souers, J. L. Maienschein, E. R. Mapoles, and J. R. Gaines, Phys. Rev. B **45**, 549 (1992).

[78] G. Feher, Phys. Rev. **103**, 834 (1956).

[79] G. W. Collins, J. L. Maienschein, E. R. Mapoles, R. T. Tsugawa, E. M. Fearon, P. C. Souers, J. R. Gaines, and P. A. Fedders, Phys. Rev. B **48**, 12620 (1993).

[80] Tetsuo Miyazaki, Hiromichi Morikita, Kenji Fueki, and Tatsuya Hiraku, Chem. Phys. Lett. **182**, 35 (1991).

[81] J. H. Van Vleck, Phys. Rev. **74**, 1168 (1948).

[82] C. Kittel and Elihu Abrahams, Phys. Rev. **90**, 238 (1953).

[83] C. P. Slichter, *Principles of Magnetic Resonance*, Lecture Notes in Computer Science (Springer, 1996).

[84] J. R. Gaines, R. T. Tsugawa, and P. C. Souers, Phys. Rev. Lett. **42**, 1717 (1979).

[85] T. Kumada, N. Kitagawa, T. Noda, J. Kumagai, Y. Aratono, and T. Miyazaki, Chem. Phys. Lett. **288**, 755 (1998).

[86] T. Miyazaki, N. Iwata, K. Fueki, and H. Hase, J. Phys. Chem. **94**, 1702 (1990).

[87] A. V. Frolov, V. A. Shevtsov, and I. I. Lukashevitch, Fiz. Nizk. Temper. **17**, 675 (1991).

[88] Tetsuo Miyazaki, Chem. Phys. Lett. **176**, 99 (1991).

[89] G. T. Trammell, Henry Zeldes, and Ralph Livingston, Phys. Rev. **110**, 630 (1958).

[90] Takayuki Kumada, Shoji Mori, Jun Kumagai, Yasuyuki Aratono, and Tetsuo Miyazaki, J. Phys. Chem. A **103**, 8966 (1999).

[91] G. W. Collins, P. C. Souers, F. Magnotta, E. R. Mapoles, and J. R. Gaines, Phys. Rev. B **53**, 8143 (1996).

[92] Tetsuo Miyazaki, Kenji Yamamoto, and Yasuyuki Aratono, Chem. Phys. Lett. **232**, 229 (1995).

[93] Jun Kumagai, Hiroki Inagaki, Susumu Kariya, Takahiro Ushida, Yuta Shimizu, and Takayuki Kumada, J. Chem. Phys. **127**, 024505 (2007).

[94] T. Miyazaki, *Atom Tunneling Phenomena in Physics, Chemistry and Biology*, Physics and Astronomy Online Library (Springer, 2004).

[95] Matthew D. Correnti, Kyle P. Dickert, Mark A. Pittman, John W. Felmly, John J. III Banisaukas, and Lon B. Knight Jr., J. Chem. Phys. **137**, 204308 (2012).

[96] G. Dresselhaus, A. F. Kip, and C. Kittel, Phys. Rev. **98**, 368 (1955).

[97] Tsuneki Ichikawa, Hiroto Tachikawa, Takayuki Kumada, Jun Kumagai, and Tetsuo Miyazaki, Chem. Phys. Lett. **307**, 283 (1999).

[98] R. L. Brooks, S. K. Bose, J. L. Hunt, Jack R. MacDonald, J. D. Poll, and J. C. Waddington, Phys. Rev. B **32**, 2478 (1985).

[99] V. S. Edel'man and M. I. Faley, J. Low Temp. Phys. **52**, 301 (1983).

[100] Jisha Hazra and N Balakrishnan, New J. Phys. **17**, 055027 (2015).

[101] B. K. Kendrick, Jisha Hazra, and N. Balakrishnan, Phys. Rev. Lett. **115**, 153201 (2015).

[102] F. J. Aoiz, L. Bañares, and V. J. Herrero, Int. Rev. Phys. Chem. **24**, 119 (2005).

[103] Justin Jankunas, Mahima Sneha, Richard N. Zare, Foudhil Bouakline, Stuart C. Althorpe, Diego Herráez-Aguilar, and F. Javier Aoiz, P. Natl. Acad. Sci. USA **111**, 15 (2014).

[104] Johndale C. Solem and G. A. Rebka, Phys. Rev. Lett. **21**, 19 (1968).

[105] Haruyuki Tsuruta, Tetsuo Miyazaki, Kenji Fueki, and Naoto Azuma, J. Phys. Chem. **87**, 5422 (1983).

[106] A. V. Ivliev, A. S. Iskovskikh, A. Ya. Katunin, I. I. Lukashevich, V. V. Skl-yarevskii, V. V. Suraev, V. V. Filippov, N. I. Filippov, and V. A. Shevtsov, JETP Lett. **38**, 379 (1983).

[107] Kwang Pill Lee, Tetsuo Miyazaki, Kenji Fueki, and Kenji Gotoh, J. Phys. Chem. **91**, 180 (1987).

[108] Tetsuo Miyazaki, Nobuchika Iwata, Kwang Pill Lee, and Kenji Fueki, J. Phys. Chem. **93**, 3352 (1989).

[109] Takayuki Kumada, Shoji Mori, Toshimitsu Nagasaka, Jun Kumagai, and Tetsuo Miyazaki, J. Low Temp. Phys. **122**, 265 (2001).

[110] S. I. Kiselev, V. V. Khmelenko, and D. M. Lee, Phys. Rev. Lett. **89**, 175301 (2002).

[111] E. P. Bernard, R. E. Boltnev, V. V. Khmelenko, and D. M. Lee, J. Low Temp. Phys. **138**, 829 (2005).

[112] V. V. Khmelenko, E. P. Bernard, S. A. Vasiliev, and D. M. Lee, Russ. Chem. Rev. **76**, 1107 (2007).

[113] Toshiyuki Takayanagi, Nobuyuki Masaki, Kazutaka Nakamura, Makoto Okamoto, Shin Sato, and George C. Schatz, J. Chem. Phys. **86**, 6133 (1987).

[114] Toshiyuki Takayanagi, Kazutaka Nakamura, and Shin Sato, J. Chem. Phys. **90**, 1641 (1989).

[115] Toshiyuki Takayanagi and Shin Sato, J. Chem. Phys. **92**, 2862 (1990).

[116] Gene C. Hancock, C. Alden Mead, Donald G. Truhlar, and Antonio J. C. Varandas, J. Chem. Phys. **91**, 3492 (1989).

[117] Takayuki Kumada, Kenji Komaguchi, Yasuyuki Aratono, and Tetsuo Miyazaki, Chem. Phys. Lett. **261**, 463 (1996).

[118] W. J. Moore, *Physical Chemistry (4th Edition)* (Prentice-Hall, 1962), pp. 260–263.

[119] Albert W. Overhauser, Phys. Rev. **92**, 411 (1953).

[120] Thomas R. Carver and Charles P. Slichter, Phys. Rev. **102**, 975 (1956).

[121] A. Abragam, Phys. Rev. **98**, 1729 (1955).

[122] Chester F. Hwang and Daniel A. Hill, Phys. Rev. Lett. **19**, 1011 (1967).

[123] David S. Wollan, Phys. Rev. B **13**, 3671 (1976).

[124] G. Feher and E. A. Gere, Phys. Rev. **114**, 1245 (1959).

[125] A. Abragam and M. Goldman, *Nuclear Magnetism: Order and Disorder* (Clarendon Press, 1982). P. 339-418.

[126] A. Honig and E. Stupp, Phys. Rev. **117**, 69 (1960).

[127] A. Ya. Katunin, I. I. Lukashevich, S. T. Orosmamatov, V. V. Sklyarevskii, V. V. Suraev, V. V. Filippov, N. I. Filippov, and V. A. Shevtsov, Phys. Lett. A **87**, 483 (1982).

[128] J. Van Houten, W. Th. Wenckebach, and N. J. Poulis, Physica B+C **92**, 210 (1977).

[129] D. Banerjee, D. Shimon, A. Feintuch, S. Vega, and D. Goldfarb, J. Magn. Reson. **230**, 212 (2013).

[130] G. Feher, R. C. Fletcher, and E. A. Gere, Phys. Rev. **100**, 1784 (1955).

[131] Anatoly E. Dementyev, David G. Cory, and Chandrasekhar Ramanathan, J. Chem. Phys. **134** (2011).

[132] Lon B. Knight Jr., William E. Rice, Louie Moore, and Ernest R. Davidson, J. Chem. Phys. **103**, 5275 (1995).

[133] Lon B. Knight Jr., William E. Rice, Louie Moore, Ernest R. Davidson, and Robert S. Dailey, J. Chem. Phys. **109**, 1409 (1998).

[134] Gerald Rosen, J. Chem. Phys. **65**, 1735 (1976).

[135] R. E. Boltnev, E. P. Bernard, J. Järvinen, V. V. Khmelenko, and D. M. Lee, Phys. Rev. B **79**, 180506 (2009).

[136] John Lambe, Phys. Rev. **120**, 1208 (1960).

[137] E. R. Mapoles, F. Magnotta, G. W. Collins, and P. C. Souers, Phys. Rev. B **41**, 11653 (1990).

[138] Frank J. Zeleznik, J. Chem. Phys. **65**, 4492 (1976).

[139] Donald G. Truhlar, Roger S. Grev, and Bruce C. Garrett, J. Phys. Chem. **87**, 3415 (1983).

[140] Yasuyuki Aratono, Takuro Matsumoto, Toshiyuki Takayanagi, Takayuki Kumada, Kenji Komaguchi, and Tetsuo Miyazaki, J. Phys. Chem. A **104**, 1968 (2000).

[141] Yasuyuki Aratono, Takuro Matsumoto, Toshiyuki Takayanagi, Takayuki Kumada, Kenji Komaguchi, and Tetsuo Miyazaki, J. Phys. Chem. A **102**, 1501 (1998).

[142] N. Bloembergen and R. V. Pound, Phys. Rev. **95**, 8 (1954).

[143] G. Feher, J. P. Gordon, E. Buehler, E. A. Gere, and C. D. Thurmond, Phys. Rev. **109**, 221 (1958).

[144] E. M. Purcell, Phys. Rev. **69**, 681 (1946).

[145] S. A. Vasilyev, A. Ya. Katunin, A. I. Safonov, A. V. Frolov, and E. Tjukanov, Appl. Magn. Reson. **3**, 1061 (1992).

[146] D. Jérome and J. M. Winter, Phys. Rev. **134**, A1001 (1964).

[147] D. M. Lee and N. Ashcroft, private communication.

[148] William C. Stwalley, Chem. Phys. Lett. **88**, 404 (1982).

[149] E. Tjukanov, P. C. Souers, and W. N. Hardy, *Zero-field magnetic resonance studies of atomic tritium*, Spin Polarized Quantum Systems, edited by S. Stringari (World Scientific, Singapore, 1989), p. 240.

[150] K. E. Kürten and M. L. Ristig, Phys. Rev. B **31**, 1346 (1985).

[151] A. F. G. Wyatt, Phys. Rev. Lett. **69**, 1785 (1992).

[152] F. Pobell, *Matter and Methods at Low Temperatures* (Springer-Verlag, 2007), p. 106.

[153] C. L. Reynolds and A. C. Anderson, Phys. Rev. B **14**, 4114 (1976).